Multi-modality imaging in ischemic heart disease, arrhythmia and cardiac-mechanics

El Mahdiui, M.

Multi-modality imaging in ischemic heart disease, arrhythmia and cardiac-mechanics

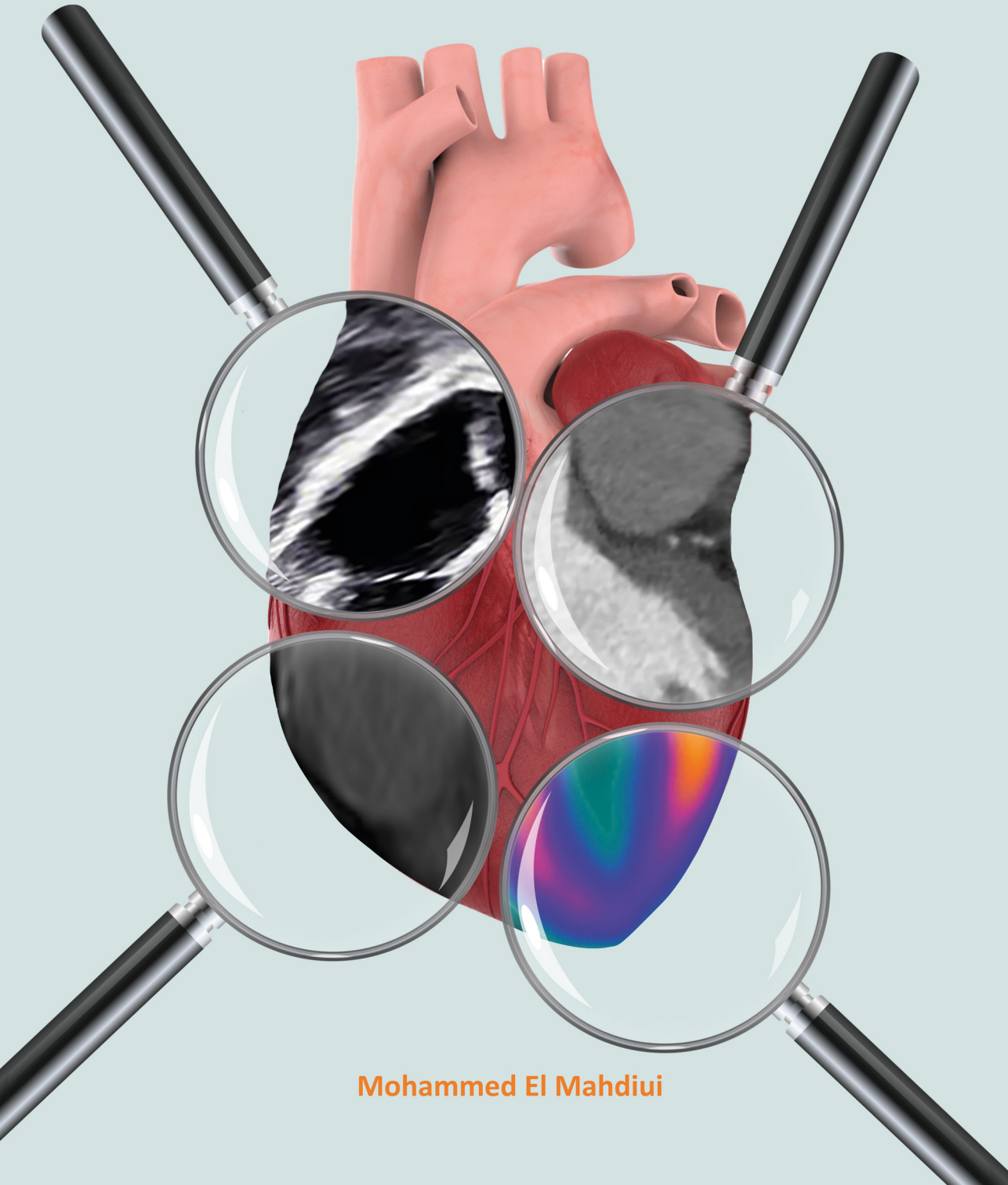

Mohammed El Mahdiui

Multi-modality imaging in ischemic heart disease, arrhythmia and cardiac-mechanics

Mohammed El Mahdiui

Colophon

The studies described in this thesis were performed at the Department of Cardiology of the Leiden University Medical Center, Leiden, The Netherlands

ISBN: 978-94-6421-717-9
Printing: Proefschriften.nl, Ede
Cover design: Loes Kema
Layout and design: Yasmin Katlich, persoonlijkproefschrift.nl

Financial support for this thesis by Boehringer Ingelheim bv, Canon Medical Systems Nederland, Medis Medical Imaging Systems bv and Chipsoft bv is gratefully acknowledged.

Multi-modality imaging in ischemic heart disease,

arrhythmia and cardiac-mechanics

Proefschrift

ter verkrijging van
de graad van doctor aan de Universiteit Leiden,
op gezag van rector magnificus prof. dr.ir. H. Bijl,
volgens besluit van het college voor promoties
te verdedigen op dinsdag 10 mei 2022
klokke 10 uur
door

Mohammed El Mahdiui
Geboren te Midar, Marokko
In 1989

Promotoren

Prof. Dr. J.J. Bax

Prof. Dr. J.W. Jukema

Co-promotor

Dr. V. Delgado

Leden promotiecommissie

Prof. Dr. Ir. J.H.C. Reiber	
Prof. Dr. A Gimelli	University of Pisa, Italië
Prof. Dr. J Knuuti	University of Turku, Finland
Dr. M. Bootsma	
Dr. N. Ajmone Marsan	

Het verschijnen van dit proefschrift werd mede mogelijk gemaakt door de steun van de Nederlandse Hartstichting

Aan mijn familie

TABLE OF CONTENTS

1

General introduction and outline of the thesis

Cardiovascular disease (CVD) is the leading cause of morbidity and mortality in adults worldwide.[1] The worldwide incidence of CVD deaths has increased from 18.1 million in 2010 to 20.5 million in 2020 and is expected to increase to 24.2 million in 2030.[2] Adequate diagnosis, risk stratification and treatment to decrease mortality, morbidity and the burden on health care systems is therefore crucial. Multimodality imaging has emerged as an important tool for the management of patients with cardiovascular disease.

Ischemic heart disease

Ischemic heart disease is the largest contributor to CVD and the single largest cause for worldwide mortality.[1] The development of coronary artery disease (CAD) is a complex process of accumulation of atherosclerotic plaque in the span of several years before the development of symptoms.[3] Although sex-related differences in CAD have been reported, the role of sex on plaque progression and composition has not been studied in a low-to-intermediate risk population in stable clinical conditions over a long follow-up period. While assessment of coronary plaque composition was previously reserved solely for invasive imaging modalities or histology, increased spatial resolution has allowed cardiac computed tomography (CT) to quantitatively asses plaque composition.[4,5] Indeed, cardiac CT has demonstrated a dramatic change in the last decade with increasingly lower radiation exposure and better imaging quality.[4,6]

The clinical manifestation of CAD is divers, and includes stable angina and myocardial infarction with possible adverse effects on left ventricular (LV) function leading to heart failure and sudden cardiac death. In patients presenting with symptoms of stable angina, risk stratification is indicated. Both coronary artery calcium (CAC) score, an anatomical marker of CAD, and nuclear imaging, a functional marker of CAD, have demonstrated independent and complementary prognostic value in patients with stable CAD, with also intermodality correlation.[7,8] The relationship between CAC score and CT myocardial perfusion, also a functional marker of CAD, which could be performed directly after CAC score, has however not been studied before.

In post-myocardial infarction patients, following treatment, imaging is performed to assess possible treatment options; for that purpose, assessment of ischemia, the extent of damage and myocardial viability is important.[9] Late gadolinium

contrast enhanced cardiac magnetic resonance (LGE CMR) has a high diagnostic accuracy for assessment of the extent of transmural scar. [10] Although, LGE CMR has several important advantages, it is not without limitations, for instance the need for intravenous contrast, the limited clinical availability and the relative high cost. Non-invasive myocardial work is a novel echocardiographic based parameter for assessment of LV function which overcomes these limitations. [11,12]

Arrhythmias

Heart failure is an important complication following myocardial infarction. Heart failure patients have an increased risk for developing ventricular arrythmias and therefore implantable cardioverter defibrillator (ICD) therapy might be appropriate. Evaluation of patients with heart failure, both ischemic and non-ischemic, who might benefit from ICD therapy continues to be a clinical challenge. Currently, LV ejection fraction <35% is used as a cut-off value to recommend ICD therapy. However, a substantial portion of patients with an ICD never develop ventricular arrythmias. Anatomical and functional characterization of the arrhythmogenic substrate using multimodality imaging may permit superior risk stratification for the occurrence of ventricular arrythmias (and accordingly, the need for ICD implantation).

Atrial fibrillation (AF) is the most prevalent arrhythmic disease worldwide with considerable impact on morbidity and mortality. AF catheter ablation is a safe and established treatment option for AF and is more effective in maintaining sinus rhythm compared to medical therapy.[13] However, AF recurrence rates remain high following AF catheter ablation.[13,14] Adequate patient selection prior to ablation might prevent unnecessary interventions and complications. Epicardial adipose tissue (EAT) in close proximity of the LA, is the adipose tissue which actively secretes hormones and cytokines and may play a role in the development of AF.[15,16] The quantity and attenuation of EAT can be derived from cardiac CT scans, and may provide a marker of inflammation. It is however, unknown whether volumetric assessment of quantity and attenuation of EAT (located posterior to the LA) predicts AF recurrence following catheter ablation.

Objectives and outline of the thesis

The main objective of this thesis is to investigate the role of multi-modality imaging in ischemic heart disease. Specifically various chapters have been dedicated to how and when cardiac mechanics (a new, echocardiographically derived parameter of LV function) and other novel imaging parameters can be used for risk stratification and treatment guidance in ischemic heart disease.

In Part 1 of this thesis, different imaging modalities are utilized to evaluate the extent and severity of CAD in different patient populations. In Chapter 2, the progression of CAD is evaluated with focus on the role of sex (with longer term follow-up) in a low-to-intermediate risk population. In Chapter 3, the relationship between an anatomical marker of CAD (CAC score derived from CT) and a functional marker of CAD (CT perfusion imaging), is assessed. A novel imaging parameter for evaluating LV function based on non-invasive pressure-strain loops, is introduced in Chapter 4 and reference values of global LV myocardial efficiency are presented in distinct patient populations. In Chapter 5, this novel imaging parameter is then further related to infarct transmurality, which is characterized on LGE CMR in patients with previous ST-segment elevation myocardial infarction.

In Part 2 of this thesis the role of multimodality imaging in arrythmias is assessed. Several imaging parameters are evaluated for risk stratification of ventricular arrhythmias in heart failure patients in Chapter 6, while in Chapter 7, imaging parameters are tested for prediction of AF recurrence following catheter ablation.

REFERENCES

1. Global health estimates 2019: Life expectancy, 2000–2019. Geneva: World Health Organization; 2018 (https://www.who.int/docs/default-source/gho-documents/global-health-estimates/ghe2019_cod_global_2000_20194e572f53-509f-4578-b01e-6370c65d9fc5.xlsx?sfvrsn=eaf8ca5_7, accessed 18 July 2021).
2. World Health Organization. The top 10 causes of death. Geneva: World Health Organization; 2012 (https://www.who.int/cardiovascular_diseases/en/cvd_atlas_25_future.pdf?ua=1, accessed 18 July 2021).
3. Man JJ, Beckman JA, Jaffe IZ. Sex as a Biological Variable in Atherosclerosis. Circ Res 2020;126:1297-1319.
4. Heseltine TD, Murray SW, Ruzsics B, Fisher M. Latest Advances in Cardiac CT. Eur Cardiol 2020;15:1-7.
5. de Graaf MA, Broersen A, Kitslaar PH, Roos CJ, Dijkstra J, Lelieveldt BP, et al. Automatic quantification and characterization of coronary atherosclerosis with computed tomography coronary angiography: cross-correlation with intravascular ultrasound virtual histology. Int J Cardiovasc Imaging 2013;29:1177-1190.
6. Stocker TJ, Deseive S, Leipsic J, Hadamitzky M, Chen MY, Rubinshtein R, et al. Reduction in radiation exposure in cardiovascular computed tomography imaging: results from the PROspective multicenter registry on radiaTion dose Estimates of cardiac CT angIOgraphy iN daily practice in 2017 (PROTECTION VI). Eur Heart J 2018;39:3715-3723.
7. Chang SM, Nabi F, Xu J, Peterson LE, Achari A, Pratt CM, et al. The coronary artery calcium score and stress myocardial perfusion imaging provide independent and complementary prediction of cardiac risk. J Am Coll Cardiol 2009;54:1872-1882.
8. Engbers EM, Timmer JR, Ottervanger JP, Mouden M, Knollema S, Jager PL. Prognostic Value of Coronary Artery Calcium Scoring in Addition to Single-Photon Emission Computed Tomographic Myocardial Perfusion Imaging in Symptomatic Patients. Circ Cardiovasc Imaging 2016;9.
9. Ibanez B, James S, Agewall S, Antunes MJ, Bucciarelli-Ducci C, Bueno H, et al. 2017 ESC Guidelines for the management of acute myocardial infarction in patients presenting with ST-segment elevation: The Task Force for the management of acute myocardial infarction in patients presenting with ST-segment elevation of the European Society of Cardiology (ESC). Eur Heart J 2018;39:119-177.
10. Kim RJ, Wu E, Rafael A, Chen E-L, Parker MA, Simonetti O, et al. The Use of Contrast-Enhanced Magnetic Resonance Imaging to Identify Reversible Myocardial Dysfunction N Engl J Med 2000;343:1445-1453.
11. Russell K, Eriksen M, Aaberge L, Wilhelmsen N, Skulstad H, Remme EW, et al. A novel clinical method for quantification of regional left ventricular pressure-strain loop area: a non-invasive index of myocardial work. Eur Heart J 2012;33:724-733.
12. Russell K, Eriksen M, Aaberge L, Wilhelmsen N, Skulstad H, Gjesdal O, et al. Assessment of wasted myocardial work: a novel method to quantify energy loss due to uncoordinated left ventricular contractions. Am J Physiol Heart Circ Physiol 2013;305:H996-1003.
13. Kirchhof P, Benussi S, Kotecha D, Ahlsson A, Atar D, Casadei B, et al. 2016 ESC Guidelines for the management of atrial fibrillation developed in collaboration with EACTS. Europace 2016;18:1609-1678.

14. Sultan A, Luker J, Andresen D, Kuck KH, Hoffmann E, Brachmann J, et al. Predictors of Atrial Fibrillation Recurrence after Catheter Ablation: Data from the German Ablation Registry. Sci Rep 2017;7:16678.

15. Thanassoulis G, Massaro JM, O'Donnell CJ, Hoffmann U, Levy D, Ellinor PT, et al. Pericardial fat is associated with prevalent atrial fibrillation: the Framingham Heart Study. Circ Arrhythm Electrophysiol 2010;3:345-350.

16. Sacks HS, Fain JN. Human epicardial adipose tissue: a review. Am Heart J 2007;153:907-917.

PART I

Imaging modalities in coronary artery disease

2

Sex Differences in Coronary Plaque Changes assessed by Serial Computed Tomography Angiography

El Mahdiui M, Smit JM, van Rosendael AR, Neglia D, Knuuti J, Saraste A, Buechel RR, Teresinska A, Pizzi MN, Roque A, Magnacca M, Mertens BJ, Caselli C, Rocchiccioli S, Parodi O, Pelosi G, Scholte AJ.

Int J Cardiovasc Imaging. 2021 Mar 10.

ABSTRACT

Long-term data on sex-differences in coronary plaque changes over time is lacking in a low-to-intermediate risk population of stable coronary artery disease (CAD). The aim of this study was to evaluate the role of sex on long-term plaque progression and evolution of plaque composition. Furthermore, the influence of menopause on plaque progression and composition was also evaluated. Patients that underwent a coronary computed tomography angiography (CTA) were prospectively included to undergo a follow-up coronary CTA. Total and compositional plaque volumes were normalized using the vessel volume to calculate a percentage atheroma volume (PAV). To investigate the influence of menopause on plaque progression, patients were divided into two groups, under and over 55 years of age. In total, 211 patients were included in this analysis, 146 (69%) men. The mean interscan period between baseline and follow-up coronary CTA was 6.2 ± 1.4 years. Women were older, had higher HDL levels and presented more often with atypical chest pain. Men had 434 plaque sites and women 156. On a per-lesion analysis, women had less fibro-fatty PAV compared to men (β -1.3 ± 0.4%; $p < 0.001$), with no other significant differences. When stratifying patients by 55 years age threshold, fibro-fatty PAV remained higher in men in both age groups ($p < 0.05$) whilst women younger than 55 years demonstrated more regression of fibrous (β -0.8 ± 0.3% per year; $p = 0.002$) and non-calcified PAV (β -0.7 ± 0.3% per year; $p = 0.027$). In a low-to-intermediate risk population of stable CAD patients, no significant sex differences in total PAV increase over time were observed. Fibro-fatty PAV was lower in women at any age and women under 55 years demonstrated significantly greater reduction in fibrous and non-calcified PAV over time compared to age-matched men. (ClinicalTrials.gov number, NCT04448691.)

INTRODUCTION

Several studies have highlighted distinct sex-related differences for coronary artery disease (CAD). Women tend to be older when presenting with CAD[1], have lower rates of obstructive disease[2] but higher risk of major adverse cardiac events compared to men[2-5]. This discrepancy might arise from differences in plaque characteristics between men and women.[6] Postmortem histology studies reported plaque morphological differences between men and women[7-10]. However, in vivo intravascular studies have shown conflicting data regarding plaque burden and morphology between men and women.[11-22] These invasive studies were though performed in patients with an acute coronary syndrome (ACS), did not evaluate the plaques in the whole coronary tree or did not prospectively investigate sex differences in the natural plaque evolution over a long follow-up period. Coronary computed tomography angiography (CTA) allows for a fast and non-invasive assessment of coronary plaque burden and characterization of plaque composition comparable with intravascular ultrasound virtual histology (IVUS-VH).[23] The aim of the current study was to evaluate the influence of sex on long-term in vivo plaque progression and evolution of plaque composition in a low-to-intermediate risk population in stable clinical conditions. Furthermore, the role of menopause on plaque progression and composition was also evaluated.

MATERIALS AND METHODS

Study design

The SMARTool (Simulation Modeling of coronary ARTery disease: a tool for clinical decision support, Horizon 2020) project, is a prospective, international, multicenter study with the aim of integrating clinical, molecular, cellular and imaging data to provide a patient-specific risk stratification model exploitable for clinical decision support in stable CAD management.[24,25] Patients who had undergone a coronary CTA at baseline for suspected CAD were prospectively included and subsequently underwent a follow-up coronary CTA. Patients with stable CAD without a history of myocardial infarction, heart failure or surgical procedures related to heart diseases were included. The complete inclusion and exclusion criteria are provided in the supplementary material.

Study population

Patients who had undergone clinically indicated coronary CTA in the period 2009-2012 or were part of the EVINCI (FP7-222915) or the ARTreat (FP7-224297) clinical studies were included. The Diamond-Forrester model was used to estimate the pretest probability of CAD.[26] Inclusion and exclusion criteria have been described previously.[25] Data on cardiovascular risk factors and medical therapy were prospectively collected at baseline and follow-up. Statin intensity was classified according to the American College of Cardiology and American Heart Association guidelines.[27] In total, 275 patients from 5 European countries (Finland, Italy, Poland, Spain and Switzerland) were recruited in 7 centers. Of the 263 patients who underwent a follow-up coronary CTA, 52 patients were excluded because of uninterpretable coronary CTA for visual (n=5) or quantitative CTA analysis (n=11) or absence of coronary plaques at follow-up (n=36). Thus, 211 patients were finally included in the present analysis (Figure 1).

Fig. 1 Flow diagram of the study population

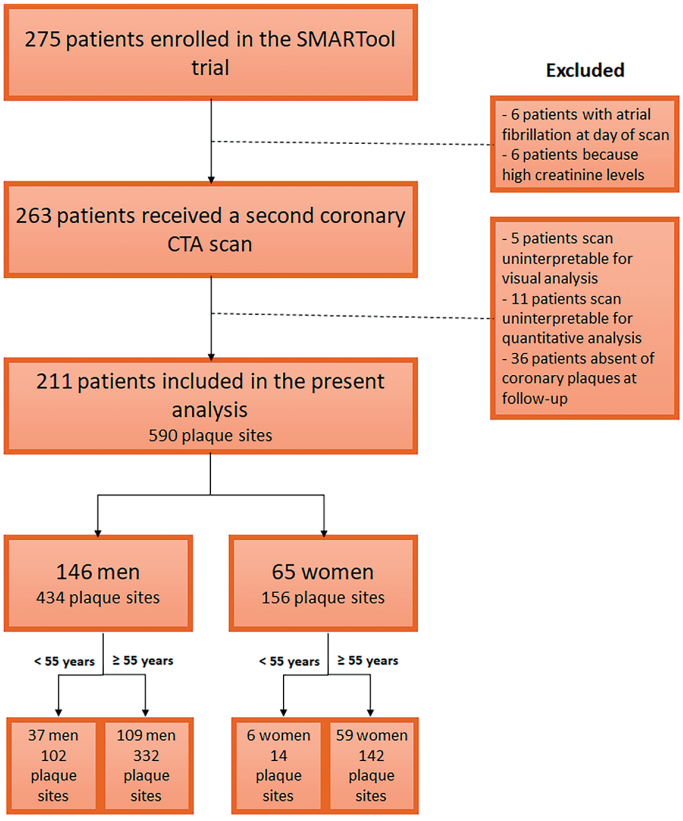

Coronary CTA analysis protocol

The coronary CTA protocol has been described previously.[25] In brief, anonymized coronary CTA data were transferred to a core laboratory (Leiden University Medical Center) for visual and quantitative analysis (supplementary material) and researchers were blinded to patients clinical data. Quantitative analysis was performed on visually identified plaques using a dedicated software package (QAngio CT Research Edition version 3.1.2.0, Medis Medical Imaging Systems, Leiden, the Netherlands). The software automatically detects the centerline, lumen and the vessel wall and allows the user for manual adjustment if needed.[23,28] The baseline and follow-up coronary CTA were analyzed side-by-side and lesions were identified using anatomical markers. Several parameters were derived from the quantitative analysis: percentage diameters stenosis, lesion length, remodeling index, total vessel volume, total plaque volume and plaque composition volumes. Plaque composition volumes were determined using predefined Hounsfield units (HU) cutoff values: >350 HU for calcified plaque and -30 to 350 HU for non-calcified plaque. Non-calcified plaque was further classified in necrotic core plaque (-30 to 75 HU), fibro-fatty plaque (76 to 130 HU) and fibrous plaque (131 to 350 HU). Total plaque volume and plaque composition volumes were normalized for the vessel volume and the percentage atheroma volume (PAV) calculated as follows: (plaque volume/ total vessel volume) x100% and reported as a percentage. The inter- and intra-observer variability have been described previously.[28-30]

Statistical analysis

Continuous variables are expressed as mean ± standard deviation (SD) if normally distributed and median and interquartile range (IQR) if non-normally distributed. Normality was assessed using histograms and Q-Q plots. Categorical variables are presented as frequencies and percentages and compared using the Chi square test or the Fisher's exact test. Normally distributed continuous variables were compared using the Student's *t*-test and the Mann-Whitney *U*-test if not normally distributed. Quantitative analysis parameters were compared on a per-lesion basis. Analysis of annual rate of lesion progression was performed using linear mixed models (LMM) to correct for per lesion and per patient factors. Fixed effects in the models included sex, interscan period and the interaction between sex and interscan period. In addition, the LMM was adjusted for age, hypertension, diabetes mellitus, smoking, family history of CAD, obesity, LDL and HDL at baseline. Random effects included intercept and an unstructured covariance was used to account for within-

patient and within-plaque correlation over time. A sub-analysis was performed in patients aged under and over 55 years at baseline coronary CTA scan to assess the influence of menopause on plaque progression in women compared to men. The models provide a test for systematic between-group difference across time, as well as a test for between-group differences in the trend. The estimated difference (β) of women compared to men and the interaction are presented with standard error (SE), 95% confidence interval (CI) and p-values. Statistical analyses were performed using SPSS version 25.0 (SPSS, Armonk, NY) and a two-sided p-value <0.05 was considered statistically significant.

RESULTS

Baseline patient characteristics

Of the 211 patients included in the present analysis, 146 (69%) were men and 65 (31%) were women. Women were generally older, had higher HDL levels and presented more often with atypical chest pain. The mean interscan period between baseline and follow-up coronary CTAs was 6.2 ± 1.4 years (minimum 1.9- maximum 11.3). Baseline patient characteristics are shown in Table 1. When stratifying the population according to age groups, 43 (20%) were under 55 years at the time of baseline coronary CTA scan and 168 (80%) were 55 years or older.

Table 1. Patient characteristics

	Total (n=211)	Men (n=146)	Women (n=65)	p-value
Clinical				
Age, years	62 ± 8	61 ± 8	64 ± 7	**0.001**
Body mass index, kg/m^2	27.6 ± 3.8	27.6 ± 3.4	27.5 ± 4.5	0.835
Family history of CAD	96 (46)	59 (40)	37 (57)	**0.049**
Current smoker	33 (16)	25 (17)	8 (12)	0.306
Diabetes mellitus	41 (19)	25 (17)	16 (25)	0.266
Dyslipidemia	138 (65)	91 (62)	47 (72)	0.305
Hypertension	136 (65)	90 (62)	46 (71)	0.370
Chest pain	47 (22)	34 (23)	13 (20)	0.310
Typical	96 (46)	56 (38)	40 (62)	**0.017**
Atypical	1 (1)	1 (1)	0 (0)	1.000
Non-anginal				

Table 1. Continued.

	Total (n=211)	Men (n=146)	Women (n=65)	p-value
Medication				
ACE-inhibitors/ARB's	96 (46)	64 (44)	32 (49)	0.839
Aspirin	133 (63)	90 (62)	43 (66)	0.891
Beta-blockers	86 (41)	55 (38)	31 (48)	0.366
Diuretics	32 (15)	13 (9)	19 (29)	**<0.001**
Statin therapy				
Statins at baseline	112 (53)	74 (51)	38 (59)	0.296
-High-intensity	7 (6)	4 (5)	3 (8)	0.687
-Low-/Moderate-intensity	34 (30)	25 (34)	9 (24)	0.271
Statins at follow-up	145 (69)	105 (72)	40 (62)	0.133
-High-intensity	27 (19)	19 (19)	8 (20)	0.792
-Low-/Moderate-intensity	110 (76)	78 (77)	32 (80)	0.472
Biochemical				
Creatinine, mg/dl	0.873 ± 0.197	0.943 ± 0.174	0.734 ± 0.166	**<0.001**
Glucose, mg/dl	109.51 ± 26.63	110.55 ± 26.80	107.42 ± 26.38	0.458
Triglycerides, mg/dL	121.93 ± 62.51	126.92 ± 65.04	111.66 ± 56.13	0.125
Total Cholesterol, mg/dL	185.52 ± 48.32	182.55 ± 48.29	192.23 ± 48.10	0.190
LDL, mg/dL	110.28 ± 41.24	108.35 ± 41.42	114.65 ± 40.84	0.318
HDL, mg/dL	51.33 ± 14.87	49.28 ± 14.53	55.97 ± 14.69	**0.003**

Bold indicates statistical significance of p-value <0.05.
Patient characteristics are at baseline unless otherwise indicated. Values are presented as mean ± standard deviation or n (%)
ACE = angiotensin-converting enzyme; ARB = angiotensin-II-receptor blocker; CAD = coronary artery disease; HDL = high-density lipoprotein; LDL = low-density lipoprotein

Baseline plaque characteristics and changes of total and compositional PAV

A total of 590 plaques were identified, 434 (74%) plaques were found in men and 156 (26%) in women. Baseline plaque characteristics are shown in Table 2. At baseline men had higher degree of stenosis (p<0.05). Men also had higher absolute volumes of fibro-fatty and necrotic core (p<0.05), but after correction for vessel volume only fibro-fatty PAV remained higher in men (p<0.001). Table 3 summarizes the differences in plaque changes between men and women. Total PAV increased 0.42 %/ per lesion/ per year and 0.34 %/ per lesion/ per year, in men and women respectively, no difference in the progression was observed (β -0.1 ± 0.1 (95% CI -0.2 to 0.1) % per year; p=0.320). Similarly, no sex differences in compositional changes

were observed, although women had less fibro-fatty PAV per-lesion compared to men during follow-up (β -1.3 ± 0.4 (95% CI -2.0 to -0.6) %; p<0.001), despite no difference in the rate of plaque progression compared to men (p=0.416) (Figure 2). Examples of quantitative coronary plaque analysis are demonstrated in Figure 3.

Table 2. Plaque characteristics at baseline

Variables	Total (n=590)	Men (n=434)	Women (n=156)	p-value
Lesion length, mm	13.3 (6.5-30.5)	13.4 (6.6-31.6)	13.1 (6.1-24.9)	0.196
Diameter stenosis, %	23.8 (14.5-32.8)	24.6 (14.9-33.5)	21.5 (13.3-30.8)	**0.044**
Remodeling index	0.85 ± 0.16	0.85 ± 0.16	0.85 ± 0.15	0.973
Total vessel volume, mm³	247.7 (116.2-528.1)	252.1 (123.5-550.0)	229.6 (101.3-426.4)	0.072
Total plaque volume, mm³	141.0 (67.5-302.8)	143.3 (70.6-322.3)	133.2 (60.0-239.4)	0.094
Calcified plaque volume, mm³	7.7 (1.7-23.0)	7.3 (1.7-22.4)	8.5 (1.8-23.3)	0.659
Non-calcified plaque volume, mm³	123.3 (57.3-269.7)	128.0 (58.7-284.1)	114.7 (52.4-205.7)	0.082
Fibrous plaque volume, mm³	53.6 (24.7-113.4)	54.3 (24.7-119.1)	50.9 (23.8-105.6)	0.383
Fibro-fatty plaque volume, mm³	27.8 (12.9-63.1)	29.3 (13.2-68.9)	24.5 (11.0-49.8)	**0.009**
Necrotic core plaque volume, mm³	34.4 (15.1-75.4)	37.3 (16.0-82.3)	30.2 (12.5-62.8)	**0.032**
Total PAV, %	57.9 ± 7.8	57.7 ± 7.7	58.3 ± 7.9	0.453
Calcified PAV, %	3.4 (0.8-7.7)	3.2 (0.8-7.5)	4.1 (1.4-8.3)	0.062
Non-calcified PAV, %	50.6 ± 8.6	50.8 ± 9.0	50.0 ± 7.4	0.304
Fibrous PAV, %	23.0 ± 8.1	22.7 ± 8.1	23.8 ± 8.2	0.167
Fibro-fatty PAV, %	12.0 ± 3.4	12.4 ± 3.5	10.9 ± 2.8	**<0.001**
Necrotic core PAV, %	15.6 ± 6.6	15.7 ± 6.5	15.3 ± 6.9	0.492

Bold indicates statistical significance of p-value <0.05
Values are presented as mean ± standard deviation or median (interquartile range).
PAV = percentage atheroma volume.

Table 3. Plaque morphological and compositional changes on a per-lesion analysis shown for women compared to men

	Total (n=590) β ± SE (95% CI)	p-value
Lesion length, mm - Between group comparison - Interaction	-4.4 ± 2.8 (-9.9 to 1.1) -0.0 ± 0.0 (-0.0 to 0.0)	0.116 0.744
Diameter stenosis, % - Between group comparison - Interaction	-0.0 ± 0.0 (-0.1 to 0.0) 0.0 ± 0.0 (-0.0 to 0.0)	0.061 0.981
Remodeling Index - Between group comparison - Interaction	0.0 ± 0.0 (-0.1 to 0.0) -0.0 ± 0.0 (-0.0 to 0.0)	0.758 0.121
Total PAV, % - Between group comparison - Interaction	0.6 ± 1.0 (-1.4 to 2.6) -0.1 ± 0.1 (-0.2 to 0.1)	0.551 0.320
Calcified PAV, % - Between group comparison - Interaction	0.6 ± 0.7 (-0.8 to 2.1) -0.1 ± 0.1 (-0.3 to 0.0)	0.391 0.126
Non-calcified PAV, % - Between group comparison - Interaction	-0.6 ± 1.0 (-2.5 to 1.2) -0.0 ± 0.1 (-0.2 to 0.2)	0.500 0.811
Fibrous PAV, % - Between group comparison - Interaction	1.0 ± 0.9 (-0.8 to 2.9) -0.1 ± 0.1 (-0.3 to 0.1)	0.270 0.559
Fibro-fatty PAV, % - Between group comparison - Interaction	-1.3 ± 0.4 (-2.0 to -0.6) 0.0 ± 0.0 (-0.1 to 0.1)	**<0.001** 0.416
Necrotic core PAV, % - Between group comparison - Interaction	-0.3 ± 0.7 (-1.7 to 1.1) -0.0 ± 0.1 (-0.2 to 0.2)	0.704 0.996

Bold indicates statistical significance of p-value <0.05
Values are presented as estimates (β) ± standard error (SE) (95% confidence interval)
CI = confidence interval; PAV = percentage atheroma volume

Fig. 2 Plaque changes on a per-lesion analysis shown for women and men

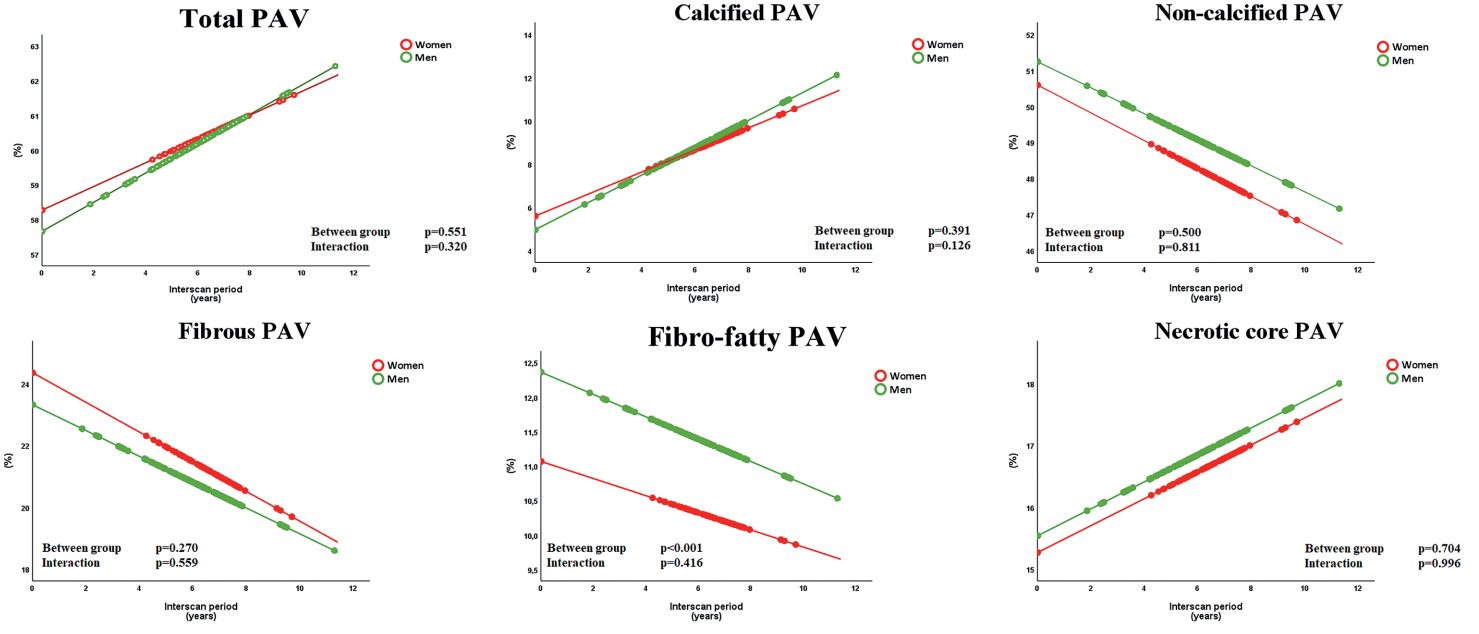

The line graphs represent the estimated average trend from baseline to 12 years for both groups based on a linear mixed modelling, with tests for the systematic between-group differences as well as for differences in trend. Circles represent the estimated mean percentage at the time point the follow-up scan was performed. PAV = percentage atheroma volume

Fig. 3 Quantitative assessment of coronary plaques in a male and female patient at baseline and follow-up.

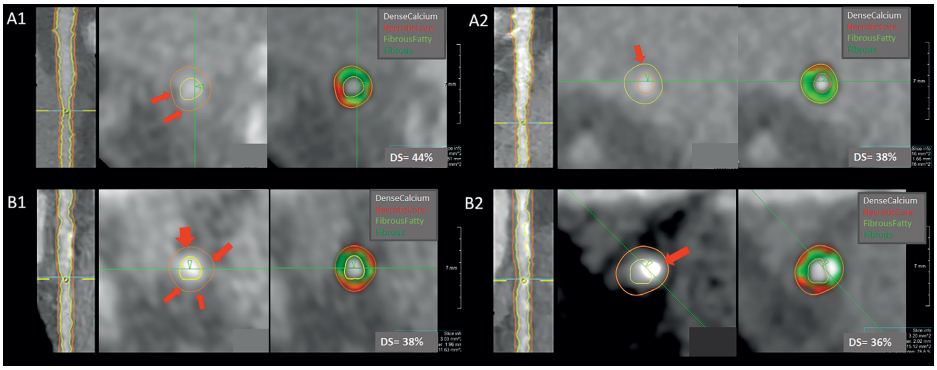

Panel A represents quantitative coronary plaque analysis of a 62-year-old male patient of the mid-left anterior descending artery at baseline (A1) and after 5.4 years follow-up (A2). During follow-up reduction of necrotic core and an increase in fibrous and fibrous fatty can be observed. Panel B represents quantitative coronary plaque analysis of a 58-year-old female patient of the proximal circumflex artery at baseline (B1) and after 5.9 years follow-up (B2). A reduction of necrotic core and the formation of dense calcium can be observed during follow-up. DS = diameter stenosis

Sex differences and the role of menopause on plaque progression

Table 4 summarizes the differences in plaque progression between men and women stratified according to age (<55 vs ≥55 years). Women had less fibro-fatty PAV in both age groups (<55 vs ≥55 years) compared to men ($p<0.05$). Women younger than 55 years showed more regression of fibrous PAV (β -0.8 ± 0.3 (95% CI -1.3 to -0.3) % per year; $p=0.002$) and non-calcified PAV (β -0.7 ± 0.3 (95% CI -1.4 to -0.1) % per year; $p=0.027$), compared to men. These differences were absent in the age group ≥ 55 years old (Figure 4).

Table 4. Plaque morphological and compositional changes on a per-lesion analysis shown for women compared to men stratified according to <55 or ≥55 years of age

	<55 years (n=112) β ± SE (95% CI)	p-value	≥ 55 years (n=478) β ± SE (95% CI)	p-value
Lesion length, mm				
Between group comparison	-9.0 ± 9.2 (-27.5 to 9.4)	0.329	-4.2 ± 2.9 (-10.1 to 1.6)	0.151
Interaction	0.0 ± 0.1 (-0.1 to 0.1)	0.871	-0.0 ± 0.0 (-0.1 to 0.0)	0.580
Diameter stenosis, %				
Between group comparison	-0.0 ± 0.0 (-0.1 to 0.1)	0.659	-0.0 ± 0.0 (-0.1 to 0.0)	**0.031**
Interaction	0.0 ± 0.0 (-0.0 to 0.0)	0.965	0.0 ± 0.0 (-0.0 to 0.0)	0.823
Positive remodeling				
Between group comparison	-0.0 ± 0.1 (-0.1 to 0.1)	0.649	0.0 ± 0.0 (-0.0 to 0.0)	0.563
Interaction	-0.0 ± 0.0 (-0.0 to 0.0)	0.487	-0.0 ± 0.0 (-0.0 to 0.0)	0.125
Total PAV, %				
Between group comparison	1.5 ± 2.9 (-4.3 to 7.3)	0.600	0.1 ± 1.1 (-2.1 to 2.3)	0.919
Interaction	-0.1 ± 0.2 (-0.6 to 0.3)	0.583	-0.1 ± 0.1 (-0.2 to 0.1)	0.329
Calcified PAV, %				
Between group comparison	-0.5 ± 1.4 (-3.3 to 2.4)	0.750	0.3 ± 0.8 (-1.3 to 1.9)	0.733
Interaction	-0.0 ± 0.2 (-0.4 to 0.4)	0.987	-0.1 ± 0.1 (-0.3 to 0.0)	0.130
Non-calcified PAV, %				
Between group comparison	-1.3 ± 2.6 (-6.6 to 4.0)	0.632	-0.5 ± 1.0 (-2.5 to 1.6)	0.652
Interaction	-0.7 ± 0.3 (-1.4 to -0.1)	**0.027**	0.0 ± 0.1 (-0.2 to 0.2)	0.881
Fibrous PAV, %				
Between group comparison	0.1 ± 2.8 (-5.4 to 5.7)	0.968	0.7 ± 1.0 (-1.2 to 2.7)	0.449
Interaction	-0.8 ± 0.3 (-1.3 to -0.3)	**0.002**	0.0 ± 0.1 (-0.2 to 0.2)	0.923
Fibro-fatty PAV, %				
Between group comparison	-2.4 ± 1.0 (-4.4 to -0.4)	**0.020**	-1.0 ± 0.4 (-1.8 to -0.3)	**0.010**
Interaction	-0.1 ± 0.2 (-0.4 to 0.2)	0.676	0.0 ± 0.0 (-0.1 to 0.1)	0.476
Necrotic core PAV, %				
Between group comparison	0.7 ± 2.0 (-3.3 to 4.8)	0.725	-0.0 ± 0.8 (-1.5 to 1.4)	0.965
Interaction	0.1 ± 0.2 (-0.3 to 0.6)	0.590	-0.0 ± 0.1 (-0.2 to 0.2)	0.744

Bold indicates statistical significance of p-value <0.05
Values are presented as estimates (β) ± standard error (SE) (95% confidence interval)
CI = confidence interval; PAV = percentage atheroma volume

Fig. 4 Plaque changes on a per-lesion analysis shown for women and men stratified according to the age group (<55 vs ≥55 years old)

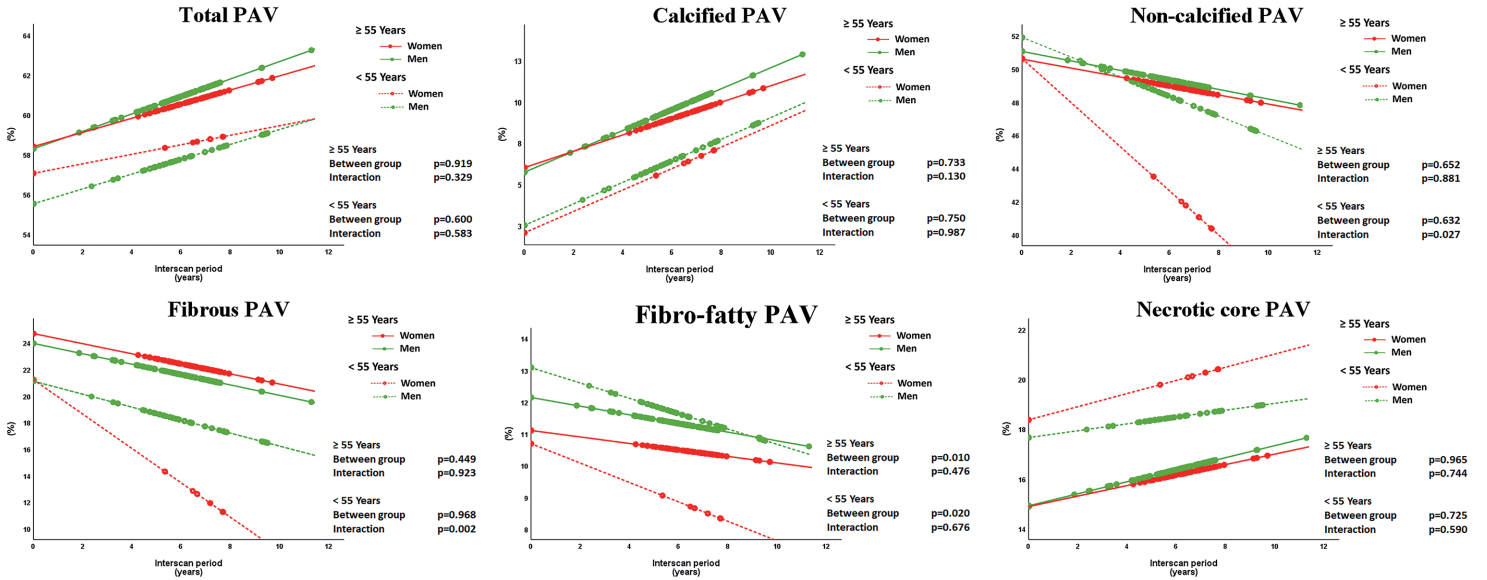

The line graphs represent the estimated average trend from baseline to 12 years for both groups based on a linear mixed modelling, with tests for the systematic between-group differences as well as for differences in trend. Circles represent the estimated mean percentage at the time point the follow-up scan was performed. PAV = percentage atheroma volum

DISCUSSION

In this prospective and multicenter study of serial coronary CTA we demonstrated that fibro-fatty PAV was higher in men compared to women at any age. During long-term follow-up no sex differences were detected in the change of total or compositional PAV on a per-lesion analysis after correction for multiple cardiovascular risk factors. However, when stratifying patients according to age groups (< 55 vs ≥ 55 years), coronary plaques in women younger than 55 years demonstrated more pronounced reduction of fibrous and non-calcified PAV compared to age-matched men. These results provide further insight in the understanding of the role of sex on long-term evolution of plaque morphology in stable CAD.

Similar to previous studies, we found that women had fewer lesions compared to men.[8,15] However, the total PAV per-lesion at baseline was comparable for men and women, which was also demonstrated in several other studies using IVUS.[11,14,15,31] In a sub analysis of the PROSPECT (Providing Regional Observations to Study Predictors of Events in the Coronary Tree) trial, women had fewer lesions and fewer diseased vessels than men, yet comparable plaque burden on a per-lesion analysis. More importantly, we did not find sex differences in the progression of total PAV during long-term follow-up. Few studies have investigated the influence of sex on quantitatively assessed plaque progression. In a population of 727 men and 251 women, Nicholls et al. also demonstrated no sex differences in the progression of total PAV using IVUS during a follow-up of 18-24 months.[12] Plaque compositional differences between men and women were first reported from limited postmortem studies in patients with advanced CAD and demonstrated coronary plaques in women, especially young women, contained less dense fibrous tissue compared to men.[7,8] More recently, IVUS-VH studies in patients with ACS demonstrated women tend to have lower fibrous tissue compared to men.[14,15] This is in agreement with our findings of a greater reduction of fibrous PAV in women younger than 55 years compared to age-matched men. Absolute values of fibro-fatty PAV were higher in men compared to women in both age groups, and at both CTA scan time points, as previously described[15] but its change in time did not differ between men and women. Non-calcified PAV regressed more in women younger than 55 years than in younger men, without any difference in subjects of 55 years or older. Given the known association between non-calcified

plaques with ischemia and ACS, these findings might partially explain the lower risk of symptomatic CAD in young women.[32-34]

Cardiovascular diseases are increased in women after menopause and the loss of protective female sex hormones has been suggested to play an important role.[35] Sex hormones demonstrate a wide range of effects on endothelial cells, vascular tone, lipids, coagulation and cardiomyocytes.[35] Consequently, several large randomized trials were conducted to investigate hormone replacement therapy (HRT) following menopause for reducing risk of cardiovascular disease. Although the Women's Health Initiative trials demonstrated no benefit of HRT initiated late after menopause on cardiovascular events,[36,37] other trials demonstrated that timely starting of HRT was associated with lower progression of atherosclerosis, but did not find evidence for an effect on coronary atherosclerosis progression.[38-41] Our findings of a similar progression of total PAV between men and women in both age groups, but differences in compositional changes between men and women younger than 55 years but not in those of 55 years or older is a new insight. Although previous trials have not demonstrate an effect of HRT on total coronary atherosclerosis changes, our findings suggest coronary plaques should be evaluated for compositional changes following HRT. HRT might potentially positively influence plaque compositional changes.

Clinical implications

The higher regression of fibrous and non-calcified PAV in women compared to men younger than 55 years old is an clinically important finding. Non-calcified plaques are associated with ischemia and ACS. [28-30] The absence of this difference in the, likely post-menopausal, women of 55 years or older hints to a slowing of the regression of non-calcified PAV to match that of the men and thereby increasing the risk for symptomatic CAD. Several strategies could be considered for this increased risk. Monitoring and treatment of cardiovascular risk factors of women around the age of menopause could be employed. Coronary CTA with quantitative plaque assessment might provide additional information on risk for future symptomatic CAD which could prompt early treatment of cardiovascular risk factors. Moreover, HRT might potentially positively influence plaque compositional changes and should be investigated.

Study limitations

Similar to other trials, women were underrepresented in our study. We used 55 years as a proxy for menopause, since menopause status was unavailable from clinical records. Although, the mean age of menopause has been demonstrated to be lower than 55 years, we cannot exclude the fact that premenopausal subjects might have been included in the ≥55 years age group.[42] Furthermore, information on HRT or sex hormone levels, which might have added relevant information, was also unavailable. A relative limited number of patients were included in this study and the sub analysis of sex differences in the different age groups should be interpreted with caution. As coronary CTA scanners from different vendors were used, a predefined standard operating procedure was applied to minimize variances among centers and quantitative analysis was performed in the core lab exclusively on visually recognized plaques: however, although careful visual examination was performed in the whole coronary tree, some plaques might have been unrecognized.

CONCLUSIONS

In a low-to-intermediate risk population of stable CAD with serial CTA scan during a follow-up of 6.2 ± 1.4 years women younger than 55 years demonstrated, after correction for several cardiovascular risk factors, a more pronounced reduction of fibrous and non-calcified PAV compared to age-matched men. No differences in the change of total or compositional PAV were observed between women and men of 55 years or older. Finally, the absolute value of fibro-fatty PAV was consistently higher in men than in women at any age.

REFERENCES

1. Anand SS, Islam S, Rosengren A, Franzosi MG, Steyn K, Yusufali AH, et al. Risk factors for myocardial infarction in women and men: insights from the INTERHEART study. Eur Heart J 2008;29:932-940.
2. Shaw LJ, Bairey Merz CN, Pepine CJ, Reis SE, Bittner V, Kelsey SF, et al. Insights from the NHLBI-Sponsored Women's Ischemia Syndrome Evaluation (WISE) Study: Part I: gender differences in traditional and novel risk factors, symptom evaluation, and gender-optimized diagnostic strategies. J Am Coll Cardiol 2006;47:S4-s20.
3. Sedlak TL, Lee M, Izadnegahdar M, Merz CN, Gao M, Humphries KH. Sex differences in clinical outcomes in patients with stable angina and no obstructive coronary artery disease. Am Heart J 2013;166:38-44.
4. Vaccarino V, Parsons L, Every NR, Barron HV, Krumholz HM. Sex-based differences in early mortality after myocardial infarction. National Registry of Myocardial Infarction 2 Participants. N Engl J Med 1999;341:217-225.
5. Lawesson SS, Stenestrand U, Lagerqvist B, Wallentin L, Swahn E. Gender perspective on risk factors, coronary lesions and long-term outcome in young patients with ST-elevation myocardial infarction. Heart 2010;96:453-459.
6. Virmani R, Burke AP, Farb A, Kolodgie FD. Pathology of the vulnerable plaque. J Am Coll Cardiol 2006;47:C13-18.
7. Dollar AL, Kragel AH, Fernicola DJ, Waclawiw MA, Roberts WC. Composition of atherosclerotic plaques in coronary arteries in women less than 40 years of age with fatal coronary artery disease and implications for plaque reversibility. Am J Cardiol 1991;67:1223-1227.
8. Mautner SL, Lin F, Mautner GC, Roberts WC. Comparison in women versus men of composition of atherosclerotic plaques in native coronary arteries and in saphenous veins used as aortocoronary conduits. J Am Coll Cardiol 1993;21:1312-1318.
9. Farb A, Burke AP, Tang AL, Liang Y, Mannan P, Smialek J, et al. Coronary Plaque Erosion Without Rupture Into a Lipid Core. Circulation 1996;93:1354-1363.
10. Burke AP, Farb A, Malcom GT, Liang Y-h, Smialek J, Virmani R. Effect of Risk Factors on the Mechanism of Acute Thrombosis and Sudden Coronary Death in Women. Circulation 1998;97:2110-2116.
11. Kornowski R, Lansky AJ, Mintz GS, Kent KM, Pichard AD, Satler LF, et al. Comparison of men versus women in cross-sectional area luminal narrowing, quantity of plaque, presence of calcium in plaque, and lumen location in coronary arteries by intravascular ultrasound in patients with stable angina pectoris. Am J Cardiol 1997;79:1601-1605.
12. Nicholls SJ, Wolski K, Sipahi I, Schoenhagen P, Crowe T, Kapadia SR, et al. Rate of progression of coronary atherosclerotic plaque in women. J Am Coll Cardiol 2007;49:1546-1551.
13. Qian J, Maehara A, Mintz GS, Margolis MP, Lerman A, Rogers J, et al. Impact of gender and age on in vivo virtual histology-intravascular ultrasound imaging plaque characterization (from the global Virtual Histology Intravascular Ultrasound [VH-IVUS] registry). Am J Cardiol 2009;103:1210-1214.
14. Hong YJ, Jeong MH, Choi YH, Ma EH, Cho SH, Ko JS, et al. Gender differences in coronary plaque components in patients with acute coronary syndrome: virtual histology-intravascular ultrasound analysis. J Cardiol 2010;56:211-219.

15. Lansky AJ, Ng VG, Maehara A, Weisz G, Lerman A, Mintz GS, et al. Gender and the extent of coronary atherosclerosis, plaque composition, and clinical outcomes in acute coronary syndromes. J Am Coll Cardiol Img 2012;5:S62-72.

16. Stegman B, Shao M, Nicholls SJ, Elshazly M, Cho L, King P, et al. Coronary atheroma progression rates in men and women following high-intensity statin therapy: A pooled analysis of REVERSAL, ASTEROID and SATURN. Atherosclerosis 2016;254:78-84.

17. Ten Haaf ME, Rijndertse M, Cheng JM, de Boer SP, Garcia-Garcia HM, van Geuns RM, et al. Sex differences in plaque characteristics by intravascular imaging in patients with coronary artery disease. EuroIntervention 2017;13:320-328.

18. Chia S, Christopher Raffel O, Takano M, Tearney GJ, Bouma BE, Jang IK. In-vivo comparison of coronary plaque characteristics using optical coherence tomography in women vs. men with acute coronary syndrome. Coron Artery Dis 2007;18:423-427.

19. Guagliumi G, Capodanno D, Saia F, Musumeci G, Tarantini G, Garbo R, et al. Mechanisms of atherothrombosis and vascular response to primary percutaneous coronary intervention in women versus men with acute myocardial infarction: results of the OCTAVIA study. J Am Coll Cardiol Interv 2014;7:958-968.

20. Kataoka Y, Puri R, Hammadah M, Duggal B, Uno K, Kapadia SR, et al. Sex Differences in Nonculprit Coronary Plaque Microstructures on Frequency-Domain Optical Coherence Tomography in Acute Coronary Syndromes and Stable Coronary Artery Disease. Circ Cardiovasc Imaging 2016;9.

21. Mariani L, Burzotta F, Aurigemma C, Romano A, Niccoli G, Leone AM, et al. Frequency-domain optical coherence tomography plaque morphology in stable coronary artery disease: sex differences. Coron Artery Dis 2017;28:472-477.

22. Tian J, Wang X, Tian J, Yu B. Gender differences in plaque characteristics of nonculprit lesions in patients with coronary artery disease. BMC Cardiovasc Disord 2019;19:45.

23. de Graaf MA, Broersen A, Kitslaar PH, Roos CJ, Dijkstra J, Lelieveldt BP, et al. Automatic quantification and characterization of coronary atherosclerosis with computed tomography coronary angiography: cross-correlation with intravascular ultrasound virtual histology. Int J Cardiovasc Imaging 2013;29:1177-1190.

24. Sakellarios A, Siogkas P, Georga E, Tachos N, Kigka V, Tsompou P, et al. A Clinical Decision Support Platform for the Risk Stratification, Diagnosis, and Prediction of Coronary Artery Disease Evolution. Conf Proc IEEE Eng Med Biol Soc 2018;2018:4556-4559.

25. Smit JM, van Rosendael AR, El Mahdiui M, Neglia D, Knuuti J, Saraste A, et al. Impact of Clinical Characteristics and Statins on Coronary Plaque Progression by Serial Computed Tomography Angiography. Circ Cardiovasc Imaging 2020;13:e009750.

26. Diamond GA, Forrester JS. Analysis of probability as an aid in the clinical diagnosis of coronary-artery disease. N Engl J Med 1979;300:1350-1358.

27. Grundy SM, Stone NJ, Bailey AL, Beam C, Birtcher KK, Blumenthal RS, et al. 2018 AHA/ACC/AACVPR/AAPA/ABC/ACPM/ADA/AGS/APhA/ASPC/NLA/PCNA Guideline on the Management of Blood Cholesterol: Executive Summary: A Report of the American College of Cardiology/American Heart Association Task Force on Clinical Practice Guidelines. Circulation 2019;139:e1046-e1081.

28. Boogers MJ, Broersen A, van Velzen JE, de Graaf FR, El-Naggar HM, Kitslaar PH, et al. Automated quantification of coronary plaque with computed tomography: comparison with intravascular ultrasound using a dedicated registration algorithm for fusion-based quantification. Eur Heart J 2012;33:1007-1016.

29. Budoff MJ, Ellenberg SS, Lewis CE, Mohler ER, 3rd, Wenger NK, Bhasin S, et al. Testosterone Treatment and Coronary Artery Plaque Volume in Older Men With Low Testosterone. JAMA 2017;317:708-716.

30. de Knegt MC, Haugen M, Linde JJ, Kühl JT, Nordestgaard BG, Køber LV, et al. Reproducibility of quantitative coronary computed tomography angiography in asymptomatic individuals and patients with acute chest pain. PloS one 2018;13:e0207980.

31. Bharadwaj AS, Vengrenyuk Y, Yoshimura T, Baber U, Hasan C, Narula J, et al. Multimodality Intravascular Imaging to Evaluate Sex Differences in Plaque Morphology in Stable CAD. J Am Coll Cardiol Img 2016;9:400-407.

32. Versteylen MO, Kietselaer BL, Dagnelie PC, Joosen IA, Dedic A, Raaijmakers RH, et al. Additive value of semiautomated quantification of coronary artery disease using cardiac computed tomographic angiography to predict future acute coronary syndrome. J Am Coll Cardiol 2013;61:2296-2305.

33. Driessen RS, Stuijfzand WJ, Raijmakers PG, Danad I, Min JK, Leipsic JA, et al. Effect of Plaque Burden and Morphology on Myocardial Blood Flow and Fractional Flow Reserve. J Am Coll Cardiol 2018;71:499-509.

34. Chang HJ, Lin FY, Lee SE, Andreini D, Bax J, Cademartiri F, et al. Coronary Atherosclerotic Precursors of Acute Coronary Syndromes. J Am Coll Cardiol 2018;71:2511-2522.

35. Mendelsohn ME, Karas RH. Molecular and cellular basis of cardiovascular gender differences. Science 2005;308:1583-1587.

36. Rossouw JE, Anderson GL, Prentice RL, LaCroix AZ, Kooperberg C, Stefanick ML, et al. Risks and benefits of estrogen plus progestin in healthy postmenopausal women: principal results From the Women's Health Initiative randomized controlled trial. JAMA 2002;288:321-333.

37. Anderson GL, Limacher M, Assaf AR, Bassford T, Beresford SA, Black H, et al. Effects of conjugated equine estrogen in postmenopausal women with hysterectomy: the Women's Health Initiative randomized controlled trial. JAMA 2004;291:1701-1712.

38. Hodis HN, Mack WJ, Henderson VW, Shoupe D, Budoff MJ, Hwang-Levine J, et al. Vascular Effects of Early versus Late Postmenopausal Treatment with Estradiol. N Engl J Med 2016;374:1221-1231.

39. Herrington DM, Reboussin DM, Brosnihan KB, Sharp PC, Shumaker SA, Snyder TE, et al. Effects of estrogen replacement on the progression of coronary-artery atherosclerosis. N Engl J Med 2000;343:522-529.

40. Hodis HN, Mack WJ, Lobo RA, Shoupe D, Sevanian A, Mahrer PR, et al. Estrogen in the prevention of atherosclerosis. A randomized, double-blind, placebo-controlled trial. Ann Intern Med 2001;135:939-953.

41. Hodis HN, Mack WJ, Azen SP, Lobo RA, Shoupe D, Mahrer PR, et al. Hormone therapy and the progression of coronary-artery atherosclerosis in postmenopausal women. N Engl J Med 2003;349:535-545.

42. Variations in reproductive events across life: a pooled analysis of data from 505 147 women across 10 countries. Human reproduction 2019;34:881-893.

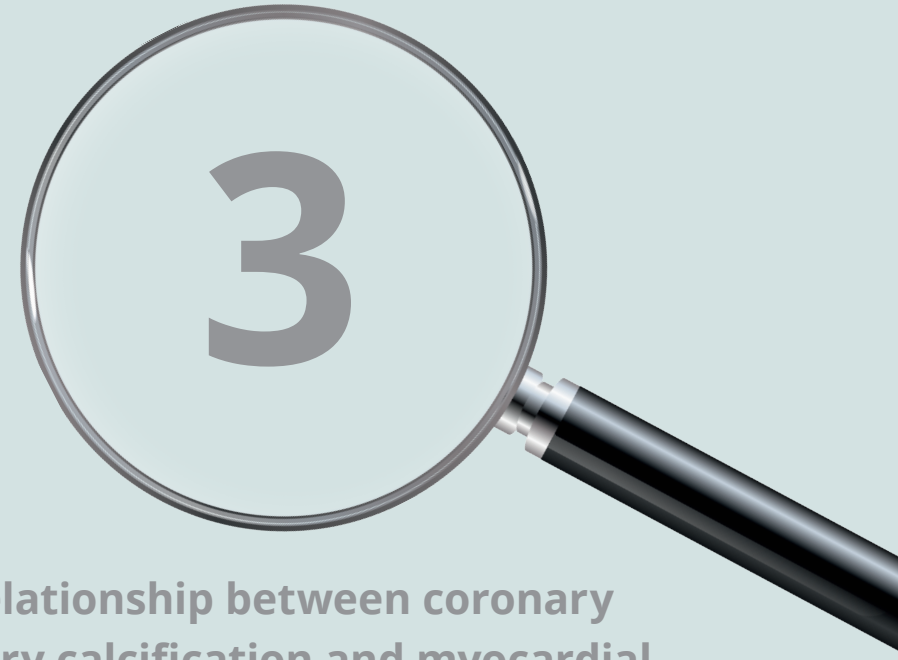

Relationship between coronary artery calcification and myocardial ischemia on computed tomography myocardial perfusion in patients with stable chest pain

El Mahdiui M, Smit JM, van Rosendael AR, Jukema JW, Bax JJ, Scholte AJHA.
J Nucl Cardiol. 2019 Sep 16.

ABSTRACT

Coronary artery calcium (CAC) score has shown to provide incremental prognostic information when added to the Framingham risk score. Although the relation between CAC and myocardial ischemia has been evaluated, there has been little evaluation of the relationship between CAC score and inducible myocardial ischemia on computed tomography myocardial perfusion (CTP). Patients who were referred with stable chest pain from the outpatient clinic and who underwent non-contrast computed tomography scan, coronary computed tomography angiography and adenosine stress CTP were included in this study. CAC score was subdivided in four groups (1-99; 100-399, 400-999 and ≥1000). Inducible myocardial ischemia was considered when reversible perfusion defects were observed in ≥1 segment. A total of 131 patients (age 62±9.4 years; 56% male) were included. The median CAC score was 241 (73-539). Forty-nine patients (37%) had evidence of inducible myocardial ischemia. The presence of inducible myocardial ischemia increased with increasing CAC score from 22% in the CAC score 1-99 subgroup, to 35%, 47% and 65% in the 100-399, 400-999 and ≥1000 CAC score subgroup, respectively. In multivariable analysis CAC score was the only determinant that significantly predicted the presence of inducible myocardial ischemia on CTP. In a population of symptomatic patients, the majority of patients with extensive calcification had evidence of inducible myocardial ischemia on CTP. CAC score was the only independent predictor of inducible myocardial ischemia on CTP.

INTRODUCTION

Coronary artery calcium (CAC) score measures calcification in the coronary arterial wall along the whole coronary artery tree and is a good indicator of the extent of coronary artery disease (CAD).[1,2] CAC score has shown excellent prognostic value in asymptomatic patients and has also shown its prognostic value in patients with stable chest pain.[3-14] The degree of CAC correlates well with inducible myocardial ischemia as assessed on single-photon emission computed tomography (SPECT) myocardial perfusion imaging (MPI).[15-17] Computed tomography (CT) myocardial perfusion (CTP) also provides functional information of coronary stenosis.[18] Previous studies have advocated not to perform coronary computed tomography angiography (CTA) when high CAC score is present but straight away CTP.[19,20] However, no studies have assessed the direct relation of CAC score and inducible myocardial ischemia on CTP.

Therefore, the aim of the current study is to examine the relation between CAC score and inducible myocardial ischemia on CTP in patients with stable chest pain.

METHODS

Study population

The study population consisted of patients with stable chest pain who were referred for cardiac CT from the outpatient clinic between March 2013 until June 2018. Patients with presence of calcium on non-contrast CT scan and subsequently underwent coronary CTA and adenosine stress CTP were included in this study. The updated Diamond-Forrester risk model was used to calculate the pre-test likelihood of CAD.[21] The imaging protocol design at our center has been reported before.[22,23] Patients with ≥1 uninterpretable myocardial segments on CTP were excluded from analysis. Patients with a history of myocardial infarction or revascularization were also excluded from analysis. Contraindications for cardiac CT were atrial fibrillation, renal insufficiency, second or third degree atrioventricular block, known allergy to iodine-containing contrast agents and pregnancy. Clinical data were prospectively entered into the departmental cardiology information system (EPD-Vision©, Leiden University Medical Center, The Netherlands). The Dutch Central Committee on Human-related Research allows the use of anonymous patient data

without previous approval of an institutional review board, provided that the data are acquired for routine patient care. All data used for this study were acquired for clinical purposes.

Cardiac CT acquisition

Non-contrast CT, coronary CTA and CTP were acquired on the same day, using a 320-row volumetric scanner (from 2013 until November 2015 Aquilion ONE, Canon Medical Systems, Otawara, Japan and from November 2015 the Aquilion ONE Genesis Edition, Canon Medical Systems, Otawara, Japan).

Patients were instructed not to consume caffeine products 24h before examination since CTP with adenosine might be performed. On the day of examination patients were evaluated 1h prior to CT acquisition, by measuring the patient's heart rate and blood pressure. Metoprolol, 25mg up until 150mg, was administrated orally if a patient's heart rate exceeded 60 beats per minutes (bpm) and no contraindications were present. Additional metoprolol could be administrated intravenously if the heart rate remained above 60 bpm during scout images.

First, a low dose non-contrast enhanced scan was performed to determine the CAC score. Nitro-glycerine (0.4mg) was sprayed sublingual prior to coronary CTA. The coronary CTA was performed with the following scan parameters: detector collimation of 320 x 0.5 mm, 350 ms gantry rotation time and temporal resolution of 175 ms for the Aquilion ONE and 275 ms gantry rotation time and temporal resolution of 137 ms for the Aquilion ONE Genesis Edition. Peak tube voltage was between 100 and 135 kV and tube current between 140 and 580mA, depending on body mass index. The contrast agent (Iomeron 400, Bracco, Milan, Italy) was injected in the antecubital vein. First, 50–90 mL (depending on patient weight) contrast agent (flow rate 5– 6 mL/s) was administrated, followed by 20 mL of a 1:1 mixture of contrast and saline and finally 25 mL of saline (flow rate 3 mL/s). Prospective ECG triggering was used to scan 70-80% of the RR-interval, in patients with heart rate >65 pm, 30-80% of the RR-interval was covered. Real-time bolus tracking was performed in the descending aorta, and coronary CTA was performed the next beat when the threshold of 300 Hounsfield units (HU) was reached.

Stress CTP was performed at least 20 minutes after coronary CTA to achieve adequate myocardial contrast wash-out. After 4 minutes of continuous adenosine

infusion (0.14 mg/kg/min) and continuous electrocardiogram and blood pressure monitoring, contrast agent was given. After reaching the target threshold of 300 HU in the descending aorta, CTP images were acquired the next heart beat scanning 80-99% of the RR-interval. The tube settings, injection protocol, and contrast agent were similar to the coronary CTA acquisition. If side-effects occurred during adenosine infusion, the administration was discontinued which resolved the side-effects rapidly and theophylline or atropine could be administrated if needed. The effective radiation dose was calculated by multiplying the dose-length-product by a conversion coefficient 0.014 mSv/(mGy x cm).[24]

Image reconstruction and analysis

Collected images were transferred to a workstation and analyzed using dedicated post-processing software (Vitrea FX 6.5; Vital Images, Minnetonka, Minnesota, USA). For the assessment of the CAC score, images with a 3 mm slice thickness were reconstructed from the non-contrast CT. To analyze the CAC score, pixels exceeding 130 HU were recognized and encircled in the course of a coronary artery and calculated according to the Agatston method.[1] CAC score was categorized into 4 subgroups, minimal to mild calcification (CAC score =1-99), moderate calcification (CAC score = 100-399), severe calcification (CAC score =400-999) and extensive calcification (CAC score ≥1000). For myocardial perfusion analysis, cardiac phases were reconstructed every 2% of the scanned interval. The phase with the best image quality was selected and interpreted with a narrow window width and level setting (W300/L150), according to the standard 17 myocardial segment model.[25] For per vessel analysis, individual myocardial segments were assigned to the 3 major coronary arteries using also the standard 17 myocardial segment model. After the initial analysis, observers were allowed to adjust the display settings. All images were analyzed and interpreted by two trained observers. For the present analysis CTA images were exclusively used for rest perfusion data and not for stenosis degree and/or plaques analysis. For stress data, CTP images during adenosine infusion were used. CTP images were arranged in the short axis, vertical long axis and horizontal long axis with a slice thickness of 3mm. Each segment was scored for perfusion defects and if present, other phases were checked to differentiate between real perfusion defects or artifacts.[26] When perfusion defects were observed in ≥1 segment, the CTP was considered abnormal. Summed difference score (SDS) was calculated by subtracting the summed rest score (SRS) from the summed stress score (SSS). To calculate the SRS and the SSS, all abnormal segments

were added from the rest data and stress data, respectively. Inducible myocardial ischemia was defined by a SDS ≥ 1.

Statistical analysis

Continuous variables are depicted as mean ± standard deviation when normally distributed and median with 25-75th percentile (interquartile range (IQR)) when non-normally distributed. Normally distributed variables were analyzed using the independent sample t-test and non-normally distributed variables using the Mann Whitney U-test or the Kruskal Wallis. Summed scores are depicted as mean and range. Categorical variables are depicted as percentages and numbers and analyzed using the χ^2 test. Correlation between CAC score as a continuous variable and extent of myocardial ischemia as assessed by SDS was tested with the Spearman correlation coefficient. Univariable and multivariable analysis were performed to evaluate the variables that were significantly associated with myocardial ischemia on CTP. Variables with a P-value <0.1 in univariable analysis and age and gender were included in the multivariable analysis. A P-value <0.05 was considered statistically significant. All statistical analyses were performed using SPSS version 23.0 (SPSS, Armonk, NY, USA).

RESULTS

Clinical characteristics

A total of 146 patients were identified. One patient was revascularized and was excluded from further analysis. We excluded 14 patients because of 1 or more uninterpretable myocardial segments on CTP, leaving 131 patients (age 62±9.4 years; 56% male) for analysis. Clinical characteristics are shown in Table 1. Prevalence of cardiovascular risk factors was high in the total population. There was no differences between both groups regarding the presence of cardiovascular risk factors, pre-test likelihood or medication use.

Table 1. Clinical characteristics divided according to the presence of inducible myocardial ischemia

	Total population (n= 131)	Myocardial ischemia (n= 49)	No myocardial ischemia (n=82)	P-value
Age (years)	62 ± 9.4	63 ± 7.9	61 ± 10.2	0.332
Male, n (%)	73 (56)	27 (55)	46 (56)	0.912
BMI (kg/m²)	27 ± 4	26 ± 4	27 ± 5	0.449
Cardiovascular risk factors				
Current smoking, n(%)	18 (14)	9 (18)	9 (11)	0.296
Diabetes, n(%)	32 (24)	11 (22)	21 (26)	0.684
Family history of CVD, n(%)	67 (51)	27 (55)	40 (49)	0.484
Hypercholesterolemia, n(%)	57 (44)	24 (49)	33 (40)	0.329
Hypertension, n(%)	80 (61)	35 (71)	45 (55)	0.060
Updated Diamond-Forrester risk score (%)				
Intermediate (20-80%) pre-test risk, n(%)	84 (64)	34 (69)	50 (61)	0.376
Medication				
Aspirin, n(%)	35 (27)	14 (29)	21 (26)	0.711
Thienopyridine, n(%)	3 (2)	2 (4)	1 (1)	0.556
OAC, n(%)	14 (11)	6 (12)	8 (10)	0.772
β-blocker, n(%)	70 (53)	30 (61)	40 (49)	0.167
Statin, n(%)	61 (47)	24 (49)	37 (45)	0.668
Diuretic, n(%)	26 (20)	10 (20)	16 (20)	0.901
ACE-I/ARB	55 (42)	23 (47)	32 (39)	0.374

Values are shown as n (%) or as mean ± standard deviation.
ACE-I: angiotensin-converting enzyme inhibitor, ARB: angiotensin receptor blocker, BMI: body mass index, CABG: coronary artery bypass grafting, CVD: cardiovascular disease, OAC: oral anticoagulants, PCI: percutaneous coronary intervention.

Coronary artery calcium score

The median CAC score of the study population was 241 (73-539). 41 (31%) patients had minimal to mild calcification (CAC score 1-99), 43 (33%) had moderate calcification (CAC score 100-399), 30 (23%) had severe calcification (CAC score 400-999), while 17 (13%) patients had extensive calcifications (CAC score ≥1000).

CT myocardial perfusion

A total of 55 (42%) patients had myocardial perfusion abnormalities at stress, 6 (5%) patients had only perfusion defects at rest and 49 (37%) patients had 1 or more segments with reversible defects on CTP, indicating inducible myocardial ischemia.

The mean (range) SRS, SSS and SDS were 0.22 (0-12), 2.26 (0-17) and 2.04 (0-16), respectively. The median effective radiation dose for CTP was 2.8 mSv (IQR: 1.8-4.4).

Figure 1. Relationship between percentage of patients with inducible myocardial ischemia and CAC score subgroups.

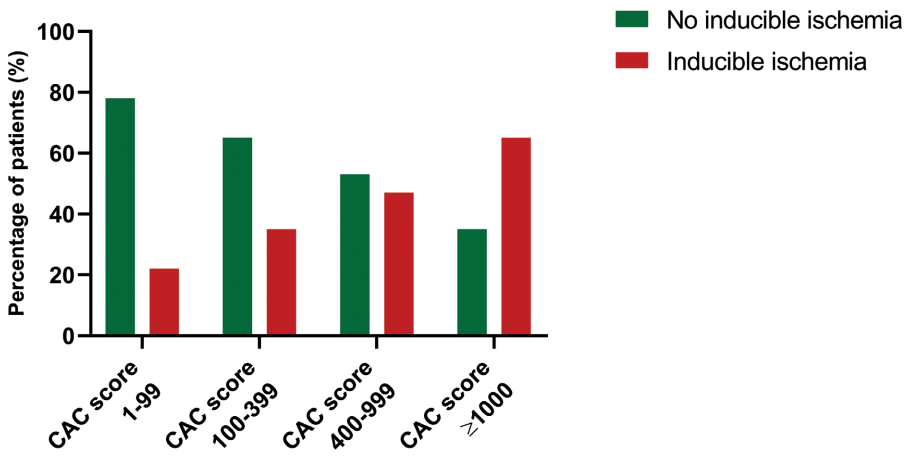

The percentage of subjects with inducible myocardial ischemia on CTP increased with increasing CAC score severity. CAC score = coronary artery calcium score.

Relation between CAC score and inducible myocardial ischemia on CTP

In the subgroups CAC score 1-99, CAC score 100-399, CAC score 400-999 and CAC score ≥1000 evidence of inducible myocardial ischemia on CTP was seen in 9 (22%), 15 (35%), 14 (47%) and 11 (65%), respectively. (Figure 1) The relation between CAC score and inducible myocardial ischemia per coronary artery is shown in Table 2. The LAD had higher CAC score independent of the presence of inducible myocardial ischemia or not. The extent of inducible myocardial ischemia (SDS) related to the predefined CAC score subgroups is shown in Figure 2 and the per vessel analysis is shown in Table 3. There was a moderate but significant positive correlation between CAC score and SDS (r= 0.368; P<0.0001).

Table 2. CAC score divided according to the presence of inducible myocardial ischemia

	Total population (n=131)	Myocardial ischemia (n=49)	No myocardial ischemia (n=82)	P-value
CAC score	241 (73-539)	438 (189-905)	167 (40-421)	0.001
Per vessel				
CAC score LAD	119 (30-280)	216 (94- 415)	84 (21-228)	0.001
CAC score RCA	24 (0-124)	71 (4-216)	11 (0-84)	0.005
CAC score LCX	9 (0-101)	34 (1-186)	6.5 (0-73)	0.019

Bold indicates statistical significance of p-value <0.05
Values are presented as median (25^{th}-75^{th} percentile).
CAC score = coronary artery calcium score, LAD = left anterior descending coronary artery, LCX = left circumflex coronary artery, RCA = right coronary artery.

Figure 2. Relationship between extent of inducible myocardial ischemia and CAC score subgroups.

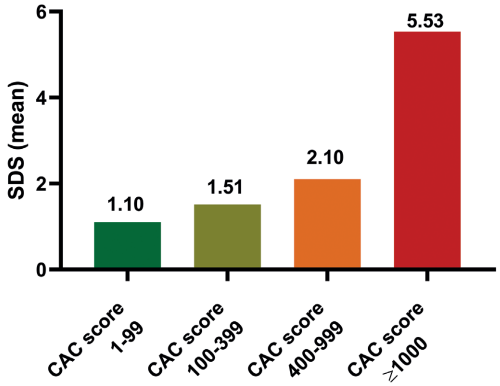

A significant difference was found for the extent of inducible myocardial ischemia between the CAC score subgroups (P=0.002). CAC score = coronary artery calcium score, SDS = summed difference score.

Table 3. SDS per coronary artery according to the CAC score subgroups

	CAC score 1-99 (n=41)	CAC score 100-399 (n=43)	CAC score 400-999 (n=30)	CAC score ≥1000 (n=17)	P-value
SDS LAD	0.63 (0-12)	0.67 (0-7)	1.07 (0-6)	3.82 (0-15)	**<0.001**
SDS RCA	0.10 (0-2)	0.42 (0-5)	0.43 (0-2)	1.18 (0-6)	**0.013**
SDS LCX	0.37 (0-6)	0.42 (0-4)	0.60 (0-6)	0.53 (0-4)	0.672

Bold indicates statistical significance of p-value <0.05
Values are presented as mean (minimum-maximum).
CAC score: coronary artery calcium score, LAD: left anterior descending coronary artery, LCX: left circumflex coronary artery, RCA: right coronary artery. SDS: summed difference score.

Uni- and multivariable analysis for inducible myocardial ischemia on CTP

The uni- and multivariable analysis for the presence of inducible myocardial ischemia on CTP are shown in Table 4. No cardiovascular risk factors were significantly correlated with inducible myocardial ischemia (Table 3). CAC score was significantly correlated with inducible myocardial ischemia on CTP in univariable analysis (OR: 1.001; 95% CI: 1.000-1.001; P= 0.013) and remained significant in the multivariable analysis (OR: 1.001 per 1 Agatston Unit; 95% CI: 1.000-1.001; P= 0.029).

Table 4. Uni- and multivariable analysis for inducible myocardial ischemia

	Univariable Odds ratio (95% CI)	p-value	Multivariable Odds ratio (95% CI)	P-value
Age	1.018 (0.980- 1.058)	0.361	1.000 (0.958- 1.045)	0.985
Male	0.960 (0.471- 1.958)	0.912	0.800 (0.350- 1.829)	0.597
BMI	0.968 (0.891- 1.052)	0.447		
Current smoking	1.825 (0.671- 4.967)	0.239		
Diabetes	0.841 (0.365- 1.937)	0.684		
Family history of CVD	1.289 (0.633- 2.622)	0.484		
Hypercholesterolemia	1.425 (0.699- 2.908)	0.330		
Hypertension	2.056 (0.964- 4.383)	0.062	1.626 (0.731- 3.618)	0.234
CAC score	1.001 (1.000-1.001)	**0.013**	1.001 (1.000-1.001)	**0.029**

Bold indicates statistical significance of p-value <0.05
CAC score = coronary artery calcium score, CVD = cardiovascular disease.

DISCUSSION

This study is the first to describe the relationship between CAC score and the presence of inducible myocardial ischemia on CTP. We observed a positive correlation between the burden of CAC and inducible myocardial ischemia on CTP. The frequency of inducible myocardial ischemia on CTP was three times higher for patients with extensive calcification compared to patients with mild calcifications. Moreover, the majority of symptomatic patients referred for CAC scoring with extensive calcifications had inducible myocardial ischemia on CTP.

CAC score

Several large retrospective and prospective studies have shown the prognostic value of CAC score measured by coronary CT in asymptomatic patients and its value to improve risk detection over traditional risk factors.[3-9] The prognostic value of CAC score has also been demonstrated in symptomatic patients.[10-14]

CAC score and CTP

Previous studies applying both CAC score and CTP have primarily focused on the incremental diagnostic value of CTP in the setting of decreased interpretability of coronary CTA in patients with high CAC score.[19,20] Sharma et al. investigated the diagnostic performance of CTP and coronary CTA in 381 patients with intermediate and high risk for CAD and patients with known CAD.[20] The population was divided in patients with a CAC score 1-399 and CAC score ≥400. In patients with an CAC score ≥400 combined use of coronary CTA and CTP showed superior diagnostic accuracy than coronary CTA or CTP alone, using stenosis ≥50% on invasive coronary angiography with corresponding stress perfusion defect on SPECT-MPI as a reference standard. Ladeiras-Lopes et al., reached the same conclusions in a cohort of 95 symptomatic patients with an intermediate pretest probability of CAD using invasive fractional flow reserve (FFR) as a gold standard.[19] The direct relationship between CAC score and the presence of inducible myocardial ischemia on CTP has not been investigated before.

CAC score and SPECT-MPI

The relationship between CAC and myocardial ischemia on SPECT-MPI has been investigated previously. He et al., showed in a population of 411 predominantly asymptomatic patients that CAC severity was the strongest predictor for the

presence of silent myocardial ischemia on SPECT-MPI.[15] Several studies have shown similar results with increasing rates of myocardial ischemia on SPECT-MPI and PET-MPI with increasing CAC score subgroup.[16,17] A meta-analysis from Bavishi et al., including 20 studies showed a wide range of prevalence of inducible myocardial ischemia on SPECT-MPI or PET-MPI, among the different studies but a consistent increase of inducible myocardial ischemia with increasing CAC score subgroup.[16] In a large a cohort of 4897 symptomatic patients with low-to-intermediate risk, Engbers et al. showed that CAC score was an independent predictor for abnormal SPECT-MPI.[17] The frequency of abnormal SPECT-MPI increased with higher CAC score, from 19% in patients with mild calcifications to 50% in patients with extensive calcifications, similar to the results in our study. Interestingly, Engbers et al. also showed that combined evaluation of SPECT-MPI and CAC score provided incremental prognostic information over the individual modalities.[17] This was also shown by Nappi et al. in a population of 156 patients.[27] Chang et al. reached the same conclusions in 1126 mostly asymptomatic subjects.[28] Moreover, in a study by Assante et al., the combined evaluation of CAC score and coronary vascular function as assessed by coronary flow reserve also provided incremental risk stratification for the prediction of adverse cardiac events.[29]

CAC score and other functional tests

The relation between CAC score and other functional tests has also been investigated. Ramakrishna et al., investigated the relationship between CAC score and exercise echocardiography in a population of 556 patients.[30] The correlation between CAC score and exercise wall motion score index (WMSI) was significant, but limited (r=0.17), underscoring the difference between anatomical and functional testing. Patients with both CAC score >100 and also exercise WMSI >1 were 4 times more likely to experience a myocardial infarction or die during a follow-up of 5 years compared to patients with a CAC score ≤100 and a normal exercise WMSI. Janssen et al., investigated the relation between CAC score and dobutamine cardiovascular magnetic resonance imaging (CMR).[31] They showed that in a population of 114 symptomatic patients a CAC score ≤100 had a negative and positive predictive value of 0.96 and 0.29, respectively, for predicting inducible myocardial ischemia during dobutamine CMR.

CTP has several benefits over SPECT-MPI and other stress testing modalities investigating myocardial ischemia. CTP allows for a fast and simultaneous

assessment of anatomical and functional parameters in one session. Furthermore, a recent meta-analysis by Takx et al., showed CTP to accurately rule out hemodynamic significant CAD using invasive FFR as a golden standard, whereas SPECT-MPI and echocardiography were less accurate.[32]

Limitations

This study has several limitations, inherent to its retrospective and single-center design. The exclusion of patients with uninterpretable CTP imaging might have introduced selection bias. We analyzed the CAC score using the Agatston method and did not incorporate the distribution of the calcifications in the coronary vessel. Although inducible myocardial ischemia has shown prognostic value, in our study we did not look at clinical endpoints.

CONCLUSIONS

In a population of symptomatic patients, the majority of patients with extensive calcification had evidence of inducible myocardial ischemia on CTP. CAC score was an independent predictor of inducible myocardial ischemia on CTP.

REFERENCES

1. Agatston AS, Janowitz WR, Hildner FJ, Zusmer NR, Viamonte M, Jr., Detrano R. Quantification of coronary artery calcium using ultrafast computed tomography. J Am Coll Cardiol 1990;15:827-832.
2. Sangiorgi G, Rumberger JA, Severson A, Edwards WD, Gregoire J, Fitzpatrick LA, et al. Arterial calcification and not lumen stenosis is highly correlated with atherosclerotic plaque burden in humans: a histologic study of 723 coronary artery segments using nondecalcifying methodology. J Am Coll Cardiol 1998;31:126-133.
3. Greenland P, LaBree L, Azen SP, Doherty TM, Detrano RC. Coronary artery calcium score combined with Framingham score for risk prediction in asymptomatic individuals. JAMA 2004;291:210-215.
4. Arad Y, Goodman KJ, Roth M, Newstein D, Guerci AD. Coronary calcification, coronary disease risk factors, C-reactive protein, and atherosclerotic cardiovascular disease events: the St. Francis Heart Study. J Am Coll Cardiol 2005;46:158-165.
5. Vliegenthart R, Oudkerk M, Hofman A, Oei HH, van Dijck W, van Rooij FJ, et al. Coronary calcification improves cardiovascular risk prediction in the elderly. Circulation 2005;112:572-577.
6. Budoff MJ, Shaw LJ, Liu ST, Weinstein SR, Mosler TP, Tseng PH, et al. Long-term prognosis associated with coronary calcification: observations from a registry of 25,253 patients. J Am Coll Cardiol 2007;49:1860-1870.
7. Detrano R, Guerci AD, Carr JJ, Bild DE, Burke G, Folsom AR, et al. Coronary calcium as a predictor of coronary events in four racial or ethnic groups. N Engl J Med 2008;358:1336-1345.
8. Elias-Smale SE, Proenca RV, Koller MT, Kavousi M, van Rooij FJ, Hunink MG, et al. Coronary calcium score improves classification of coronary heart disease risk in the elderly: the Rotterdam study. J Am Coll Cardiol 2010;56:1407-1414.
9. Geisel MH, Bauer M, Hennig F, Hoffmann B, Lehmann N, Mohlenkamp S, et al. Comparison of coronary artery calcification, carotid intima-media thickness and ankle-brachial index for predicting 10-year incident cardiovascular events in the general population. Eur Heart J 2017;38:1815-1822.
10. Detrano R, Hsiai T, Wang S, Puentes G, Fallavollita J, Shields P, et al. Prognostic value of coronary calcification and angiographic stenoses in patients undergoing coronary angiography. J Am Coll Cardiol 1996;27:285-290.
11. Keelan PC, Bielak LF, Ashai K, Jamjoum LS, Denktas AE, Rumberger JA, et al. Long-term prognostic value of coronary calcification detected by electron-beam computed tomography in patients undergoing coronary angiography. Circulation 2001;104:412-417.
12. Schmermund A, Stang A, Mohlenkamp S, Eggebrecht H, Baumgart D, Gilbert V, et al. Prognostic value of electron-beam computed tomography-derived coronary calcium scores compared with clinical parameters in patients evaluated for coronary artery disease. Prognostic value of EBCT in symptomatic patients. Z Kardiol 2004;93:696-705.
13. Sarwar A, Shaw LJ, Shapiro MD, Blankstein R, Hoffmann U, Cury RC, et al. Diagnostic and prognostic value of absence of coronary artery calcification. JACC Cardiovasc Imaging 2009;2:675-688.

14. Petretta M, Daniele S, Acampa W, Imbriaco M, Pellegrino T, Messalli G, et al. Prognostic value of coronary artery calcium score and coronary CT angiography in patients with intermediate risk of coronary artery disease. Int J Cardiovasc Imaging 2012;28:1547-1556.

15. He ZX, Hedrick TD, Pratt CM, Verani MS, Aquino V, Roberts R, et al. Severity of coronary artery calcification by electron beam computed tomography predicts silent myocardial ischemia. Circulation 2000;101:244-251.

16. Bavishi C, Argulian E, Chatterjee S, Rozanski A. CACS and the Frequency of Stress-Induced Myocardial Ischemia During MPI: A Meta-Analysis. JACC Cardiovasc Imaging 2016;9:580-589.

17. Engbers EM, Timmer JR, Ottervanger JP, Mouden M, Knollema S, Jager PL. Prognostic Value of Coronary Artery Calcium Scoring in Addition to Single-Photon Emission Computed Tomographic Myocardial Perfusion Imaging in Symptomatic Patients. Circ Cardiovasc imaging 2016;9.

18. George RT, Mehra VC, Chen MY, Kitagawa K, Arbab-Zadeh A, Miller JM, et al. Myocardial CT perfusion imaging and SPECT for the diagnosis of coronary artery disease: a head-to-head comparison from the CORE320 multicenter diagnostic performance study. Radiology 2014;272:407-416.

19. Ladeiras-Lopes R, Bettencourt N, Ferreira N, Sampaio F, Pires-Morais G, Santos L, et al. CT myocardial perfusion and coronary CT angiography: Influence of coronary calcium on a stress-rest protocol. J Cardiovasc Comput Tomogr 2016;10:215-220.

20. Sharma RK, Arbab-Zadeh A, Kishi S, Chen MY, Magalhaes TA, George RT, et al. Incremental diagnostic accuracy of computed tomography myocardial perfusion imaging over coronary angiography stratified by pre-test probability of coronary artery disease and severity of coronary artery calcification: The CORE320 study. Int J Cardiol 2015;201:570-577.

21. Genders TSS, Steyerberg EW, Alkadhi H, Leschka S, Desbiolles L, Nieman K, et al. A clinical prediction rule for the diagnosis of coronary artery disease: validation, updating, and extension. Eur Heart J 2011;32:1316-1330.

22. van Rosendael AR, Kroft LJ, Broersen A, Dijkstra J, van den Hoogen IJ, van Zwet EW, et al. Relation between quantitative coronary CTA and myocardial ischemia by adenosine stress myocardial CT perfusion. J Nucl Cardiol 2017;24:1253-1262.

23. van Rosendael AR, de Graaf MA, Dimitriu-Leen AC, van Zwet EW, van den Hoogen IJ, Kharbanda RK, et al. The influence of clinical and acquisition parameters on the interpretability of adenosine stress myocardial computed tomography perfusion. Eur Heart J Cardiovasc Imaging 2017;18:203-211.

24. Hausleiter J, Meyer T, Hermann F, Hadamitzky M, Krebs M, Gerber TC, et al. Estimated radiation dose associated with cardiac CT angiography. JAMA 2009;301:500-507.

25. Cerqueira MD, Weissman NJ, Dilsizian V, Jacobs AK, Kaul S, Laskey WK, et al. Standardized myocardial segmentation and nomenclature for tomographic imaging of the heart. A statement for healthcare professionals from the Cardiac Imaging Committee of the Council on Clinical Cardiology of the American Heart Association. Circulation 2002;105:539-542.

26. Mehra VC, Valdiviezo C, Arbab-Zadeh A, Ko BS, Seneviratne SK, Cerci R, et al. A stepwise approach to the visual interpretation of CT-based myocardial perfusion. J Cardiovasc Comput Tomogr 2011;5:357-369.

27. Nappi C, Nicolai E, Daniele S, Acampa W, Gaudieri V, Assante R, et al. Long-term prognostic value of coronary artery calcium scanning, coronary computed tomographic angiography and stress myocardial perfusion imaging in patients with suspected coronary artery disease. J Nucl Cardiol 2018;25:833-841.

28. Chang SM, Nabi F, Xu J, Peterson LE, Achari A, Pratt CM, et al. The coronary artery calcium score and stress myocardial perfusion imaging provide independent and complementary prediction of cardiac risk. Journal of the American College of Cardiology 2009;54:1872-1882.

29. Assante R, Acampa W, Zampella E, Arumugam P, Nappi C, Gaudieri V, et al. Prognostic value of atherosclerotic burden and coronary vascular function in patients with suspected coronary artery disease. Eur J Nucl Med Mol Imaging 2017;44:2290-2298.

30. Ramakrishna G, Breen JF, Mulvagh SL, McCully RB, Pellikka PA. Relationship between coronary artery calcification detected by electron-beam computed tomography and abnormal stress echocardiography: association and prognostic implications. J Am Coll Cardiol 2006;48:2125-2131.

31. Janssen CH, Kuijpers D, Vliegenthart R, Overbosch J, van Dijkman PR, Zijlstra F, et al. Coronary artery calcification score by multislice computed tomography predicts the outcome of dobutamine cardiovascular magnetic resonance imaging. Eur Radiol 2005;15:1128-1134.

32. Takx RA, Blomberg BA, El Aidi H, Habets J, de Jong PA, Nagel E, et al. Diagnostic accuracy of stress myocardial perfusion imaging compared to invasive coronary angiography with fractional flow reserve meta-analysis. Circ Cardiovasc Imaging 2015;8.

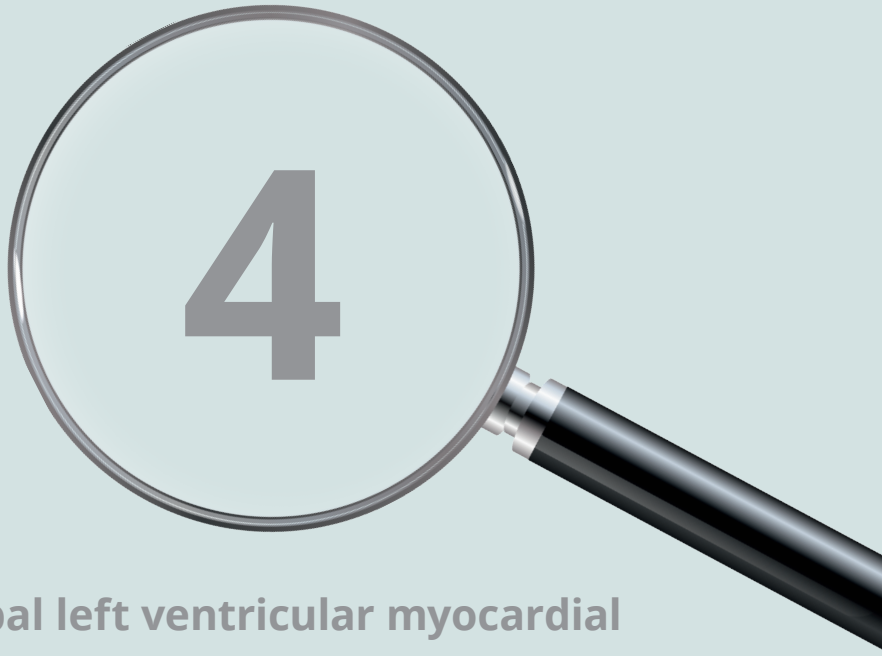

4

Global left ventricular myocardial work efficiency in healthy individuals and patients with cardiovascular disease

El Mahdiui M, van der Bijl P, Abou R, Ajmone Marsan N, Delgado V, Bax JJ.
J Am Soc Echocardiogr. 2019 Sep;32(9):1120-1127.

ABSTRACT

Global left ventricular (LV) myocardial work efficiency, the ratio of constructive to wasted work in all left ventricular segments, reflects the efficiency by which mechanical energy is expended during the cardiac cycle. Global LV myocardial work efficiency can be derived from LV pressure-strain loop analysis incorporating both non-invasively estimated blood pressure recordings and echocardiographic strain data. The aim of this study was to characterize global LV myocardial work efficiency in healthy individuals and patients with cardiovascular risk factors or overt cardiac disease. We retrospectively included healthy individuals without structural heart disease or cardiovascular (CV) risk factors were selected from an ongoing database of normal individuals, and matched for age and sex with: i) individuals without structural heart disease but with CV risk factors, ii) post-infarct patients without heart failure and iv) heart failure patients with reduced ejection fraction (HFrEF). Global LV myocardial work efficiency was estimated with a proprietary algorithm from speckle tracking strain analyses, as well as non-invasive blood pressure measurements. In total, 120 individuals (44% male, 53±13 years) were included (n=30 per group). In healthy individuals without structural heart disease or CV risk factors, global LV myocardial work efficiency was 96.0% (IQR 95.0-96.3). Myocardial efficiency of the LV did not differ significantly between individuals without structural heart disease and those with CV risk factors (96.0% vs. 96.0%; p=0.589). Global LV myocardial work efficiency however, was significantly decreased in post-infarct patients (96.0% vs. 93.0%, p<0.001) and those with HFrEF (96.0% vs. 69.0%; p<0.001). In conclusion, while global LV myocardial work efficiency was similar in normal individuals and those with CV risk factors, it was decreased in post-infarct and HFrEF patients. The global LV myocardial work efficiency values presented here show distinct patterns in different cardiac pathologies.

INTRODUCTION

Non-invasive myocardial work is a relatively new parameter for assessing left ventricular (LV) systolic function, derived from LV pressure-strain loop analysis incorporating both non-invasively estimated blood pressure recordings and echocardiographic strain data.[1] Russell et al. demonstrated that non-invasive LV pressure-strain loops corresponded well with invasively-measured LV pressure-strain loops,[1,2] and these results have been confirmed in subsequent studies.[3] Non-invasive myocardial work has been shown to be a strong predictor of response to cardiac resynchronization therapy (CRT)[4,5] and superior to LV ejection fraction (LVEF) and LV global longitudinal strain (LV GLS) in identifying patients with acute coronary syndromes.[6] Despite showing great clinical potential, there are few data on normal values of global LV myocardial work efficiency in different cardiac pathologies.
The aim of this study is to characterize global LV myocardial work efficiency in four groups: i) normal individuals without structural heart disease or cardiovascular (CV) risk factors, ii) individuals without structural heart disease but with CV risk factors, iii) post-infarct patients without heart failure and iv) heart failure patients with reduced ejection fraction (HFrEF).

METHODS

Study population

We retrospectively included healthy individuals without structural heart disease or CV risk factors selected from a database of normal individuals,[7] and matched for age and sex with: i) individuals without structural heart disease but with CV risk factors, ii) post-infarct patients without heart failure (from an ongoing registry of patients with ST-segment elevation myocardial infarction (STEMI), treated with primary percutaneous coronary intervention)[8] and iii) HFrEF (from an ongoing registry of cardiac resynchronization therapy recipients).[9] Heart failure etiology was considered ischemic in the presence of significant coronary artery disease and/or a history of prior myocardial infarction or revascularization. Demographics and clinical data were collected from the departmental cardiology information system (EPD-vision; Leiden University Medical Centre, Leiden, The Netherlands), as well as electronic medical records (HiX; ChipSoft, Amsterdam, The Netherlands). For retrospective analysis of clinically acquired data, the institutional review board

waived the need of written patient informed consent. All data used for this study were acquired for clinical purposes and handled anonymously.

Echocardiographic data acquisition

Transthoracic echocardiographic images were recorded using a Vivid 7 or E9 ultrasound system (General Electric Vingmed Ultrasound, Milwaukee, USA) with patients at rest, in the left lateral decubitus position. ECG-triggered echocardiographic data were acquired with 3.5 MHz or M5S transducers and digitally stored in cine-loop format for offline analysis with EchoPac (EchoPac 202, General Electric Vingmed Ultrasound, Milwaukee, USA).[10] LV end-diastolic and end-systolic volumes were measured in the apical 2- and 4-chamber views, and the LVEF calculated using the biplane Simpson's method.[10]

Quantification of global LV myocardial work efficiency

Global LV myocardial work efficiency was quantified using a novel, non-invasive method which employs echocardiographic strain data as well as brachial cuff blood pressure recordings.[1] This method has been validated in different patient subgroups.[1,2,4,6,11,12] Strain was measured using 2-dimensional speckle tracking echocardiography by manually tracing the LV endocardial border in the apical long-axis, 2- and 4-chamber views. A non-invasively estimated LV pressure-strain loop curve was then constructed using the strain and blood pressure data, and a normalized reference curve adjusted according to the duration of the different cardiac cycle phases (defined by the timing of aortic and mitral valve events).[1] LV myocardial work was subsequently computed segmentally by differentiation of the strain values over time, giving the segmental shortening rate, which was then multiplied by the instantaneous LV pressure. Instantaneous power (the result) was integrated over time to yield the segmental (as well as the global) LV myocardial work values as a function of time.

Constructive work was defined as work performed during segmental shortening in systole or during lengthening in isovolumic relaxation. Wasted work was then defined as work performed during segmental lengthening in systole or work performed during segmental shortening against a closed aortic valve in isovolumic relaxation. Global LV myocardial work efficiency was calculated as the sum of constructive work in all LV segments, divided by the sum of constructive and wasted work in all LV segments, expressed as a percentage (Figure 1).

Figure 1. Global LV myocardial work efficiency in a healthy individual (panel A), a patient with cardiovascular risk factors (panel B), a post-infarct patient (panel C) and a heart failure patient with reduced ejection fraction (panel D).

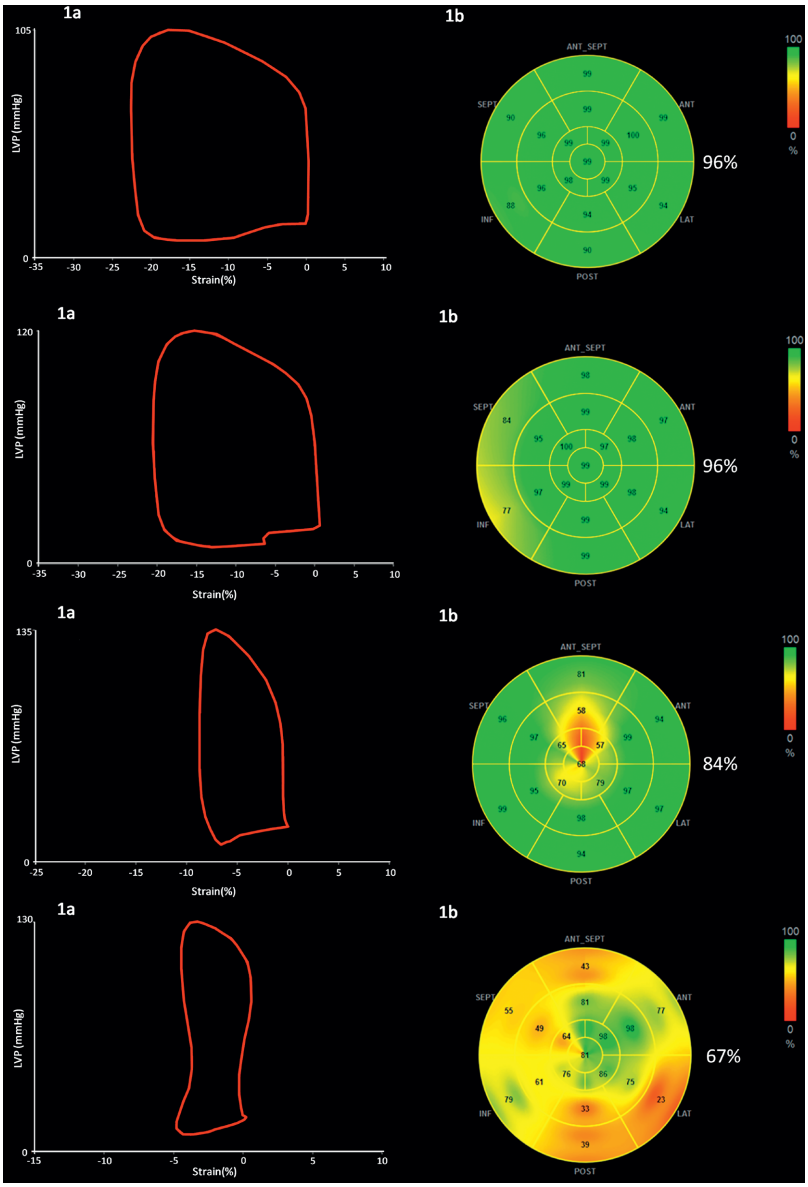

On the left, the pressure-strain loop (1a) is depicted and the global LV myocardial work efficiency presented as a parametric map (1b) is shown on the right. Note the progressive reduction in global LV myocardial work as the LV damage increases: from 96% in the healthy individual (panel A) to 67% in the patient with heart failure with reduced ejection fraction (panel D).
LVP: left ventricular pressure.

Statistical analysis

Categorical data are presented as frequencies and percentages. Continuous variables are reported as mean±standard deviation if normally distributed, and as median and interquartile range (IQR) if non-normally distributed. Categorical data were compared with the $\chi 2$ test, followed by post-hoc analysis of subgroups. Continuous data were compared using the Student's *t* test if normally distributed or the Mann-Whitney U test or the Kruskal-Wallis test if non-normally distributed. Pearson correlation was used to investigate the relationship between LVEF and global LV myocardial work efficiency. Twenty random individuals were selected for inter- and intra-observer agreements and analyzed using Bland-Altman plots and the intraclass correlation coefficient (ICC). Intra-observer measurements were performed after a 2-week interval. The second observer was blinded to the measurements of the first observer, as well as to all previous measurements, when performing the inter-observer assessments. A p-value <0.05 was considered statistically significant. All statistical analyses were performed using SPSS version 23.0 (SPSS, Armonk, NY, USA).

RESULTS

Clinical characteristics

A total of 120 individuals (44% male, age 53±13 years) were included. Clinical characteristics are shown in Table 1. The left anterior descending (LAD) was the culprit vessel in 20 (67%) post-infarct patients. The etiology of heart failure was non-ischemic in 17 (57%) patients.

Table 1. Clinical characteristics

	Normal (n=30)	With CV risk factors (n=30)	Post-infarct (n=30)	HFrEF (n=30)
Age (years)	56 (41-64)	54 (35-69)	55 (48-63)	54 (51-57)
Male, n (%)	13 (43)	13 (43)	13 (43)	14 (47)
BSA (m^2)	1.9 (1.8-2.0)	1.8 (1.7-2.1)	2.0 (1.8-2.1)	1.9 (1.7-2.1)
BMI (kg/m^2)	24.6 (21.9-26.9)	24.2 (21.5-26.7)	26.7 (24.7-29.5)*†	26.1 (22.7-28.8)
Systolic blood pressure (mmHg)	128 (110-139)	127 (110-141)	120 (110-135)	120 (107-129)
Diastolic blood pressure (mmHg)	75 (70-85)	78 (70-90)	73 (69-80)	72 (69-79)
Mean arterial pressure (mmHg)	93 (86-101)	95 (85-107)	90 (81-96)	88 (82-93)
CV risk factors				
Hypertension, n (%)	0 (0)	7 (23.3)*	18 (60.0)*†	12 (40.0)*
Hypercholesterolemia, n (%)	0 (0)	4 (13.3)	6 (20.0)	9 (30.0)*
Diabetes, n (%)	0 (0)	4 (13.3)	5 (16.7)	2 (6.7)
Current smoking, n (%)	0 (0)	7 (23.3)*	15 (50.0)*	14 (46.7)*
Family history of CVD, n (%)	0 (0)	20 (66.7)*#	9 (30.0)*	12 (40.0)*
Medication, n (%)				
Aspirin	1 (3.3)	2 (6.7)	28 (93.3)*†‡	10 (33.3)
Thienopyridine	0 (0)	0 (0)	26 (86.7)*†‡	1 (3.3)
β-blocker	0 (0)	2 (6.7)	28 (93.3)*†	26 (86.7)*†
Statin	0 (0)	3 (10.0)	30 (100.0)*†‡	17 (56.7)*†
Diuretic	0 (0)	3 (10.0)	9(30.0)*	25 (83.3)*†#
ACE-I/ARB	0 (0)	5 (16.7)	29 (96.7)*†	28 (93.3)*†

ACE-I: angiotensin-converting enzyme inhibitor, ARB: angiotensin receptor blocker, BMI: body mass index, BSA: body surface area, CV: cardiovascular, CVD: cardiovascular disease, HFrEF: heart failure with reduced ejection fraction. Data are presented as mean ± standard deviation if normally distributed or median (25^{th}-75^{th} percentile) if not normally distributed. * $p<0.05$ compared to normal individuals, † $p<0.05$ compared to individuals with CV risk, # $p<0.05$ compared to post-infarct patients, ‡ $p<0.05$ compared to HFrEF patients

Conventional echocardiographic parameters

Conventional echocardiographic findings are summarized in Table 2. Patients with HFrEF had larger cavity sizes and worse LVEF, compared to all other groups. In addition, the post-infarct patients had worse LVEF compared to the healthy individuals without CV risk factors and those with CV risk factors.

Table 2. Echocardiographic characteristics

	Normal (n=30)	With CV risk factors (n=30)	Post-infarct (n=30)	HFrEF (n=30)
Heart rate (bpm)	69 (61-76)	68 (63-75)	63 (57-70)	73 (62-85) ǂ
Left ventricular mass index (g/m²)	92 (72-112)	90 (74-99)	102 (87-122)	158 (139-191)*†ǂ
Interventricular septal thickness (mm)	10 (8-11)	10 (9-12)	12 (10-12)	10 (8-11)
Left ventricular posterior wall thickness (mm)	10 (9-12)	10 (8-11)	10 (9-12)	11 (10-12)
Left ventricular end-diastolic volume (ml)	109 (96-133)	112 (88-124)	112 (85-150)	234 (160-304)*†ǂ
Left ventricular end-systolic volume (ml)	44 (37-54)	42 (33-55)	56 (43-80)†	186 (120-250)*†ǂ
Left ventricular ejection fraction (%)	58 (56-63)	61 (58-65)	50 (45-53)*†	24 (17-30)*†ǂ
Left ventricular global longitudinal strain (%)	-19.3 (-20.5 to -18.3)	-18.8 (-20.4 to -17.0)	-14.4 (-18.0 to -11.8)*†	-6.2 (-7.2 to -5.0)*†ǂ

Data are presented as mean ± standard deviation if normally distributed or median (25^{th}-75^{th} percentile) if not normally distributed.
bpm = beats per minute, CV = cardiovascular, HFrEF = heart failure with reduced ejection fraction.
* p<0.05 compared to normal individuals
† p<0.05 compared to individuals with CV risk
ǂ p<0.05 compared to post-infarct patients
‡ p<0.05 compared to HFrEF patients

Two-dimensional speckle tracking data: global LV longitudinal strain and myocardial work efficiency

HFrEF patients showed the most impaired LV GLS values as compared to post-STEMI patients, patients with CV risk factors and healthy individuals (Table 2). In healthy individuals without structural heart disease or CV risk factors, the median

global LV myocardial work efficiency was 96.0% (IQR 95.0-96.3) (Figure 1), which did not differ significantly from individuals with CV risk factors 96.0% (IQR 95.0-97.0) (p=0.59, Figures 1 and 2). Compared to healthy individuals, median global LV myocardial work efficiency was significantly worse in post-STEMI patients (93.0%, IQR 88.5-95.0, p<0.001, Figures 1 and 2), and HFrEF patients (69.0%, IQR 63.8-80.0, p<0.001, Figures 1 and 2). The median global LV myocardial work efficiency was also significantly more impaired in post-STEMI patients and HFrEF patients as compared to individuals with CV risk factors (p<0.001, Figure 2). In comparison to post-STEMI patients, median global LV myocardial work efficiency was significantly lower in HFrEF patients (p<0.001, Figure 2). The global LV myocardial work efficiency did not differ between men and women (94.0% vs. 95.0%; p=0.489) in the overall population. There was a significant correlation between global LV myocardial work efficiency and LVEF in the total population (r=0.80, p<0.001). However, this correlation was non-significant when analyzing patients with CV risk factors (r=-0.03, p=0.876), post-STEMI patients (r=-0.226, p=0.231) and HFrEF patients (r=0.324, p=0.081) separately (Figure 3).

The ICC for intra-observer variability was 0.645 (p<0.001) and that for inter-observer variability 0.737 (p<0.001, Figure 4). Bland-Altman analysis for assessing intra-observer variability showed a bias of 0.55 with 95% limits of agreement ranging from -1.407 to 2.507 and for inter-observer variability a bias of 0.84 with 95% limits of agreement ranging from -1.950 to 3.634 (Figure 4).

Figure 2. Median global left ventricular myocardial work efficiency, compared across the different groups.

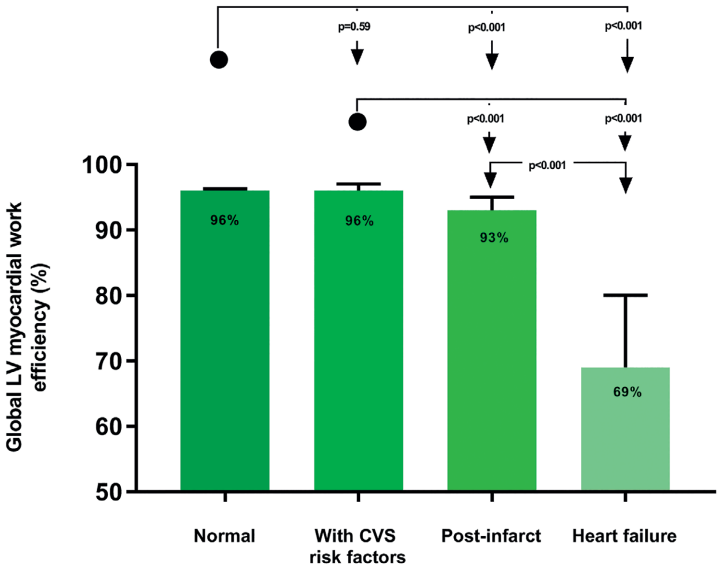

Columns represent median values, and T-bars the upper quartile. CV: cardiovascular, LV: left ventricular

Figure 3. Relation between global left ventricular myocardial work efficiency and left ventricular ejection fraction.

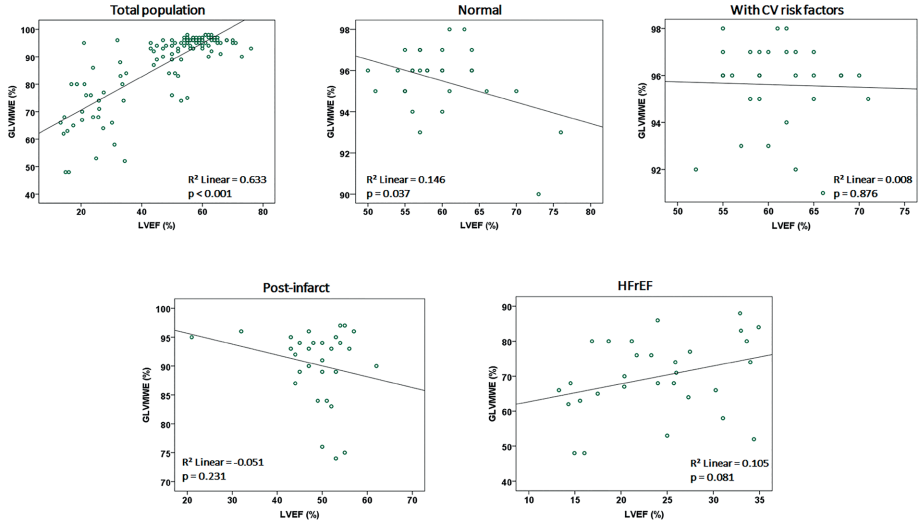

GLVMWE: global left ventricular myocardial work efficiency, LVEF: left ventricular ejection fraction, CV: cardiovascular, HFrEF: heart failure with reduced ejection fraction.

Figure 4. Bland-Altman plots depicting intra-observer (A) and inter-observer (B) variability of global left ventricular myocardial work efficiency.

A

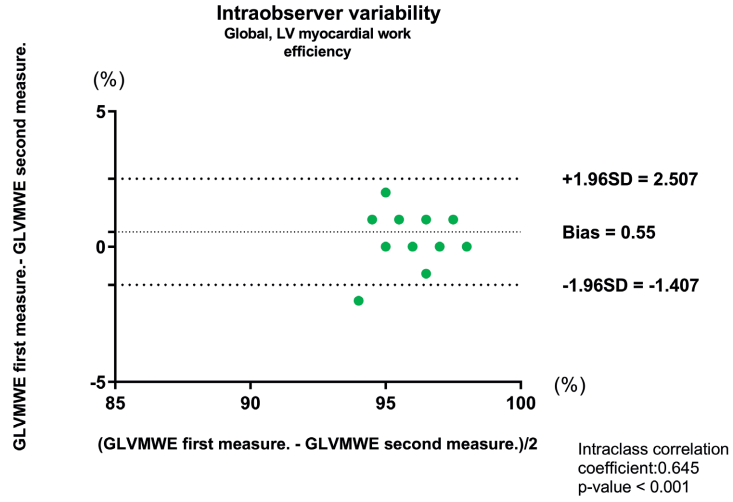

B

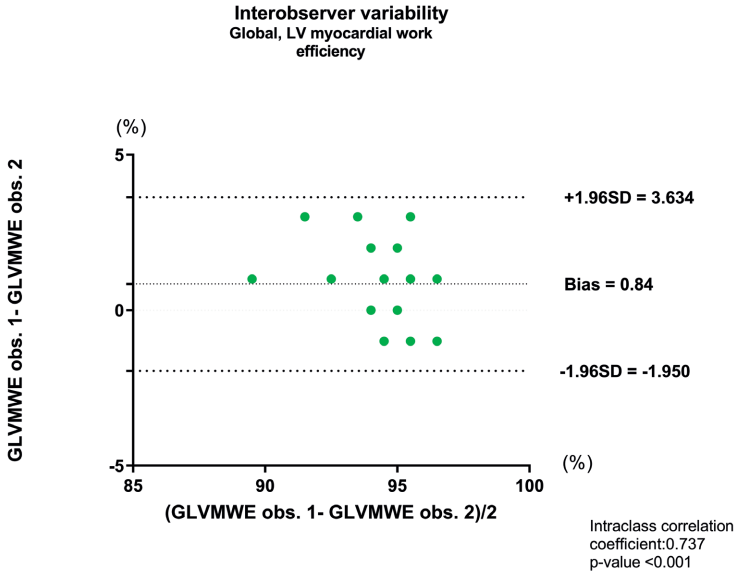

GLVMWE: global LV myocardial work efficiency, measure.: measurement, obs: observe

DISCUSSION

The values of global LV myocardial work efficiency were similar for normal individuals without structural heart disease or CV risk factors, and for individuals with CV risk factors. In contrast, global LV myocardial work efficiency was decreased in post-STEMI and HFrEF patients, compared to normal individuals and those with CV risk factors.

Non-invasive estimation of myocardial work efficiency

Myocardial work, estimated using non-invasive pressure-strain loops, is a novel approach to assess LV systolic function.[1] It overcomes the load-dependency of LVEF and global LV strain by integrating afterload into an LV function parameter. In a LV with preserved systolic function, increased afterload may lead to decreased global LV strain, which does not necessarily signify impaired contraction. In a preclinical model, aortic constriction decreased global LV strain, whereas no change was seen in the area of the non-invasive pressure-strain loop.[6] By integrating afterload, Russell et al. introduced a technique whereby non-invasively estimated blood pressure recordings are integrated with echocardiographic, speckle tracking strain values to construct pressure-strain loops of the LV.[1] The principle was tested in a canine model under a wide range of hemodynamic conditions and validated in 18 patients with chronic heart failure. An excellent correlation was found between non-invasive LV pressure-strain loop areas and invasively-measured equivalents. Similar results were shown by Hubert et al., in 9 patients with CRT, under 5 different conditions: CRT-off, right ventricular-pacing only, LV-pacing only, standard biventricular pacing and multipoint, biventricular pacing.[3] Russell et al. also demonstrated a strong correlation between myocardial glucose utilization (measured with ^{18}F-fluorodeoxyglucose positron emission tomography) and regional LV myocardial work (using non-invasive pressure-strain loops).[1] Combining cine cardiovascular magnetic resonance imaging (CMR) volumetry with quantitative phosphorus (^{31}P) magnetic resonance spectroscopy (MRS), Gabr et al. investigated the relation between non-invasive LV mechanical work and creatine kinase (CK) flux in 14 healthy subjects and 27 patients with heart failure.[13] LV mechanical efficiency was highly correlated with CK flux, supporting non-invasive LV work as valid measure of myocardial energetics. Although there is a strong correlation between LVEF and global LV myocardial work efficiency in the total population in our study, the absence of a significant correlation in the patients with CV risk

factors, post-STEMI patients and HFrEF patients, provides further support to the unique characterization of systolic function by global LV myocardial work efficiency.

Since LV work can be reliably estimated by means of a non-invasive methodology, global LV myocardial work efficiency can be derived from LV wasted and constructive work with the following formula: (constructive work / (constructive work + wasted work)) x 100%. Constructive work is defined as work performed during segmental shortening in systole or during lengthening in isovolumic relaxation, while wasted work is defined as work performed during segmental lengthening in systole or work performed during segmental shortening against a closed aortic valve in isovolumic relaxation. Unlike global LV work index, which measures the total amount of work performed (area within the LV pressure-strain loop), global LV myocardial work efficiency represents the ratio between effectively performed work and wasted work of the LV.

This technique can be applied to examine the effects of cardiac pathologies, e.g. myocardial infarction and heart failure, on myocardial energetics.

Global LV myocardial work efficiency: normal values

If all LV segments contract and relax synchronously during the cardiac cycle, with normal deformation and against an optimized afterload, global LV myocardial work efficiency should theoretically be close to 100%. Such a high level of efficiency is almost never achieved in a biological system, and we found a mean global LV myocardial work efficiency of 96.0% (IQR 95.0-96.3%) in healthy individuals. One of the reasons can be mild LV dyssynchrony as documented in healthy individuals.[14,15] Furthermore, limitations of the technique itself may cause some variation in the normal values: blood pressure values are measured sphygmomanometrically, and modelled onto reference curve, i.e. the value of global LV myocardial work remains an estimate, and not a direct measurement of cardiac efficiency.[3] Recently, Manganaro and colleagues presented normal values of global LV myocardial work efficiency in a population of 226 healthy subjects.[16] Our results are in close agreement with those of Manganaro et al., i.e. a median global LV myocardial work efficiency of 96% (IQR 94-97) in healthy individuals.

Global LV myocardial work efficiency: influence of CV risk factors

In a recent study by Chan et al. there was no difference in global LV myocardial work efficiency between patients with hypertension and normal controls.[17] Similarly, CV risk factors (including hypertension) did not lead to a decrease in LV myocardial efficiency in our cohort. The presence of CV risk factors alone, in the absence of structural or functional cardiac changes, does not seem to impact global LV myocardial work efficiency negatively. In the study of Chan and co-workers, patients with hypertension had proportionally higher values of global constructive work, which was balanced by increased amount of global wasted work.[17] The resulting global LV myocardial work efficiency was therefore similar to controls, which is in agreement with our results.

Global LV myocardial work efficiency in post-STEMI and HFrEF patients

Decreased segmental, LV myocardial work was superior to LV global longitudinal strain and LVEF in identifying coronary artery occlusion in patients with non-STEMI, in a study of 126 patients.[6] This is consistent with our results: we found lower global LV myocardial work efficiency in patients who underwent primary percutaneous coronary intervention for STEMI (generally held to indicate complete coronary artery occlusion), compared to those with CV risk factors and normal controls. Acute coronary syndromes have the ability to induce LV dyssynchrony,[18] regional decreases in longitudinal LV strain[19,20] and dynamic changes in LV afterload,[21] which can all lead to a decrease in LV mechanical efficiency. The prognostic role of measuring global LV myocardial work efficiency in patients with acute coronary syndromes, remains to be explored.

In the current study, the lowest global LV myocardial work efficiency values were seen in patients with HFrEF (with indications for cardiac resynchronization therapy). In a population of 97 HFrEF patients, with both ischemic and non-ischemic etiologies, the mean global LV myocardial work efficiency pre-CRT was 76%, which is comparable to the values we observed in the current analysis.[5] Likewise, in a pilot study of 21 HFrEF patients receiving CRT, the mean global LV myocardial work efficiency was 61%.[4] The markedly decreased global LV myocardial work efficiency in HFrEF patients may originate in the substantial degree of LV dyssynchrony experienced by these patients,[22] as well as reduced global or regional LV strain values, reflecting impaired systolic function.[23]

Several preliminary studies have shown the capacity of non-invasive derivation of myocardial work efficiency to identify CRT response.[4,5] Global LV myocardial work efficiency could therefore be a useful tool in assessing CRT candidates, although its incremental value to current CRT selection criteria remains to be proven.

Study Limitations

This study is subject to the inherent limitations of a single-center, retrospective analysis. CV risk factors were adjudicated on the basis of medical records, including patient history. The inclusion of only revascularized STEMI patients and HFrEF patients with indications for cardiac resynchronization therapy, might limit the generalizability of our results to these specific groups. Since global LV myocardial work efficiency is predicated on the measurement of speckle tracking strain echocardiography, it is not a vendor-independent measure. Currently, commercial software for the measurement of global LV myocardial work efficiency is only provided by a single vendor. For the assessment of non-invasive myocardial work, systemic arterial pressure is used as a substitute for LV pressure. This technique can therefore not be applied when systemic arterial pressure and LV pressure are discordant, e.g. in patients with LV outflow obstruction and significant aortic stenosis.[1]

CONCLUSION

Speckle tracking strain echocardiography and sphygmomanometric blood pressure measurements can be integrated to estimate global LV myocardial work efficiency non-invasively. Individuals with CV risk factors, but without structural heart disease, had global LV myocardial work efficiencies similar to normal controls. Lower myocardial efficiency was found in patients with previously revascularized STEMI who did not develop heart failure, while HFrEF patients had the lowest global LV myocardial work efficiency. The values presented here clearly demonstrate distinct profiles of myocardial efficiency in different cardiac pathologies, which may inform further studies. The echocardiographic evaluation of LV mechanical efficiency is a promising tool for both diagnosis and prognostication of various cardiac diseases.

REFERENCES

1. Russell K, Eriksen M, Aaberge L, Wilhelmsen N, Skulstad H, Remme EW, et al. A novel clinical method for quantification of regional left ventricular pressure-strain loop area: a non-invasive index of myocardial work. Eur Heart J 2012;33:724-733.
2. Russell K, Eriksen M, Aaberge L, Wilhelmsen N, Skulstad H, Gjesdal O, et al. Assessment of wasted myocardial work: a novel method to quantify energy loss due to uncoordinated left ventricular contractions. Am J Physiol Heart Circ Physiol 2013;305:H996-1003.
3. Hubert A, Le Rolle V, Leclercq C, Galli E, Samset E, Casset C, et al. Estimation of myocardial work from pressure-strain loops analysis: an experimental evaluation. Eur Heart J Cardiovasc Imaging 2018;19:1372-1379.
4. Vecera J, Penicka M, Eriksen M, Russell K, Bartunek J, Vanderheyden M, et al. Wasted septal work in left ventricular dyssynchrony: a novel principle to predict response to cardiac resynchronization therapy. Eur Heart J Cardiovasc Imaging 2016;17:624-632.
5. Galli E, Leclercq C, Hubert A, Bernard A, Smiseth OA, Mabo P, et al. Role of myocardial constructive work in the identification of responders to CRT. Eur Heart J Cardiovasc Imaging 2018;19:1010-1018.
6. Boe E, Russell K, Eek C, Eriksen M, Remme EW, Smiseth OA, et al. Non-invasive myocardial work index identifies acute coronary occlusion in patients with non-ST-segment elevation-acute coronary syndrome. Eur Heart J Cardiovasc Imaging 2015;16:1247-1255.
7. Abou R, Leung M, Tonsbeek AM, Podlesnikar T, Maan AC, Schalij MJ, et al. Effect of Aging on Left Atrial Compliance and Electromechanical Properties in Subjects Without Structural Heart Disease. Am J Cardiol 2017;120:140-147.
8. Liem SS, van der Hoeven BL, Oemrawsingh PV, Bax JJ, van der Bom JG, Bosch J, et al. MISSION!: optimization of acute and chronic care for patients with acute myocardial infarction. Am Heart J 2007;153:14.e11-11.
9. van Bommel RJ, Borleffs CJ, Ypenburg C, Marsan NA, Delgado V, Bertini M, et al. Morbidity and mortality in heart failure patients treated with cardiac resynchronization therapy: influence of pre-implantation characteristics on long-term outcome. Eur Heart J 2010;31:2783-2790.
10. Lang RM, Badano LP, Mor-Avi V, Afilalo J, Armstrong A, Ernande L, et al. Recommendations for cardiac chamber quantification by echocardiography in adults: an update from the American Society of Echocardiography and the European Association of Cardiovascular Imaging. J Am Soc Echocardiogr 2015;28:1-39.e14.
11. Delhaas T, Arts T, Prinzen FW, Reneman RS. Regional fibre stress-fibre strain area as an estimate of regional blood flow and oxygen demand in the canine heart. J Physiol 1994;477 (Pt 3):481-496.
12. Galli E, Leclercq C, Fournet M, Hubert A, Bernard A, Smiseth OA, et al. Value of Myocardial Work Estimation in the Prediction of Response to Cardiac Resynchronization Therapy. J Am Soc Echocardiogr 2018;31:220-230.
13. Gabr RE, El-Sharkawy A-MM, Schär M, Panjrath GS, Gerstenblith G, Weiss RG, et al. Cardiac work is related to creatine kinase energy supply in human heart failure: a cardiovascular magnetic resonance spectroscopy study. J Cardiovasc Magn Reson 2018;20:81.

14. Santos ABS, Kraigher-Krainer E, Bello N, Claggett B, Zile MR, Pieske B, et al. Left ventricular dyssynchrony in patients with heart failure and preserved ejection fraction. Eur Heart J 2014;35:42-47.

15. Haland TF, Almaas VM, Hasselberg NE, Saberniak J, Leren IS, Hopp E, et al. Strain echocardiography is related to fibrosis and ventricular arrhythmias in hypertrophic cardiomyopathy. Eur Heart J Cardiovasc Imaging 2016;17:613-621.

16. Manganaro R, Marchetta S, Dulgheru R, Ilardi F, Sugimoto T, Robinet S, et al. Echocardiographic reference ranges for normal non-invasive myocardial work indices: results from the EACVI NORRE study. Eur Heart J Cardiovasc Imaging 2018. Epub ahead of print. doi:10.1093/ehjci/jey188.

17. Chan J, Edwards NFA, Khandheria BK, Shiino K, Sabapathy S, Anderson B, et al. A new approach to assess myocardial work by non-invasive left ventricular pressure-strain relations in hypertension and dilated cardiomyopathy. Eur Heart J Cardiovasc Imaging 2018;20:31-39.

18. Zhang Y, Chan AK, Yu CM, Lam WW, Yip GW, Fung WH, et al. Left ventricular systolic asynchrony after acute myocardial infarction in patients with narrow QRS complexes. Am Heart J 2005;149:497-503.

19. Urheim S, Edvardsen T, Torp H, Angelsen B, Smiseth OA. Myocardial strain by Doppler echocardiography. Validation of a new method to quantify regional myocardial function. Circulation 2000;102:1158-1164.

20. Edvardsen T, Skulstad H, Aakhus S, Urheim S, Ihlen H. Regional myocardial systolic function during acute myocardial ischemia assessed by strain Doppler echocardiography. J Am Coll Cardiol 2001;37:726-730.

21. Gibson TC. Blood pressure levels in acute myocardial infarction. Am Heart J 1978;96:475-480.

22. Yu C-M, Lin H, Zhang Q, Sanderson JE. High prevalence of left ventricular systolic and diastolic asynchrony in patients with congestive heart failure and normal QRS duration. Heart 2003;89:54-60.

23. Cho GY, Marwick TH, Kim HS, Kim MK, Hong KS, Oh DJ. Global 2-dimensional strain as a new prognosticator in patients with heart failure. J Am Coll Cardiol 2009;54:618-624.

5

Myocardial Work, an Echocardiographic Measure of Post Myocardial Infarct Scar on Contrast-Enhanced Cardiac Magnetic Resonance

El Mahdiui M, van der Bijl P, Abou R, de Paula Lustosa R, van der Geest R, Ajmone Marsan N, Delgado V, Bax JJ.
Am J Cardiol. 2021 Jul 15;151:1-9.

ABSTRACT

This study investigates the relation of non-invasive myocardial work and myocardial viability following ST-segment elevation myocardial infarction (STEMI) assessed on late gadolinium contrast enhanced cardiac magnetic resonance (LGE CMR) and characterizes the remote zone using non-invasive myocardial work parameters. STEMI patients who underwent primary percutaneous coronary intervention (PCI) were included. Several non-invasive myocardial work parameters were derived from speckle tracking strain echocardiography and sphygmomanometric blood pressure, e.g.: myocardial work index (MWI), constructive work (CW), wasted work (WW) and myocardial work efficiency (MWE). LGE was quantified to determine infarct transmurality and scar burden. The core zone was defined as the segment with the largest extent of transmural LGE and the remote zone as the diametrically opposed segment without LGE. A total of 53 patients (89% male, mean age 58 ± 9 years) and 689 segments were analyzed. The mean scar burden was 14 ± 7% of the total LV mass, and 76 segments (11%) demonstrated transmural hyperenhancement, 280 (41%) non-transmural hyperenhancement and 333 (48%) no LGE. An inverse relation was observed between segmental MWI, CW and MWE and infarct transmurality ($p<0.05$). MWI, CW and MWE were significantly lower in the core zone compared to the remote zone ($p<0.05$). In conclusion, non-invasive myocardial work parameters may serve as potential markers of segmental myocardial viability in post-STEMI patients who underwent primary PCI. Non-invasive myocardial work can also be utilized to characterize the remote zone, which is an emerging prognostic marker as well as a therapeutic target.

INTRODUCTION

Accurate quantification of the extent and transmurality of myocardial infarct in patients following an ST-segment elevation myocardial infarction (STEMI) is essential in the identification of viable myocardial regions that could benefit from revascularization.[1] In addition, the remote zone, i.e. the non-infarcted myocardium remote from the infarct core, is an emerging region of interest in STEMI, with the potential to be used as a therapeutic target.[2-4] Late gadolinium contrast enhanced cardiac magnetic resonance (LGE CMR) is the gold standard for the quantification of the extent of transmural scar[5] with high reproducibility[6] and a robust association with prognosis.[5,7] The use of CMR is limited by availability, time and cost. Recently, non-invasive myocardial work has been proposed as a parameter for assessing left ventricular (LV) systolic function.[8,9] The ability of non-invasive myocardial work indices to characterize post-infarct scar and myocardial function has not been investigated. The aims of the current study were to explore the relation of non-invasive myocardial work indices to transmurality of post-infarct scar on LGE CMR, and to compare myocardial work indices between infarct core and remote zone.

METHODS

Patients admitted with an acute STEMI who underwent primary percutaneous coronary intervention (PCI) between 2004 and 2017 at the Leiden University Medical Center (LUMC) were evaluated.[10] For this study, only patients with feasible non-invasive myocardial work analysis by 2-dimensional speckle-tracking strain echocardiography and with LGE CMR data were selected for analysis. Patients with prior myocardial infarction, coronary artery bypass grafting, LGE CMR performed within 30 days of index myocardial infarction, non-feasible 2-dimensional speckle-tracking strain echocardiography, moderate to severe valve disease or missing blood pressure measurements were excluded (Figure 1). Patients were treated according to prevailing guidelines from the European Society of Cardiology, as described previously.[10] The culprit vessel was identified during invasive coronary angiography and multivessel disease was defined as the presence of >50% luminal stenosis in more than 1 vessel. Transthoracic echocardiography was performed according to the institutional, guideline-based, clinical care track protocol (MISSION!),[10] while CMR was performed at the discretion of the treating physician. Demographic and clinical data were collected from the departmental cardiology information system (EPD-vision; LUMC, Leiden, The Netherlands) and from electronic medical records (HiX; ChipSoft, Amsterdam, The Netherlands). For retrospective analysis of clinically acquired data, the institutional review board waived the need for individual patient written informed consent.

Using commercially available echocardiographic systems (E9 and E95, General Electric Vingmed Ultrasound, Milwaukee, Wisconsin) transthoracic echocardiographic images were recorded in patients at rest. Electrocardiogram-triggered echocardiographic data were acquired with M5S transducers and digitally stored in cine-loop format for offline analysis (EchoPac 202, General Electric Vingmed Ultrasound). Echocardiographic images from the study closest in time to CMR acquisition were used for analysis. The median interval between echocardiographic and CMR acquisition was 1 month (interquartile range (IQR) 0-2 months) and the median interval between STEMI and CMR acquisition was 2 months (IQR 1-3 months). LV end-systolic and end-diastolic volumes were measured in apical 2- and 4-chamber views and LV ejection fraction (LVEF) was calculated using the biplane Simpson's method.[11]

Figure 1. Flow diagram of study population.

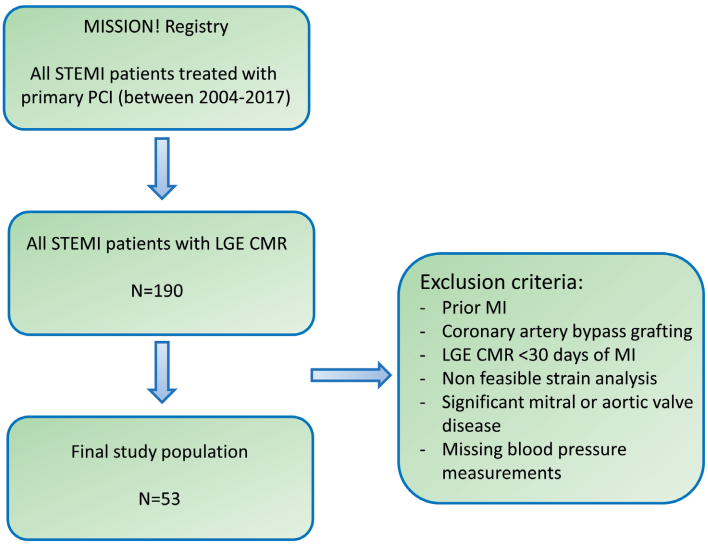

LGE CMR= late gadolinium enhancement cardiac magnetic resonance; MI= myocardial infarction; PCI=percutaneous coronary intervention; STEMI= ST-segment elevation myocardial infarction.

Quantification of non-invasive myocardial work was performed using a commercially available software package (EchoPac 202, General Electric Vingmed Ultrasound). Calculation and validation of LV myocardial work analysis from non-invasive LV pressure-strain loops has been described previously.[8,9] Non-invasive myocardial work was derived from LV pressure-strain loops by integrating LV strain data and non-invasively estimated LV pressure. This approach to echocardiographic quantification of LV work has shown a high degree of correlation with invasively-measured LV myocardial work[8,9,12] and has been validated in several patient subgroups.[8,9,12-15] LV strain data were acquired using 2-dimensional speckle-tracking echocardiography by manually tracing the LV endo- and epicardial borders in the apical long-axis, 2- and 4-chamber views. The automatically generated region of interest was manually adjusted to the myocardial thickness, as required. The LV pressure was assumed to be equal to the arterial blood pressure measured from sphygmomanometric brachial artery cuff measurements. An LV pressure-strain curve was then constructed using a normalized reference curve provided by the software and adjusted to the different cardiac cycle phases using valvular event timing (mitral and aortic valve opening and closing). Strain rate was multiplied

with LV pressure and integrated over time to produce segmental and global LV myocardial work.[9,16] Several global and segmental myocardial work indices can be derived from the construction of non-invasive LV pressure-strain loops: myocardial work index (MWI), constructive work (CW), wasted work (WW) and myocardial work efficiency (MWE). MWI is defined as the total LV work performed in a single cardiac cycle. CW is LV myocardial work performed during shortening of a myocardial segment in systole or during lengthening in isovolumic relaxation, thereby contributing to LV ejection. WW on the other hand, is LV myocardial work performed during lengthening of a myocardial segment in systole or during shortening in isovolumic relaxation, and which therefore does not contribute to LV ejection. MWE is defined as the ratio of CW, divided by the sum of CW and WW, expressed as a percentage.

Patients were imaged on a 1.5-T Gyroscan ACS-NT/Intera MR system (Philips Medical Systems, Best, the Netherlands) or on a 3.0-T Ingenia MR system (Philips Medical Systems, Best, the Netherlands) using retrospective ECG gating. Cine steady-state free precession (SSFP) CMR images were acquired in the long-(2- and 4-chamber views) and short-axes of the LV. Typical imaging parameters were as follows for the 1.5-T Gyroscan ACS-NT/Intera MR system: field of view (FOV) 400x320 mm^2; matrix, 256x206 pixels; slice thickness, 10 mm with no slice gap; flip angle (α), 35°; echo time (TE), 1.67 ms; and repetition time (TR), 3.3 ms.[17] For the 3.0-T Ingenia MR system typical parameters were: FOV 400x350 mm; matrix, 232x192 pixels; slice thickness, 8 mm with no slice gap; α, 45°; TE, 1.5 ms and TR, 3.0 ms.[18] LGE images were acquired 15 minutes after a bolus injection of gadolinium diethylenetriamine pentaacetic acid (Magnevist, Schering, Berlin, Germany) or gadoterate meglumine (Dotarem, Guerbet, Villepinte, France) (0.15 mmol/kg) with an inversion-recovery 3-dimensional turbo-field echo sequence with parallel imaging. The heart was imaged in 1 or 2 breath-holds with short-axis slices at various levels dependent on the heart size. For the 1.5-T Gyroscan ACS-NT/Intera MR system, typical parameters were as follows: FOV 400x400 mm^2; matrix, 256x206 pixels; slice thickness, 10 mm with 50% overlap; α, 10°; TE, 1.06 ms and TR, 3.7 ms.[17] For the 3.0-T Ingenia MR system typical parameters were as follows: FOV 350 × 350 mm; matrix size 188 × 125 mm; acquired pixel size 1.86 × 2.8 mm; reconstructed pixel size 1.46 × 1.46 mm; slice thickness 10 mm with 50% overlap; α, 10°; SENSE factor 3; TE, 2.09 ms and TR, 4.31 ms.[19] Images were stored digitally for offline analysis.

CMR data analysis was performed with dedicated software (MASS, Leiden University Medical Center, Leiden, the Netherlands). LV endocardial and epicardial borders were manually traced on short-axis SSFP cine images. Myocardial scar was assessed by using a previously reported method, based on the signal intensity (SI).[17] The myocardial segment with the most dense scar was visually identified and a region of interest was placed in this segment to determine the maximum SI. Subsequently, any myocardium with a SI ≥35% of the maximum SI was defined as scar and automatically identified by the software.[17]

The LV was divided into a 13-segment model and each segment was scored based on the percentage of hyperenhancement of the LV myocardial wall: transmural infarcted segments (≥50%), non-transmural infarcted segments (1-50%) and non-infarcted segments (≤1%) (Figure 2). Thereafter, 2 specific regions of interest were defined in the LV myocardial wall according to the percentage of hyperenhancement: the core zone was defined as the segment with the largest extent of transmural hyperenhancement and the remote zone as the myocardial tissue opposite to the core zone, without any evidence of hyperenhancement (Figure 2). If there was evidence of any hyperenhancement in the segment diametrically opposing the core zone, the first adjacent segment without evidence of hyperenhancement was used as the remote zone. Defining these 2 regions of interest allowed meaningful comparison of echocardiography and CMR LGE data in STEMI patients (Figure 3).

Figure 2. Determining the infarct core and the remote area.

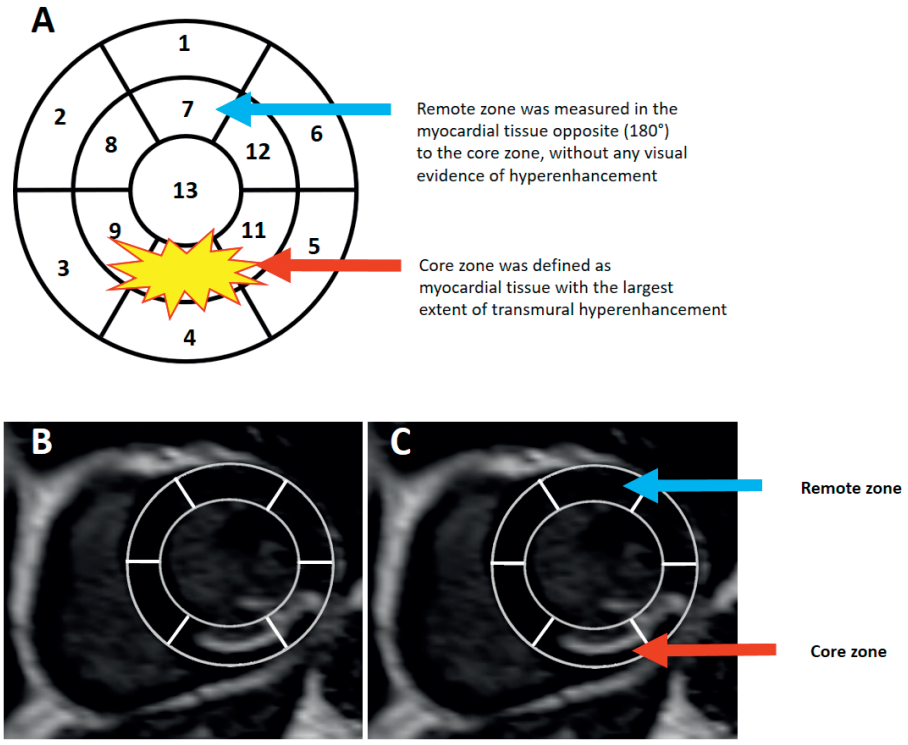

The 13-segment model shown in panel A schematically illustrates how the core zone and the remote zone were defined. After the left ventricular (LV) endo- and epicardial borders were traced, the LV segment with most transmural hyperenhancement was defined as the core zone, while the diametrically opposed segment (or next adjacent segment if the segment opposite to the core zone had any evidence of scar), without evidence of hyperenhancement, was labelled as the remote zone. Panels B and C show a patient with late gadolinium enhancement (LGE) on cardiac magnetic resonance (CMR) in the inferior and inferolateral wall after an ST-segment elevation myocardial infarction (STEMI) with complete occlusion of the right coronary artery. The midventricular inferior segment demonstrates an infarct with 73% transmurality.

Figure 3. Non-invasive pressure-strain loops and myocardial work efficiency of a patient after an ST-segment elevation myocardial infarction (STEMI).

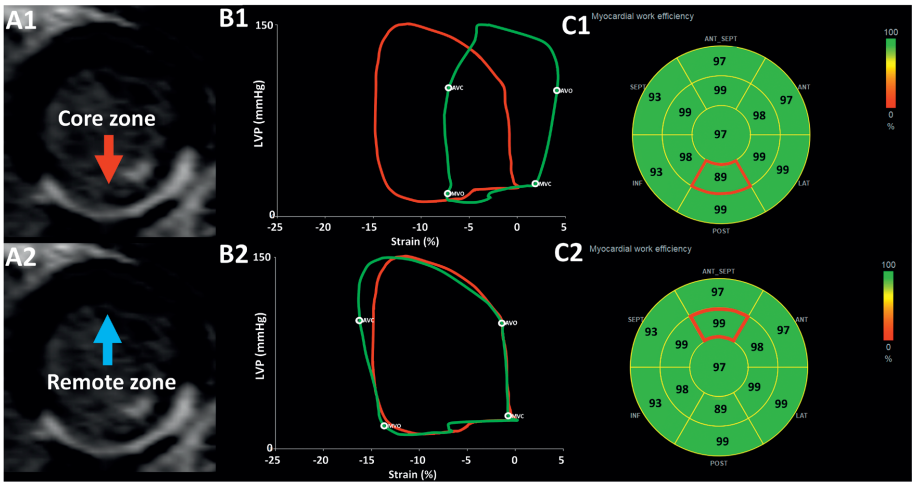

A 41 year old male patient presented with an inferior STEMI, due to complete occlusion of the right coronary artery. On late gadolinium contrast enhanced cardiac magnetic resonance (LGE CMR) imaging the total scar burden was 11.9%. Panel A represents the core zone with 73% transmurality (A1) and the remote zone (A2) on LGE CMR. Panel B displays non-invasive pressure-strain loops from which myocardial work efficiency is derived (B1 core zone and B2 remote zone). The red pressure-strain loop represents the averaged loop for all left ventricular segments, whereas the green pressure-strain loop specifically represents the selected segment outlined in Panel C. Panel C shows parametric maps of left ventricular myocardial work efficiency (C1 core zone with myocardial work efficiency (MWE) of 89% and C2 remote zone MWE of 99%).

Normally distributed continuous variables are presented as mean ± standard deviation (SD) and non-normal continuous variables as median and interquartile range (IQR). Normality was assessed using the Shapiro-Wilk test and visual assessment of a histogram and Q-Q plots. Categorical variables are presented as frequencies and percentages. Continuous variables were compared using the Student's *t*-test if normally distributed and the Mann-Whitney *U*-test if not normally distributed. For comparison of related transmural, non-transmural and non-infarcted segments, linear mixed models were used for normally distributed variables (MWI and CW) and the Friedman's two-way ANOVA with post-hoc Wilcoxon signed-rank tests for non-normally distributed variables (WW and MWE). A p-value <0.05 was considered statistically significant. Statistical analyses were performed using SPSS version 25.0 (SPSS, Armonk, NY).

RESULTS

Fifty three patients (89% male, age 58 ± 9 years) were analyzed for the presence and distribution of segmental LGE. Patient clinical characteristics are shown in Table 1. Patients received appropriate, guideline-directed pharmacotherapy following STEMI.

Table 1. Patient characteristics

Variable	(n=53)
Age (years)	58 ± 9
Men	47 (89%)
Height (cm)	178.4 ± 6.7
Weight (kg)	87.6 ± 14.0
BMI (kg/m²)	27.5 ± 4.1
BSA (m²)	2.1 ± 0.2
LAD culprit artery	33 (62%)
Peak creatine phosphokinase (U/L)	2665 (1397-4661)
Peak troponin T (μg/L)	6.8 (4.0-11.3)
Creatinine (μmol/L)	81 (71-89)
Hypertension	24 (45%)
Hypercholesterolemia	13 (25%)
Diabetes mellitus	6 (11%)
Current smoker	26 (49%)
Family history of CVD	21 (40%)
Medication at discharge	
Aspirin	51 (96%)
Thienopyridine	53 (100%)
β-blocker	52 (98%)
Statin	53 (100%)
ACE-I/ARB	53 (100%)

Values are mean ± standard deviation if normally distributed and median (interquartile range) if not normally distributed.
ACE-I = angiotensin-converting enzyme inhibitor, ARB = angiotensin receptor blocker, BMI = body mass index, BSA = body surface area, CV = cardiovascular, CVD = cardiovascular disease, LAD = left anterior descending coronary artery.

Conventional imaging variables, myocardial work indices and LGE burden on CMR are shown in Table 2. The median LVEF was 50% (IQR 44-55) and the median global LV MWE 93% (IQR 91-96). The mean scar burden was 14.0 ± 7.0% of the total LV mass.

Table 2. Imaging variables

Variable	(n=53)
Conventional echocardiographic variables	
Left ventricular end-diastolic volume (ml)	113 (89-142)
Left ventricular end-systolic volume (ml)	58 (42-84)
Left ventricular ejection fraction (%)	50 (44-55)
Myocardial work indices	
Global myocardial work index (mmHg%)	1446 ± 412
Global constructive work (mmHg%)	1671 ± 474
Global wasted work (mmHg%)	77 (58-127)
Global left ventricular (LV) myocardial work efficiency (%)	93 (91-96)
LGE CMR	
Total LV mass (g)	162 ± 41
Total scar burden (%)	14.0 ± 7.0

Values are mean ± standard deviation if normally distributed and median (interquartile range) if not normally distributed.

All segments (n=689) could be analyzed for LGE and for myocardial work variables. A total of 76 segments (11%) demonstrated transmural hyperenhancement, 280 (41%) had non-transmural hyperenhancement and 333 (48%) segments showed no evidence for hyperenhancement on LGE CMR. An inverse relationship was observed between segmental MWI, CW and MWE and the extent of hyperenhancement transmurality on LGE CMR ($p<0.05$ for all comparisons) while a trend was observed between a greater amount of WW and transmural hyperenhancement ($p=0.086$) (Figure 4).

Figure 4. Myocardial work indices stratified according to infarct transmurality on late gadolinium enhancement cardiac magnetic resonance (LGE CMR).

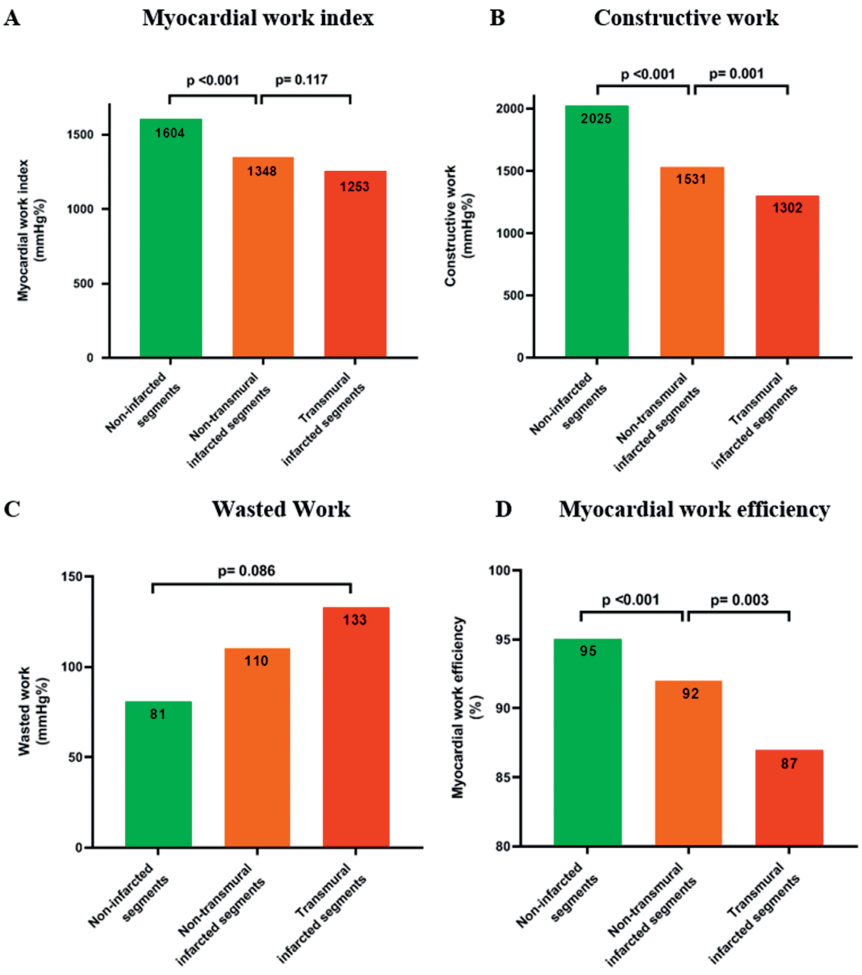

The segmental values of different myocardial work indices are presented, according to infarct transmurality on LGE CMR. Segmental values for myocardial work index (A), constructive work (B) and myocardial work efficiency (D) according to transmurality on LGE CMR

LV myocardial work indices of the infarct core and the remote zone are shown in Figure 5. Segmental MWI, CW and MWE were lower in the core zone (and WW was higher) compared to the remote zone ($p<0.05$ for all comparisons).

Figure 5. Myocardial work indices in core and remote infarct zones.

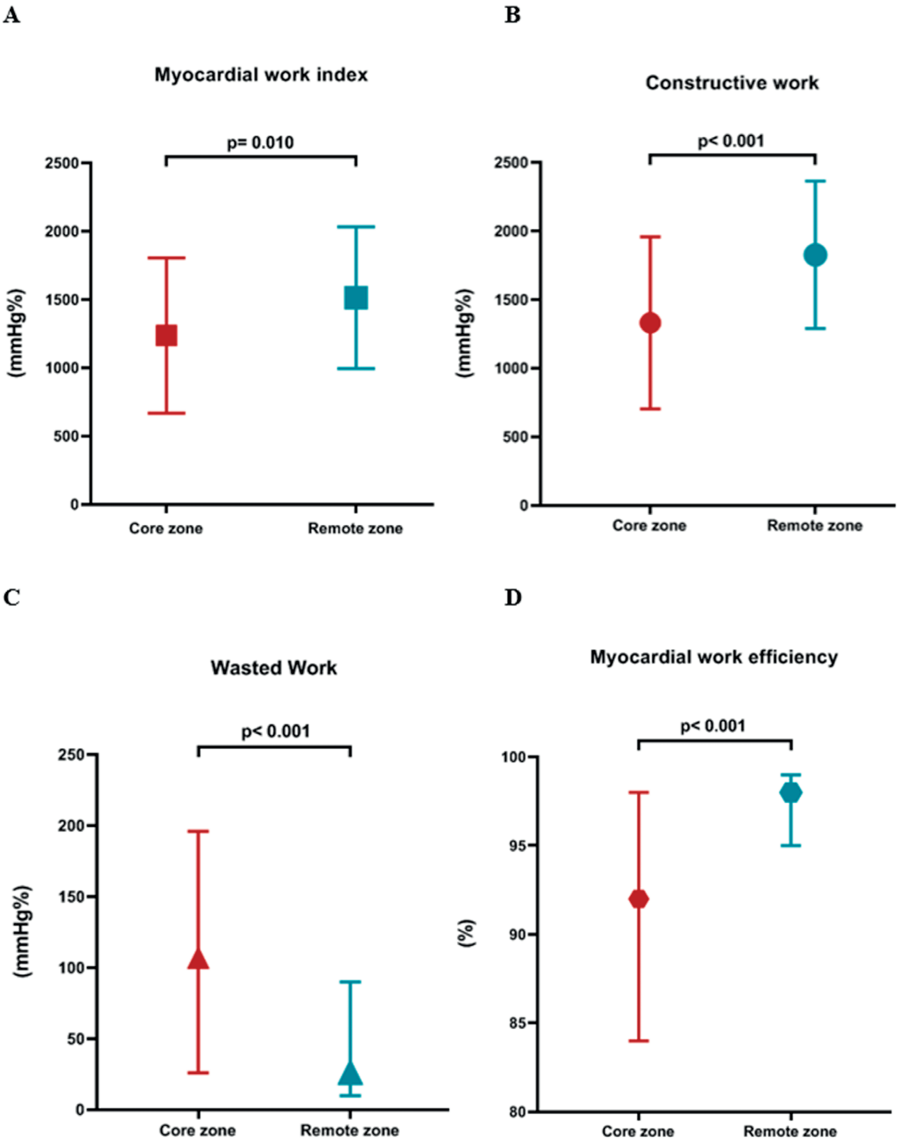

The values presented in the box-and-whisker plot for panels A and B are mean ± standard deviation and median (interquartile range) for panels C and D.

DISCUSSION

The findings from our study can be summarized as follows: MWI, CW and MWE decreased significantly with increasing transmural myocardial hyperenhancement, whereas WW increased. Moreover, MWI, CW and MWE were significantly more impaired and WW significantly larger in the core zone compared to the remote zone.

LV myocardial work, the product of force and distance, can be quantified using myocardial force-dimension loops and reflects myocardial oxygen consumption.[20,21] Invasive pressure-volume loops have typically been used to measure myocardial work, however, the invasive nature limits its application to daily practice.[21] Russell et al. introduced a non-invasive method to measure myocardial work by incorporating sphygmomanometric brachial artery cuff measurements and echocardiographic speckle tracking strain to construct pressure-strain loops.[8] This novel method demonstrated excellent agreement with invasively measured myocardial work in a canine model under different hemodynamic conditions, as well as in patients with chronic heart failure.[8,9] A robust correlation between non-invasive and invasively measured myocardial work was also found in a study of CRT recipients under different hemodynamic conditions and a variety of CRT settings, e.g. CRT off, LV pacing only, right ventricular pacing only, standard biventricular pacing and multipoint biventricular pacing.[12] Regional non-invasive myocardial work corresponds to regional glucose metabolism measured with ^{18}F-fluorodeoxyglucose (^{18}F-FDG) positron emission tomography (PET), confirming its validity as a measure of myocardial energetics.[8]

While LVEF and global LV longitudinal strain remain pillars of LV function assessment, they are limited by load-dependency.[22] Skulstad et al. demonstrated that the contraction of ischemic myocardium is heavily dependent on afterload.[23] Non-invasive myocardial work assessment has the ability to integrate the LV contraction and afterload into a single parameter, which represents a more comprehensive index of LV performance than either contractile function or afterload in isolation. Boe et al. found non-invasive myocardial work to be superior to strain analysis for the identification of acute coronary vessel occlusion in patients with non-STEMI.[13] In ischemic but viable myocardial segments, metabolism is reduced and can be quantified with ^{18}F-FDG PET.[24] The firm correlation between regional non-invasive myocardial work and regional glucose metabolism raises the exciting possibility

that non-invasive myocardial work indices may reflect segmental energetics, and allow the identification of myocardial viability.[8] LGE CMR is a proven indicator of myocardial viability through accurate distinction between viable myocardium and of nonviable scar.[5] LGE CMR is a reliable predictor of myocardial functional recovery following revascularization. In a population of 50 patients with ischemic ventricular dysfunction, Kim et al. demonstrated segmental recovery in 8% of segments with transmural hyperenhancement compared to 66% in non-transmural hyperenhancement.[1] The inverse relation between the transmural extent of LGE on CMR and segmental recovery following revascularization has been demonstrated in numerous studies.[25] The significant inverse relationship between segmental CW and transmural hyperenhancement on LGE CMR is a new insight this study provides and might indicate CW to be a valid measure of viability of myocardial segments.

Following STEMI, an inflammatory response may occur in the remote zone, eventually leading to interstitial fibrosis.[2,3,26] Several studies have investigated changes in contractile function of the remote zone following a myocardial infarction, and while some reported preserved systolic function,[27] others demonstrated reduced function.[2] In a murine model of myocardial infarction, Espe et al. demonstrated that a redistribution of myocardial work occurred from the infarcted segments to the remote zone.[28] Our data also indicate preserved or enhanced remote zone myocardial work, compared to the infarct core. The remote zone is an emerging region of interest for post-infarct risk-stratification. In a population of 288 reperfused STEMI patients who underwent CMR, native T1 values of the remote zone on CMR were independently associated with LV remodeling at 6 months, as well as with major adverse cardiac events.[3] Similar results were found in a study by Reinstandler and co-workers of 255 STEMI patients, where native T1 values of the remote zone provided incremental prognostic information beyond established markers of infarct severity.[4] Myocardial work has been compared between the remote and core zones of an infarct in a murine model.[29] In non-failing LVs, myocardial work was increased in the remote zone when compared to controls. In contrast, a compensatory increase in myocardial work in the remote zone was not seen in rats who developed cardiac failure.[29]

Several limitations should be acknowledged. This was a single center study with a retrospective design. Patients in whom echocardiographic speckle tracking strain analysis could not be performed had to be excluded. Patients with significant aortic

stenosis or patients with missing blood pressure measurements were excluded and this may have led to a selection bias. The remote zone was defined as the non-infarcted myocardial segment diametrically opposed to the infarct core, and was adopted as a reference for normal, non-invasive myocardial work values. Although such LV segments were distant from the infarct, abnormal T1 values have been recognized in the remote zone. While the significance of this finding is still unclear, it suggests that the remote zone does not represent altogether normal myocardium.[2-4] We included a homogenous population, the value of non-invasive myocardial work in a heterogenous population should be investigated. The findings of our study should be confirmed in larger, multi-center studies before implementation in clinical practice.

In conclusion, in post-STEMI patients that underwent primary PCI, CW and MWE were significantly lower in the transmural infarcted segments and non-invasive myocardial work parameters significantly different in the remote and core zone. Segmental CW may therefore serve as a low cost, non-invasive marker of myocardial viability. Furthermore, we demonstrated that non-invasive myocardial work can be utilized for the characterization of the remote, which is an emerging prognostic marker and therapeutic target post-STEMI.

REFERENCES

1. Kim RJ, Wu E, Rafael A, Chen E-L, Parker MA, Simonetti O, Klocke FJ, Bonow RO, Judd RM. The Use of Contrast-Enhanced Magnetic Resonance Imaging to Identify Reversible Myocardial Dysfunction. N Engl J Med 2000;343:1445-1453.
2. Chan W, Duffy SJ, White DA, Gao XM, Du XJ, Ellims AH, Dart AM, Taylor AJ. Acute left ventricular remodeling following myocardial infarction: coupling of regional healing with remote extracellular matrix expansion. JACC Cardiovasc Imaging 2012;5:884-893.
3. Carrick D, Haig C, Rauhalammi S, Ahmed N, Mordi I, McEntegart M, Petrie MC, Eteiba H, Lindsay M, Watkins S, Hood S, Davie A, Mahrous A, Sattar N, Welsh P, Tzemos N, Radjenovic A, Ford I, Oldroyd KG, Berry C. Pathophysiology of LV Remodeling in Survivors of STEMI: Inflammation, Remote Myocardium, and Prognosis. JACC Cardiovasc Imaging 2015;8:779-789.
4. Reinstadler SJ, Stiermaier T, Liebetrau J, Fuernau G, Eitel C, de Waha S, Desch S, Reil JC, Poss J, Metzler B, Lucke C, Gutberlet M, Schuler G, Thiele H, Eitel I. Prognostic Significance of Remote Myocardium Alterations Assessed by Quantitative Noncontrast T1 Mapping in ST-Segment Elevation Myocardial Infarction. JACC Cardiovasc Imaging 2018;11:411-419.
5. Kim RJ, Fieno DS, Parrish TB, Harris K, Chen EL, Simonetti O, Bundy J, Finn JP, Klocke FJ, Judd RM. Relationship of MRI delayed contrast enhancement to irreversible injury, infarct age, and contractile function. Circulation 1999;100:1992-2002.
6. Mahrholdt H, Wagner A, Holly TA, Elliott MD, Bonow RO, Kim RJ, Judd RM. Reproducibility of chronic infarct size measurement by contrast-enhanced magnetic resonance imaging. Circulation 2002;106:2322-2327.
7. Eitel I, de Waha S, Wohrle J, Fuernau G, Lurz P, Pauschinger M, Desch S, Schuler G, Thiele H. Comprehensive prognosis assessment by CMR imaging after ST-segment elevation myocardial infarction. JACC 2014;64:1217-1226.
8. Russell K, Eriksen M, Aaberge L, Wilhelmsen N, Skulstad H, Remme EW, Haugaa KH, Opdahl A, Fjeld JG, Gjesdal O, Edvardsen T, Smiseth OA. A novel clinical method for quantification of regional left ventricular pressure-strain loop area: a non-invasive index of myocardial work. Eur Heart J 2012;33:724-733.
9. Russell K, Eriksen M, Aaberge L, Wilhelmsen N, Skulstad H, Gjesdal O, Edvardsen T, Smiseth OA. Assessment of wasted myocardial work: a novel method to quantify energy loss due to uncoordinated left ventricular contractions. Am J Physiol Heart Circ Physiol 2013;305:H996-1003.
10. Liem SS, van der Hoeven BL, Oemrawsingh PV, Bax JJ, van der Bom JG, Bosch J, Viergever EP, van Rees C, Padmos I, Sedney MI, van Exel HJ, Verwey HF, Atsma DE, van der Velde ET, Jukema JW, van der Wall EE, Schalij MJ. MISSION!: optimization of acute and chronic care for patients with acute myocardial infarction. Am Heart J 2007;153:14.e11-**11.** Lang RM, Badano LP, Mor-Avi V, Afilalo J, Armstrong A, Ernande L, Flachskampf FA, Foster E, Goldstein SA, Kuznetsova T, Lancellotti P, Muraru D, Picard MH, Rietzschel ER, Rudski L, Spencer KT, Tsang W, Voigt JU. Recommendations for cardiac chamber quantification by echocardiography in adults: an update from the American Society of Echocardiography and the European Association of Cardiovascular Imaging. Eur Heart J Cardiovasc Imaging 2015;16:233-270.

12. Hubert A, Le Rolle V, Leclercq C, Galli E, Samset E, Casset C, Mabo P, Hernandez A, Donal E. Estimation of myocardial work from pressure–strain loops analysis: an experimental evaluation. Eur Heart J Cardiovasc Imaging 2018;19:1372-1379.

13. Boe E, Russell K, Eek C, Eriksen M, Remme EW, Smiseth OA, Skulstad H. Non-invasive myocardial work index identifies acute coronary occlusion in patients with non-ST-segment elevation-acute coronary syndrome. Eur Heart J Cardiovasc Imaging 2015;16:1247-1255.

14. El Mahdiui M, van der Bijl P, Abou R, Ajmone Marsan N, Delgado V, Bax JJ. Global Left Ventricular Myocardial Work Efficiency in Healthy Individuals and Patients with Cardiovascular Disease. J Am Soc Echocardiogr 2019;32:1120-1127.

15. Manganaro R, Marchetta S, Dulgheru R, Ilardi F, Sugimoto T, Robinet S, Cimino S, Go YY, Bernard A, Kacharava G, Athanassopoulos GD, Barone D, Baroni M, Cardim N, Hagendorff A, Hristova K, Lopez-Fernandez T, de la Morena G, Popescu BA, Penicka M, Ozyigit T, Rodrigo Carbonero JD, van de Veire N, Von Bardeleben RS, Vinereanu D, Zamorano JL, Rosca M, Calin A, Moonen M, Magne J, Cosyns B, Galli E, Donal E, Carerj S, Zito C, Santoro C, Galderisi M, Badano LP, Lang RM, Oury C, Lancellotti P. Echocardiographic reference ranges for normal non-invasive myocardial work indices: results from the EACVI NORRE study. Eur Heart J Cardiovasc Imaging 2019;20:582-590.

16. van der Bijl P, Kostyukevich M, El Mahdiui M, Hansen G, Samset E, Ajmone Marsan N, Bax JJ, Delgado V. A Roadmap to Assess Myocardial Work: From Theory to Clinical Practice. JACC Cardiovasc Imaging 2019.

17. Roes SD, Borleffs CJ, van der Geest RJ, Westenberg JJ, Marsan NA, Kaandorp TA, Reiber JH, Zeppenfeld K, Lamb HJ, de Roos A, Schalij MJ, Bax JJ. Infarct tissue heterogeneity assessed with contrast-enhanced MRI predicts spontaneous ventricular arrhythmia in patients with ischemic cardiomyopathy and implantable cardioverter-defibrillator. Circ Cardiovasc Imaging 2009;2:183-190.

18. Tao Q, van der Tol P, Berendsen FF, Paiman EHM, Lamb HJ, van der Geest RJ. Robust motion correction for myocardial T1 and extracellular volume mapping by principle component analysis-based groupwise image registration. J Magn Reson Imaging 2018;47:1397-1405.

19. Bizino MB, Tao Q, Amersfoort J, Siebelink HJ, van den Bogaard PJ, van der Geest RJ, Lamb HJ. High spatial resolution free-breathing 3D late gadolinium enhancement cardiac magnetic resonance imaging in ischaemic and non-ischaemic cardiomyopathy: quantitative assessment of scar mass and image quality. Eur Radiol 2018;28:4027-4035.

20. Hisano R, Cooper Gt. Correlation of force-length area with oxygen consumption in ferret papillary muscle. Circ Res 1987;61:318-328.

21. Delhaas T, Arts T, Prinzen FW, Reneman RS. Regional fibre stress-fibre strain area as an estimate of regional blood flow and oxygen demand in the canine heart. J Physiol 1994;477 (Pt 3):481-496.

22. Yingchoncharoen T, Agarwal S, Popovic ZB, Marwick TH. Normal ranges of left ventricular strain: a meta-analysis. J Am Soc Echocardiogr 2013;26:185-191.

23. Skulstad H, Edvardsen T, Urheim S, Rabben SI, Stugaard M, Lyseggen E, Ihlen H, Smiseth OA. Postsystolic shortening in ischemic myocardium: active contraction or passive recoil? Circulation 2002;106:718-724.

24. Elsasser A, Muller KD, Skwara W, Bode C, Kubler W, Vogt AM. Severe energy deprivation of human hibernating myocardium as possible common pathomechanism of contractile dysfunction, structural degeneration and cell death. JACC 2002;39:1189-1198.

25. Romero J, Xue X, Gonzalez W, Garcia MJ. CMR imaging assessing viability in patients with chronic ventricular dysfunction due to coronary artery disease: a meta-analysis of prospective trials. JACC Cardiovasc Imaging 2012;5:494-508.

26. Ugander M, Oki AJ, Hsu LY, Kellman P, Greiser A, Aletras AH, Sibley CT, Chen MY, Bandettini WP, Arai AE. Extracellular volume imaging by magnetic resonance imaging provides insights into overt and sub-clinical myocardial pathology. Eur Heart J 2012;33:1268-1278.

27. Husser O, Chaustre F, Sanchis J, Nunez J, Monmeneu JV, Lopez-Lereu MP, Bonanad C, Gomez C, Oltra R, Llacer A, Riegger GA, Chorro FJ, Bodi V. Function of remote non-infarcted myocardium after STEMI: analysis with cardiovascular magnetic resonance. Int J Cardiovasc Imaging 2012;28:2057-2064.

28. Espe EK, Aronsen JM, Eriksen GS, Zhang L, Smiseth OA, Edvardsen T, Sjaastad I, Eriksen M. Assessment of regional myocardial work in rats. Circ Cardiovasc Imaging 2015;8:e002695.

29. Espe EKS, Aronsen JM, Eriksen M, Sejersted OM, Zhang L, Sjaastad I. Regional Dysfunction After Myocardial Infarction in Rats. Circ Cardiovasc Imaging 2017;10.

PART II

Imaging modalities in arrythmias

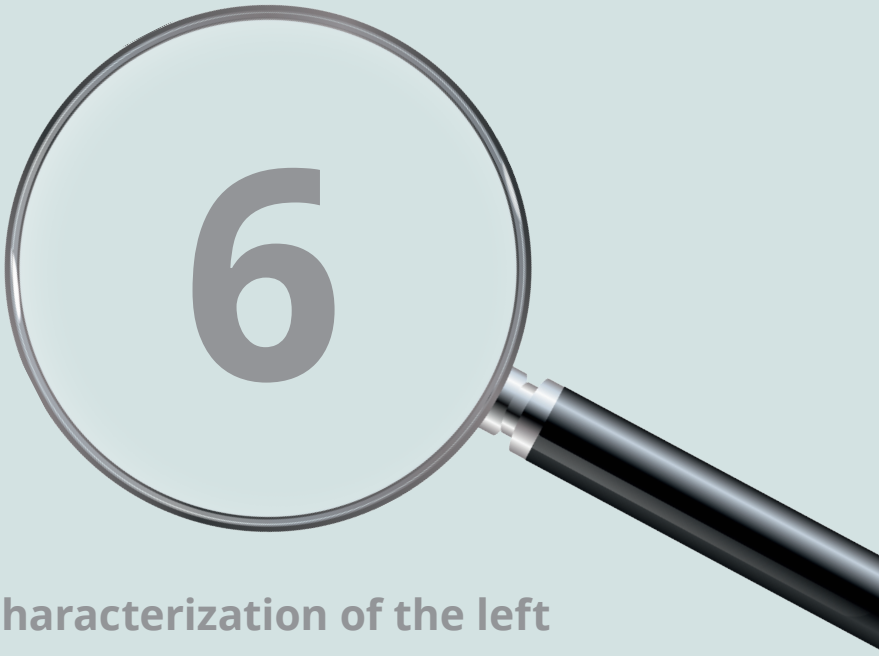

6

Characterization of the left ventricular arrhythmogenic substrate with multimodality imaging: role of innervation imaging and left ventricular global longitudinal strain

El Mahdiui M, Smit JM, van Rosendael AR, Delgado V, Ajmone Marsan N, Jukema JW, Scholte AJHA, Bax JJ.

Eur J Hybrid Imaging. 2019 Aug;3:14.

Abstract

Even though implantable cardioverter defibrillator (ICD) implantation for primary prevention has shown to reduce the risk of sudden cardiac death in chronic heart failure patients with reduced left ventricular ejection fraction (LVEF), a significant portion of these patients will never receive appropriate ICD therapy. We aimed to functionally characterize the arrhythmogenic substrate using left ventricular (LV) global longitudinal strain (GLS) and heart-to-mediastinum (H/M) ratio on ^{123}I-meta-iodobenzylguanidine (^{123}I-MIBG) scintigraphy. We included patients with heart failure with reduced LVEF who received an ICD for primary prevention. To functionally characterize the arrhythmogenic substrate we measured the LV GLS with two-dimensional speckle tracking echocardiography and cardiac innervation measured as the H/M ratio on ^{123}I-MIBG scintigraphy. An event was defined as appropriate ICD therapy. A total of 155 patients were included, 74% were male and the mean age was 72±9 years. During a median follow-up of 10 (6-12) years, 43 patients (28%) experienced appropriate ICD therapy. Patients that experienced an event were more often male, had more often ischemic cardiomyopathy and were more likely to have worse renal function. There was no difference in the left ventricular ejection fraction (LVEF) between the two groups (25±6.4% vs 26±6.0%; p=0.276). However, LV GLS was significantly more impaired in the group that experienced an event compared to patients that did not (-6.7±2.1% vs -7.6±2.1%; p=0.020). The innervation, measured as the H/M ratio on ^{123}I-MIBG scintigraphy was also significantly more impaired in the patients that experienced and event compared to patients that did not (1.34±0.2 vs 1.47±0.2; p≤0.001). Multivariable Cox regression analysis showed LV GLS and H/M ratio independently associated with appropriate ICD therapy with a hazard ratio of 1.24 (95% CI 1.027-1.491, p=0.025) and 5.71 (95% CI 1.135-28.571, p=0.034), respectively. LV GLS and H/M ratio were significantly correlated (Pearson correlation coefficient -0.30, p<0.001). In conclusion, functionally characterizing the arrhythmogenic substrate using different imaging technics defines the risk for appropriate ICD therapy, whereas LVEF did not.

INTRODUCTION

Evaluation of heart failure patients who may benefit from implantable cardioverter defibrillator (ICD) remains challenging. Current guidelines recommend an ICD implantation as primary prevention in symptomatic heart failure patients with a left ventricular ejection fraction (LVEF) ≤ 35% treated with optimal medical therapy[1]. However, around 40% of these patients receiving an ICD will not develop ventricular arrhythmias that can be appropriately treated with the ICD[2]. Therefore, a more individualized risk stratification strategy is necessary.

Characterization of the anatomical and functional substrate that may lead to re-entrant ventricular tachycardia and sudden cardiac death has been shown feasible with various imaging techniques[3]. Anatomically, the arrhythmogenic substrate is characterized by bundles of scar, fibrous tissue intermingled with viable myocardium[4,5]. Functionally, the arrhythmogenic substrate is characterized by heterogeneous regional contraction and denervated myocardium[6,7,8]. Transient factors, such as ischemia, can influence this arrhythmogenic substrate and serve as trigger for re-entry tachyarrhythmias. Left ventricular (LV) global longitudinal strain (GLS) measured with two-dimensional (2D) speckle tracking echocardiography describes better than LVEF the heterogeneous contraction of the LV myocardium and has been associated with LV myocardial scar burden[9,10,11]. In addition, in ischemic heart failure, the value of longitudinal strain of the peri-infarct zone has been associated with appropriate ICD therapy[12]. Sympathetic myocardial innervation can be assessed with ^{123}I-meta-iodobenzylguanidine (^{123}I-MIBG) scintigraphy. This radiotracer is an analogue of norepinephrine up-taken by the sympathetic nerve terminals of the heart, without being metabolized. In heart failure patients, the uptake of ^{123}I-MIBG by the heart is reduced, indicating myocardial denervation. A reduced heart-to-mediastinum (H/M) ratio of the ^{123}I-MIBG uptake on planar imaging has been associated with increased risk of ventricular arrhythmic events[7,13]. So far, there is no study using multimodality imaging to functionally assess the arrhythmogenic substrate.

The aim of the present study was to functionally characterize the arrhythmogenic substrate of heart failure patients receiving an ICD by measuring LV GLS and the H/M ratio on planar ^{123}I-MIBG scintigraphy imaging and study the differences between patients presenting with appropriate ICD therapies and patients without.

Methods

Patients and clinical evaluation

Heart failure patients who received an ICD for primary prevention, according to prevailing guidelines[1], and who underwent a ^{123}I-MIBG scintigraphy between 2004 and 2017 at the Leiden University Medical Centre (The Netherlands) were retrospectively evaluated. Demographic and clinical characteristics were collected using the departmental cardiology information system (EPD-vision; Leiden University Medical Centre, Leiden, The Netherlands) and electronic medical records (HiX; ChipSoft, Amsterdam, The Netherlands) and retrospectively analysed. Echocardiographic data were stored in the echocardiographic database and the planar ^{123}I-MIBG scintigraphy data in the department of nuclear medicine database. Clinical, echocardiographic and ^{123}I-MIBG scintigraphy data were analysed retrospectively. The association between clinical, conventional and advanced (2D speckle tracking imaging) echocardiographic variables and ^{123}I-MIBG variables and ventricular arrhythmic events was investigated. For retrospective analysis of clinically acquired data anonymously handled, the institutional review board waved the need for written patient informed consent. For a subgroup of patients, the 123I-MIBG scintigraphy was performed under a prospective study (NCT01940081) and the patients provided written informed consent.

Transthoracic echocardiography: conventional and speckle tracking analysis

Transthoracic echocardiography was performed with the patients at rest, in left lateral decubitus position using a commercially available system (Vivid 7 and E9, GE Healthcare, Horten, Norway). Bimodal, M-mode, colour, continuous and pulsed wave Doppler data were acquired with 3.5 MHz or M5S transducers and digitally stored in cine-loop format. Offline analysis was performed using the EchoPac system (version BT13, GE Medical Systems, Horten, Norway). Left ventricular end-diastolic volume (LVEDV) and left ventricular end-systolic volume (LVESV) were measured on the apical 2- and 4-chamber views according to the Simpson biplane method and the LVEF was calculated.

Using 2D speckle tracking echocardiography, the LV GLS was measured. After manually tracing the endocardial border of the left ventricle in the long-axis, 2- and 4-chamber views, the regions of interest (ROI) were automatically created and adjusted to the thickness of the myocardium. The software automatically tracks

the myocardium throughout the cardiac cycle and the quality of the tracking is evaluated. The LV GLS was calculated as the average of the peak systolic longitudinal strain of the 3 apical views and the results were displayed in a 17-segment "bull's-eye" plot.

^{123}I-MIBG scintigraphy data acquisition and analysis

For assessment of myocardial innervation, 185 MBq of ^{123}I-MIBG (AdreView, GE Healthcare, Princeton, NJ, USA) were injected intravenously, after thyroid blockage with sodium iodide. Using a dual-head gamma camera (GCA-7200, Toshiba Corp., Tokyo, Japan) equipped with a low-energy high-resolution collimators, planar anterior images of the thorax were obtained 4h (late) after tracer injection. Images were obtained with a 15% energy window centred at the 159 keV energy peak of 123I and were subsequently stored in a 256x256 matrix.

A ROI was manually drawn over the entire heart to measure the counts in the LV myocardial region. To measure the counts in de mediastinal region, a rectangular ROI was placed on the upper half of the mediastinum using the lung apex, upper cardiac border and medial contours of the lungs as borders. The late H/M ratio was calculated by dividing the mean counts in the cardiac ROI by the mean counts in the mediastinal ROI. The analysis was performed using dedicated post-processing software on a Syngo-MI workstation (Siemens Medical Solutions, Malvern, PA, USA).

Follow-up

Patients were followed-up at the heart failure outpatient clinic and the ICD devices were interrogated on 6-monthly visits. The ICD ventricular tachyarrhythmia detection criteria and therapy were programmed conventionally. The occurrence of appropriate ICD therapy was the primary endpoint. Appropriate ICD therapy was defined as anti-tachycardia pacing or shock for ventricular tachycardia or ventricular fibrillation.

Statistical analysis

Continuous variables are reported as mean±standard deviation if normally distributed, and as median and 25-75% interquartile range (IQR) if non-normally distributed. Categorical data are presented as frequencies and percentages. Patients were divided in two groups according to the occurrence of an event, appropriate ICD therapy or not. Continuous data were compared between patients

presenting with event and patients without event using the Student's t test or the Mann-Whitney U test. Categorical data were compared with the $\chi 2$ test. Cox proportional hazards regression analysis were used to evaluate the variables that were significantly associated with appropriate ICD therapy. The relationship between LV GLS and H/M ratio was investigated using Pearson correlation. A p-value <0.05 was considered statistically significant. All statistical analyses were performed using the SPSS software package (IBM Corp. Released 2015. IBM SPSS Statistics for Windows, Version 23.0. Armonk, NY, USA: IBM Corp.).

Results

A total of 155 patients with ^{123}I-MIBG scintigraphy and echocardiography with LV GLS data were included (74% were male and the mean age was 72±9 years). During a median follow-up of 10 years (25-75% IQR 6-12 years), appropriate ICD therapy occurred in 43 patients (28%). An ICD shock was the first appropriate ICD therapy in 70% of the cases. Table 1 shows the baseline clinical characteristics for the total population and the patients who did or did not experience an appropriate ICD therapy. The majority of patients referred had New York Heart Association (NYHA) functional class II or III heart failure symptoms. The two groups of patients were comparable in various demographic and clinical characteristics.

Table 1. Patient clinical characteristics

	ALL PATIENTS (N=155)	PATIENTS WITHOUT APPROPRIATE ICD THERAPY (N=112)	PATIENTS WITH APPROPRIATE ICD THERAPY (N=43)	P-VALUE
Clinical characteristics				
Age	72 ± 8.9	72 ± 8.7	71 ± 9.3	0.700
Male, n(%)	115(74)	79(71)	36(84)	0.093
NYHA functional class, n(%)				0.817
I	21(14)	16(14)	5(12)	
II	51(33)	35(31)	16(37)	
III/IV	80(52)	59(53)	21(49)	
Ischemic cardiomyopathy, n(%)	88 (57)	60 (54)	28(65)	0.194

Table 1. Continued.

	ALL PATIENTS (N=155)	PATIENTS WITHOUT APPROPRIATE ICD THERAPY (N=112)	PATIENTS WITH APPROPRIATE ICD THERAPY (N=43)	P-VALUE
Devices				
ICD, n(%) CRT-D, n(%)	51(33) 104(67)	36(32) 76(68)	15(35) 28(65)	0.745
Cardiovascular risk factors				
Dyslipidemia , n(%)	44(28)	30(27)	14(33)	0.475
Diabetes , n(%)	25 (16)	19(17)	6(14)	0.648
Hypertension, n(%)	57(37)	41(37)	16(37)	0.945
Smoking, n(%)	35 (23)	25(22)	10(23)	0.901
Medication				
ACE-I/ARB's, n(%)	132(85)	97(87)	35(81)	0.414
Diuretics, n(%)	115(74)	79(71)	36(84)	0.093
Beta-blockers, n(%) -Sotalol	118 (76) 5(4)	83(74) 4(4)	35(81) 1(2)	0.341 1.000
Calcium-blockers, n(%)	77(50)	55(49)	22(51)	0.819
Amiodarone, n(%)	30(19)	23(21)	7(16)	0.548
Digoxin, n(%)	17(11)	14(13)	3(7)	0.325
Statin, n(%)	97(63)	70(63)	27(63)	0.973
Anti-diabetic medication, n(%)	83(54)	58(52)	25(58)	0.478
Laboratory results				
Creatinine (mmol/L)	101±32	100±31	105±35	0.368
Hematocrit (%)	41.6±3.3	41.6±3.3	41.5±3.5	0.887

Values are mean ± standard deviation or n (%).
ACE-I = angiotensin converting enzyme inhibitor; ARB's = angiotensin II receptor blockers; CRT-D = cardiac resynchronization therapy defibrillator; ICD = implantable cardioverter defibrillator; NYHA = The New York Heart Association.

The imaging characteristics are shown in Table 2. Patients with an event had significantly larger LVEDV as compared to patients without an event. However, the groups were comparable in terms of LVEF (25±6.4% vs 26±6.0%; p=0.276). In contrast, patients who presented with an event showed significantly more impaired LV GLS compared to their counterparts (-6.7±2.1% vs -7.6±2.1%; p=0.020, Figure 1). In the planar ^{123}I-MIBG data, the late H/M ratio was significantly lower in the group of patients who experienced an event compared to the group who did not (1.34±0.2 vs

1.47±0.2; p≤0.001, Figure 1). Multivariate Cox regression analysis showed LV GLS and H/M ratio to be independent predictors of appropriate ICD therapy, with a Hazard ratio of 1.24 (95% CI 1.027-1.491, p=0.025) for LV GLS and 5.71 (95% CI 1.135-28.571, p=0.034) for H/M ratio when corrected for LVEDV, LVEF, LV GLS and H/M ratio.

Table 2. LV GLS and ^{123}I-MIBG characteristics

	ALL PATIENTS (N=155)	PATIENTS WITHOUT APPROPRIATE ICD THERAPY (N=112)	PATIENTS WITH APPROPRIATE ICD THERAPY (N=43)	P-VALUE
Two-dimensional echocardiography				
Left ventricular end-diastolic volume, (ml)	247 ± 87	236 ± 83	274 ± 90	**0.017**
Left ventricular end-systolic volume, (ml)	186 ± 72	181 ± 71	201 ± 73	0.117
Left ventricular ejection fraction, (%)	25 ± 6.3	25 ± 6.4	26 ± 6.0	0.276
Left ventricular GLS, (%)	-7.4 ± 2.2	-7.6 ± 2.1	-6.7 ± 2.2	**0.020**
^{123}I-MIBG SPECT				
Heart mediastinum ratio late	1.43 ± 0.2	1.47 ± 0.2	1.34 ± 0.2	**<0.001**

Bold indicates statistical significance of p-value <0.05
Values are mean ± standard deviation.
^{123}I-MIBG = 123I-meta-iodobenzylguanidine; GLS = global longitudinal strain.

Fig. 1 Example of H/M-ratio and LV GLS

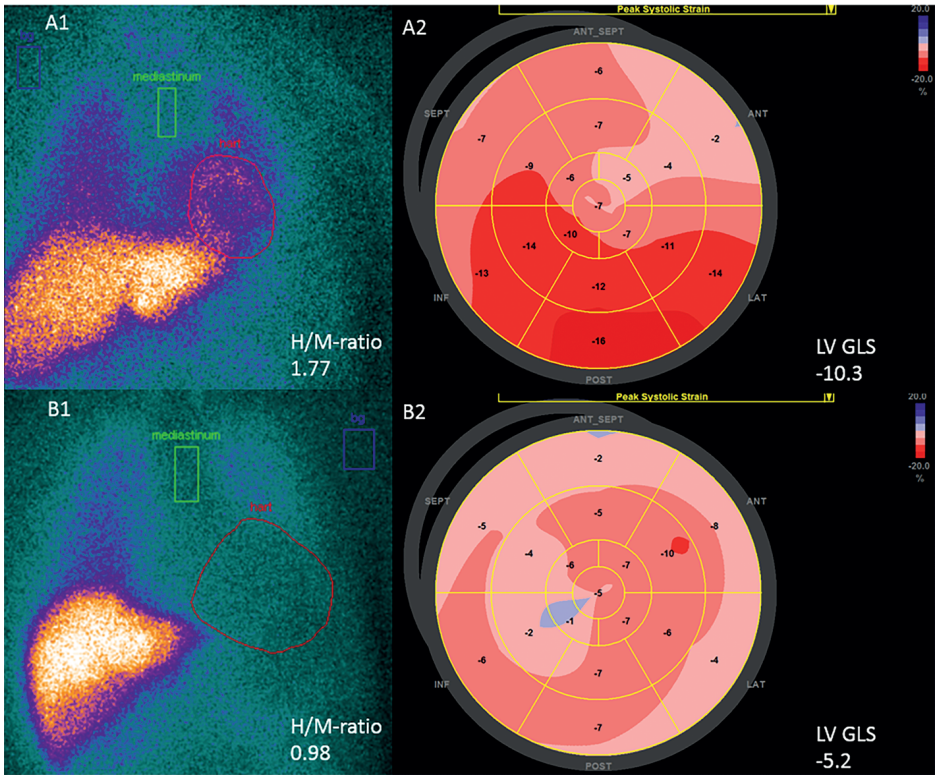

Example of heart-to-mediastinum (H/M) ratio on planar images (A1 and B1) and left ventricular (LV) global longitudinal strain (GLS) (A2 and B2) of two patients. Patient A , 70 years old male, with ischemic cardiomyopathy, left ventricular ejection fraction (LVEF) 34%. Patient B, 72 years old male, with ischemic cardiomyopathy, LVEF 25%. Patient A did not experience an event, whereas patient B experienced appropriate ICD therapy.

There was a moderate, but significant correlation between LV GLS and H/M ratio (r=0.30, p<0.001, Figure 2). This correlation remained significant in the group that did not experience an event (r=-0.21, p=0.027) and was stronger in the group that did experience an event (r=-0.50, p=0.002). (Figure 2)

Fig. 2 Correlation between H/M-ratio and LV GLS

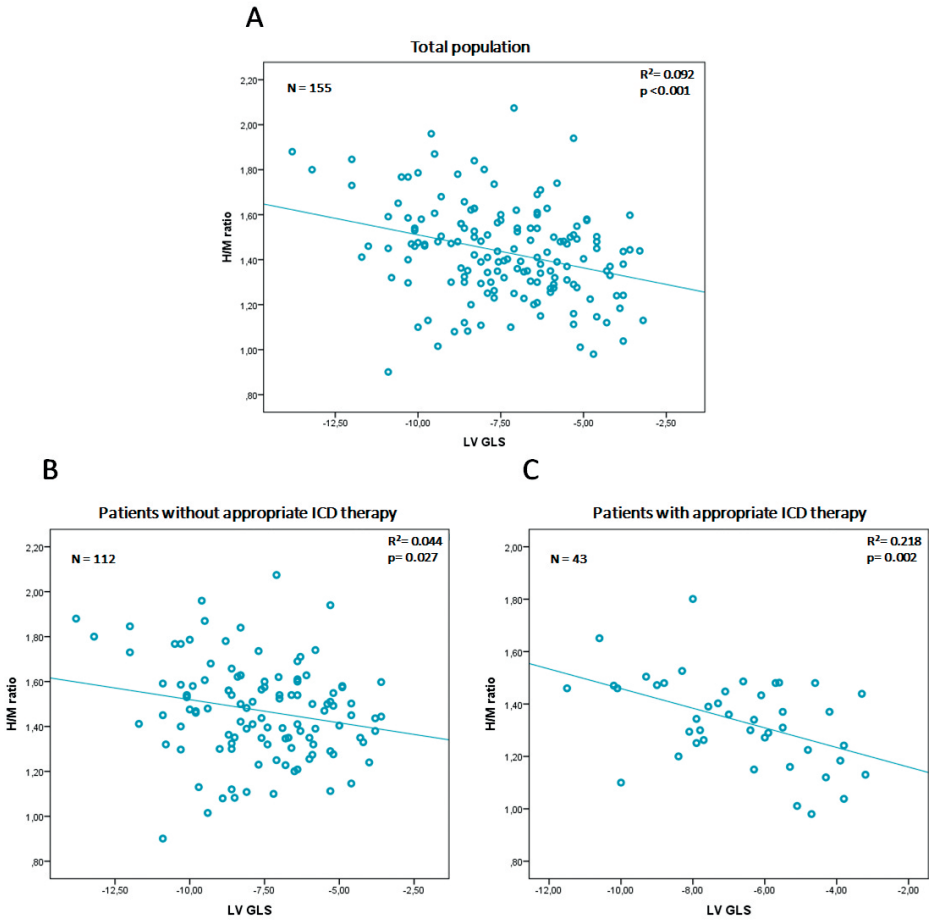

Correlation between heart-to-mediastinum (H/M) ratio and left ventricular global longitudinal strain (LV GLS) in the total population (A), patients that did not experience an event (B) and patients that did experience an event (C). There was a significant correlation between H/M ratio and LV GLS using the Pearson correlation coefficient for the total population (r=0.30, p<0.001), patients that did not experience an event (r=-0.21, p=0.027) and those that did (r=-0.50, p=0.002).

Discussion

Despite showing similar LVEF, heart failure patients experiencing appropriate ICD therapy showed more impaired LV systolic function when measured with 2D speckle tracking GLS and more impaired myocardial innervation as assessed with ^{123}I-MIBG scintigraphy. These results provide additional evidence on the limited value of LVEF to identify heart failure patients who will benefit from an ICD.

Assessment of arrhythmogenic substrate

The structural LV changes that underlie heart failure with reduced LVEF include expansion of extracellular matrix with increase of collagen and fibroblasts. Scar or fibrotic tissue (bundles of collagen) are not per se pro-arrhythmic since they are electrically inert tissue. However, the areas where the fibrous/scar tissue intermingles with viable myocytes create a substrate where re-entry circuits may form and lead to ventricular arrhythmias[15]. After myocardial infarction, this area is known as border zone.

The border zone can be characterized using different imaging modalities. On late gadolinium contrast enhanced cardiovascular magnetic resonance (LGE CMR), the border zone shows intermediate signal intensity between normal myocardium and dense myocardial scar. Applying specific thresholds, the amount of border zone can be quantified. In 91 patients with ischemic heart disease and indication for ICD implantation as primary prevention, Roes et al demonstrated that each 10 g increase in the mass of border zone was associated with 51% increased risk of ventricular arrhythmias and appropriate ICD shocks[16]. The functional properties of the scar zone, border zone and normal myocardium can be evaluated with 2-dimensional speckle tracking echocardiography and the measurement of LV regional longitudinal strain. In ischemic heart failure, LV segments with values of longitudinal strain more impaired than -4.5% (less negative) have been shown to correspond to areas of transmural scar (sensitivity 81.2% and specificity 81.6%)[17]. The areas surrounding the LV segments with a value of longitudinal strain more negative than -4.5%, can be considered border zone. In 424 ischemic heart failure patients who received an ICD as primary prevention, Ng et al showed that the occurrence of ventricular arrhythmias and appropriate ICD shocks during follow-up was more frequent as the longitudinal strain of the border zone was more impaired (hazard ratio 1.25)[12]. The present study provides additional evidence on the

association between impaired LV GLS and occurrence of appropriate ICD therapies. More impaired LV GLS reflects larger burden of myocardial fibrosis which may lead to areas of slow conduction and conduction block and favour the formation of re-entry circuits and ventricular arrhythmias. In addition, the association between LV GLS and sudden cardiac death, ventricular arrhythmias or appropriate ICD therapy has been also demonstrated in previous studies including 988 patients with acute myocardial infarction and LVEF>35% in 91% of them[8]. On multivariate analysis, LV GLS was independently associated with the occurrence of sudden cardiac death or ventricular arrhythmias with a hazard ratio of 1.24, similar to the hazard ratio reported in the current study.

Moreover, the border zone is also characterized by viable myocardium with abnormal innervation. Previous studies have shown that in ischemic cardiomyopathy patients the areas of denervation exceed the area of perfusion defects on single photon emission tomography (SPECT)[18,19,20]. The higher susceptibility of sympathetic nerve fibres to ischemia compared to myocytes leads to larger areas of denervation than scar after myocardial infarction (denervation-perfusion mismatch)[18,21,22]. By assessing myocardial denervation with ^{123}I-MIBG SPECT and myocardial perfusion with ^{99m}Technetium-tetrofosmin SPECT, the mismatch can be quantified. Patients with larger areas of denervation-perfusion mismatch have shown higher incidence of ventricular arrhythmia events[6]. Using planar ^{123}I-MIBG scintigraphy, the AdreView Myocardial Imaging for Risk Evaluation in Heart Failure (ADMIRE-HF) study, the largest study so far including 964 heart failure patients followed for 2 years, showed that patients with an H/M ratio between 1.2 and 1.6 had more frequent ventricular arrhythmic events as compared to patients with an H/M ratio ≥1.6[7]. This parameter reflects the global cardiac sympathetic innervation rather than characterizing the border zone where the re-entrant ventricular arrhythmias may start. In the present study, patients who received appropriate ICD therapy showed more impaired H/M ratio compared to those who remain without event.

The correlation between LV GLS and H/M ratio was moderate, indicating the distinct differences between both modalities. Our findings are in agreement with previously published studies, who found similar correlations between LV GLS and H/M ratio[23,24].

In clinical practice combination of multimodality imaging to characterize the arrhythmogenic substrate from the anatomical and functional point of view may be important to accurately identify the patients who will benefit from an ICD implantation. The present study provides further evidence on the importance of such characterization by combining speckle tracking echocardiography and innervation imaging.

Study limitations

There are several limitations that should be acknowledged. First, this was a retrospective, single-centre study. Furthermore, since 2D speckle tracking echocardiography requires good image quality for reliable analysis, selection bias might have been introduced. The patient population was heterogeneous, with ischemic and non-ischemic cardiomyopathy patients. Also, ischemia might have risen during the long follow-up of the study and have influenced the results. Finally, the event rate for appropriate ICD therapy in our population was relatively low compared to previous study[2]. This might be reflected by the difference in study populations.

Conclusions

In conclusion, LV GLS measured by 2D speckle tracking echocardiography and H/M ratio measured by planar ^{123}I-MIBG SPECT were significantly more impaired in patients who experienced an appropriate ICD therapy compared to patients that did not. In contrast, no differences were observed between groups of patients in terms of LVEF. Multivariate Cox regression analysis showed LV GLS and H/M ratio to be independent predictors of appropriate ICD therapy. These results underscore the importance of multimodality imaging for the characterization of the arrhythmogenic substrate and the identification of patients who will benefit from an ICD.

REFERENCES

1. Priori SG, Blomstrom-Lundqvist C, Mazzanti A, Blom N, Borggrefe M, Camm J, et al. 2015 ESC Guidelines for the management of patients with ventricular arrhythmias and the prevention of sudden cardiac death: The Task Force for the Management of Patients with Ventricular Arrhythmias and the Prevention of Sudden Cardiac Death of the European Society of Cardiology (ESC). Endorsed by: Association for European Paediatric and Congenital Cardiology (AEPC). Eur Heart J 2015;36:2793-2867.
2. Moss AJ, Greenberg H, Case RB, Zareba W, Hall WJ, Brown MW, et al. Long-term clinical course of patients after termination of ventricular tachyarrhythmia by an implanted defibrillator. Circulation 2004;110:3760-3765.
3. Bertini M, Schalij MJ, Bax JJ, Delgado V. Emerging role of multimodality imaging to evaluate patients at risk for sudden cardiac death. Circ Cardiovasc Imaging 2012;5:525-535.
4. Lin LY, Su MY, Chen JJ, Lai LP, Hwang JJ, Tseng CD, et al. Conductive channels identified with contrast-enhanced MR imaging predict ventricular tachycardia in systolic heart failure. JACC Cardiovasc Imaging 2013;6:1152-1159.
5. Fernandez-Armenta J, Berruezo A, Andreu D, Camara O, Silva E, Serra L, et al. Three-dimensional architecture of scar and conducting channels based on high resolution ce-CMR: insights for ventricular tachycardia ablation. Circulation Arrhythmia and electrophysiology 2013;6:528-537.
6. Boogers MJ, Borleffs CJ, Henneman MM, van Bommel RJ, van Ramshorst J, Boersma E, et al. Cardiac sympathetic denervation assessed with 123-iodine metaiodobenzylguanidine imaging predicts ventricular arrhythmias in implantable cardioverter-defibrillator patients. J Am Coll Cardiol 2010;55:2769-2777.
7. Jacobson AF, Senior R, Cerqueira MD, Wong ND, Thomas GS, Lopez VA, et al. Myocardial iodine-123 meta-iodobenzylguanidine imaging and cardiac events in heart failure. Results of the prospective ADMIRE-HF (AdreView Myocardial Imaging for Risk Evaluation in Heart Failure) study. J Am Coll Cardiol 2010;55:2212-2221.
8. Ersboll M, Valeur N, Andersen MJ, Mogensen UM, Vinther M, Svendsen JH, et al. Early echocardiographic deformation analysis for the prediction of sudden cardiac death and life-threatening arrhythmias after myocardial infarction. JACC Cardiovasc Imaging 2013;6:851-860.
9. Bello D, Fieno DS, Kim RJ, Pereles FS, Passman R, Song G, et al. Infarct morphology identifies patients with substrate for sustained ventricular tachycardia. J Am Coll Cardiol 2005;45:1104-1108.
10. Schmidt A, Azevedo CF, Cheng A, Gupta SN, Bluemke DA, Foo TK, et al. Infarct tissue heterogeneity by magnetic resonance imaging identifies enhanced cardiac arrhythmia susceptibility in patients with left ventricular dysfunction. Circulation 2007;115:2006-2014.
11. Gulati A, Jabbour A, Ismail TF, Guha K, Khwaja J, Raza S, et al. Association of fibrosis with mortality and sudden cardiac death in patients with nonischemic dilated cardiomyopathy. JAMA 2013;309:896-908.
12. Ng AC, Bertini M, Borleffs CJ, Delgado V, Boersma E, Piers SR, et al. Predictors of death and occurrence of appropriate implantable defibrillator therapies in patients with ischemic cardiomyopathy. Am J Cardiol 2010;106:1566-1573.

13. Nagahara D, Nakata T, Hashimoto A, Wakabayashi T, Kyuma M, Noda R, et al. Predicting the need for an implantable cardioverter defibrillator using cardiac metaiodobenzylguanidine activity together with plasma natriuretic peptide concentration or left ventricular function. J Nucl Med 2008;49:225-233.

14. Lang RM, Badano LP, Mor-Avi V, Afilalo J, Armstrong A, Ernande L, et al. Recommendations for cardiac chamber quantification by echocardiography in adults: an update from the American Society of Echocardiography and the European Association of Cardiovascular Imaging. J Am Soc Echocardiogr 2015;28:1-39.e14.

15. Morita N, Mandel WJ, Kobayashi Y, Karagueuzian HS. Cardiac fibrosis as a determinant of ventricular tachyarrhythmias. Journal of arrhythmia 2014;30:389-394.

16. Roes SD, Borleffs CJ, van der Geest RJ, Westenberg JJ, Marsan NA, Kaandorp TA, et al. Infarct tissue heterogeneity assessed with contrast-enhanced MRI predicts spontaneous ventricular arrhythmia in patients with ischemic cardiomyopathy and implantable cardioverter-defibrillator. Circ Cardiovasc imaging 2009;2:183-190.

17. Roes SD, Mollema SA, Lamb HJ, van der Wall EE, de Roos A, Bax JJ. Validation of echocardiographic two-dimensional speckle tracking longitudinal strain imaging for viability assessment in patients with chronic ischemic left ventricular dysfunction and comparison with contrast-enhanced magnetic resonance imaging. Am J Cardiol 2009;104:312-317.

18. Matsunari I, Schricke U, Bengel FM, Haase HU, Barthel P, Schmidt G, et al. Extent of cardiac sympathetic neuronal damage is determined by the area of ischemia in patients with acute coronary syndromes. Circulation 2000;101:2579-2585.

19. Gimelli A, Masci PG, Liga R, Grigoratos C, Pasanisi EM, Lombardi M, et al. Regional heterogeneity in cardiac sympathetic innervation in acute myocardial infarction: relationship with myocardial oedema on magnetic resonance. Eur J Nucl Med Mol Imaging 2014;41:1692-1694.

20. Bax JJ, Kraft O, Buxton AE, Fjeld JG, Parizek P, Agostini D, et al. 123 I-mIBG scintigraphy to predict inducibility of ventricular arrhythmias on cardiac electrophysiology testing: a prospective multicenter pilot study. Circ Cardiovasc Imaging 2008;1:131-140.

21. Zipes DP. Influence of myocardial ischemia and infarction on autonomic innervation of heart. Circulation 1990;82:1095-1105.

22. McGhie AI, Corbett JR, Akers MS, Kulkarni P, Sills MN, Kremers M, et al. Regional cardiac adrenergic function using I-123 meta-iodobenzylguanidine tomographic imaging after acute myocardial infarction. Am J Cardiol 1991;67:236-242.

23. Bulten BF, Verberne HJ, Bellersen L, Oyen WJ, Sabate-Llobera A, Mavinkurve-Groothuis AM, et al. Relationship of promising methods in the detection of anthracycline-induced cardiotoxicity in breast cancer patients. Cancer Chemother Pharmacol 2015;76:957-967.

24. Cruz MC, Abreu A, Portugal G, Santa-Clara H, Cunha PS, Oliveira MM, et al. Relationship of left ventricular global longitudinal strain with cardiac autonomic denervation as assessed by (123)I-mIBG scintigraphy in patients with heart failure with reduced ejection fraction submitted to cardiac resynchronization therapy : Assessment of cardiac autonomic denervation by GLS in patients with heart failure with reduced ejection fraction submitted to CRT. J Nucl Cardiol 2019;26:869-879.

Posterior left atrial adipose tissue attenuation assessed by computed tomography and recurrence of atrial fibrillation after catheter ablation

El Mahdiui M, Simon J, Smit JM, Kuneman JH, van Rosendael AR, Steyerberg EW, van der Geest RJ, Száraz L, Herczeg S, Szegedi N, Gellér L, Delgado V, Merkely B, Bax JJ, Maurovich-Horvat P.

Circ Arrhythm Electrophysiol. 2021 Apr;14(4):e009135.

ABSTRACT

Atrial fibrillation (AF) recurrence following catheter ablation remains high. Recent studies have shown a relation between epicardial adipose tissue (EAT) and AF. EAT secretes several pro- and anti-inflammatory adipokines that directly interact with the adjacent myocardium. The aim of the current study was to evaluate whether posterior left atrial (LA) adipose tissue attenuation, as marker of inflammation, is related to AF recurrences after catheter ablation. Consecutive patients with symptomatic AF referred for first AF catheter ablation who underwent CT were included. The total EAT and posterior LA adipose tissue were manually traced and adipose tissue was automatically recognized as tissue with Hounsfield units (HU) between -195 and -45. The attenuation value of the posterior LA adipose tissue was assessed and the population divided according to the mean HU value (-96.4 HU). In total, 460 patients (66% male, age 61 ± 10 years) were included in the analysis. After a median follow-up of 18 months (IQR 6-32), 168 (37%) patients had AF recurrence. Patients with higher attenuation (≥-96.4 HU) of the posterior LA adipose tissue showed higher AF recurrence rates compared to patients with lower attenuation (<-96.4 HU) (log-rank test p=0.046). Univariate analysis showed an association between AF recurrence and higher posterior LA adipose tissue attenuation (≥-96.4 HU) (p<0.05). On multivariable analysis posterior LA adipose tissue attenuation (HR 1.26; 95% CI 0.90-1.76; p=0.181) remained a promising predictor of AF recurrence following catheter ablation. In conclusion, posterior LA adipose tissue attenuation is a promising predictor of AF recurrence in patients who undergo catheter ablation. Higher adipose tissue attenuation might signal increased local inflammation and serve as an imaging biomarker of increased risk of AF recurrence.

INTRODUCTION

Atrial fibrillation (AF) remains the most prevalent arrhythmic disease worldwide and is associated with increased morbidity and mortality. Currently it is projected that AF prevalence will continue to rise, which is partially explained by increasing prevalence of obesity worldwide. Body mass index (BMI) is related to new-onset AF and patients with weight loss have reduced AF burden, symptom severity and less AF recurrences following AF catheter ablation.[1,2] However, AF recurrence rates are high following AF catheter ablation and adequate patient selection is crucial.[3] Recently, the relation between epicardial adipose tissue (EAT) surrounding the myocardium and AF has been reported.[4,5] EAT is a unique energy depot and is composed of adipocytes, stromovascular cells, immune cells, ganglia and interconnecting nerves.[6] There is no fascial layer separating the EAT and the myocardium which allows for direct paracrine and vasocrine effects on the myocardium.[6] This is important since EAT secretes both pro- and anti-inflammatory adipokines and direct effect on the myocardium has been demonstrated.[4] Computed tomography (CT) attenuation values for adipose tissue range between -195 and -45 Hounsfield units (HU).[7] Inflammation shifts the attenuation of the adipose tissue from a more lipid phase, closer to -195 HU, towards a more aqueous phase, closer to -45 HU. Attenuation of EAT on CT as a marker of inflammation has been linked to culprit coronary lesions in acute coronary syndrome[8] and cardiac mortality[9]. One study suggested a correlation between AF recurrence after AF catheter ablation and higher EAT attenuation, i.e. closer to -45 HU, obtained from one slice on a four-chamber view.[10] Volumetric assessment of EAT however may further increase accuracy since variability exists in EAT thickness at different myocardial regions.[11] Furthermore, recent studies have demonstrated that adipose tissue posterior to the left atrium (LA) had the strongest relationship with AF.[12,13] Whether the posterior LA adipose tissue mass and/or attenuation are related to AF recurrence following AF catheter ablation is evaluated in the current study.

METHODS

Patient population

The data that support the findings of this study are available upon reasonable request to the corresponding author. Consecutive patients with symptomatic AF who underwent preprocedural CT imaging for a first AF catheter ablation between January 2014 and June 2018 at the Heart and Vascular Center of the Semmelweis University Hungary, were included. CT was performed for evaluation of LA anatomical characteristics and location of pulmonary veins. Patients with uninterpretable CT images or who did not undergo a catheter ablation procedure after CT were excluded. Patients were followed at the outpatient clinic and a three month blanking period was implemented for AF recurrence following catheter ablation. Outpatient clinical visits were scheduled at 3, 6 and 12 months and at least yearly thereafter or when patients experienced symptoms. Follow-up visits included clinical assessment, 12-lead ECG and 24h Holter monitoring. Recurrence was prospectively recorded in the electronical medical records and defined as documented AF or atrial tachycardia episode lasting for more than 30seconds. Echocardiographic data, including left ventricular ejection fraction (LVEF) and E/A-ratio were collected from the echocardiographic database. Demographic and clinical data were collected from the electronic medical records. For retrospective analysis of clinically acquired data, the institutional review board waived the need of written patient informed consent. All data used for this study were acquired for clinical purposes and handled anonymously.

CT acquisition

Patients were scanned using a 256-slice CT scanner (Brilliance iCT 256, Phillips Healthcare, Best, The Netherlands) with 270msec rotation-time, 128 x 0.625mm collimation and tube voltage of 100-120kV. Patients were pretreated with beta-blockers if the heart rate exceeded 65 beats per minutes. Four-phasic injection protocol with 85-95ml of iodinated contrast agent was used (Iomeron 400, Bracco Ltd; Milan, Italy) at a rate of 4.5-5.5ml/s. CT was acquired using prospective ECG-gating covering 75 to 81% of the RR-interval. The CT datasets were reconstructed with 0.8mm slice thickness and 0.4mm increment with hybrid iterative reconstruction technique (iDose5, Philips Healthcare, Best, The Netherlands)

CT image and LA adipose tissue analysis

LA adipose tissue measurements were performed using MASS software (Leiden University Medical Centre, Leiden, the Netherlands) as described previously.[14] In short, a cross-sectional view of the LA was obtained from the mitral annulus to the LA roof from reconstructed two-and four-chamber views with a slice thickness of 2mm. The LA adipose tissue located posterior of the LA was manually traced from the base of the LA until the mitral annulus. Adipose tissue was automatically recognized by the software as tissue with HU between -195 and -45 and the mean HU of the adipose tissue was calculated (Figure S1 in Data Supplement). LA volume was calculated on CT images using IntelliSpace Portal (Philips Healthcare, Best, The Netherlands).

Catheter ablation procedure

The indications for performed AF ablation procedures were in accordance with the current guidelines.[15] Paroxysmal AF was defined as self-terminating AF, while persistent AF was defined as AF lasting longer than 7 days.[15] Intravenous fentanyl, midazolam, and propofol were used in all cases for conscious sedation. Femoral venous access was used for all procedures. Transseptal puncture was performed under fluoroscopy positioning and pressure monitoring. Intracardiac echocardiography was used for visualization of the interatrial septum in case of difficulty in performing safe transseptal puncture. An electroanatomical mapping system (CARTO, Biosense Webster, Inc., Diamond Bar, CA, USA or ENSITE, St. Jude Medical, Inc., MN, USA), and left atrial fast anatomical map was merged with the cardiac CT images to guide ablation. Temperature controlled ablation was performed with an irrigated 4mm tip catheter, with an standard target power delivery of 25-35W in the majority of cases. Pulmonary vein isolation was the goal of each initial procedure.

Statistical analysis

Categorical variables are presented as frequencies and percentages. Continuous variables are presented as mean ± standard deviation (SD) if normally distributed and median and interquartile range (IQR) if not normally distributed. Categorical variables were compared using the $\chi 2$ test. Continuous variables were compared using the Student's *t*-test if normally distributed and the Mann-Whitney *U*-test if not normally distributed. The relation of BMI with total EAT, posterior LA adipose tissue mass and attenuation was investigated using Pearson correlation. Recurrent

AF incidence rates were calculated from the end of the blanking period. Kaplan-Meier analysis was performed for cumulative AF recurrence. The study population was divided into two groups according to the mean posterior LA adipose tissue attenuation (-96.4 HU) and compared with a log-rank test. We performed a multivariable Cox proportional-hazards analyses and adjusted posterior LA adipose tissue mass and attenuation for age[16], sex[3], type of AF[3], BMI[2], antiarrhythmic drugs[17], LVEF[18], E/A-ratio[18] and LA volume[19]. Any missing values among these variables were statistically imputed. Four observers independently performed all measurements and were blinded to patient outcome data. Ten patients were randomly selected for inter-observer agreement and analyzed using inter-class correlation coefficient. A p-value <0.05 was considered statistically significant. Statistical analyses were performed using SPSS version 23.0 (SPSS, Armonk, NY, USA).

RESULTS

Patient characteristics

A total of 460 patients (66% male, age 61 ± 10 years) were included in the analysis. Clinical characteristics are shown in Table 1. There were 168 (37%) patients that developed AF recurrence after catheter ablation during a median follow-up period of 18 months (IQR 6-32). Patients with AF recurrence after catheter ablation were older (62 ± 10 vs 60 ± 10 years; p=0.038), more often females (42 vs 30%, p=0.012) and had more often persistent AF (33 vs 18%, p<0.001).

Table 1. Patient characteristics

	Total patients (n=460)	With recurrence (n=168)	No recurrence (n=292)	p-value
Clinical variables				
Age (years)	61±10	62±10	60±10	0.038
Male, n(%)	302 (66)	98 (58)	204 (70)	0.012
BMI (kg/m^2)	29±5	29±5	29±4	0.285
Persistent AF, n(%)	106 (23)	54 (32)	52 (18)	<0.001
Hypertension, n(%)	330 (72)	125 (74)	205 (70)	0.335
Diabetes mellitus, n(%)	70 (15)	22 (13)	48 (16)	0.336
Hyperlipidemia, n(%)	116 (25)	43 (26)	73 (25)	0.887

Table 1. Continued.

	Total patients (n=460)	With recurrence (n=168)	No recurrence (n=292)	p-value
Smoking, n(%)	130 (28)	59 (35)	71 (24)	0.054
Prior myocardial infarction, n(%)	14 (3)	6 (4)	8 (3)	0.689
Medication				
Antiarrhythmic drugs	252 (55)	98 (58)	154 (53)	0.347
β-blocker	147 (32)	53 (32)	94 (32)	0.702
Calcium antagonist	70 (15)	23 (14)	47 (16)	0.393
ACE-I/ARB	144 (31)	51 (30)	93 (32)	0.551
Diuretics	91 (20)	34 (20)	57 (20)	0.996
Statins	164 (36)	64 (38)	100 (34)	0.583
Aspirin	52 (11)	18 (11)	34 (12)	0.660
Coumarins	193 (42)	79 (47)	114 (39)	0.095
DOAC's	153 (33)	55 (33)	98 (34)	0.857
Laboratory findings				
eGFR ml/min/1.73 m2	82 (60-90)	83 (60-90)	80 (60-90)	0.779

Values are mean ± standard deviation if normally distributed and median (interquartile range) if not normally distributed.
ACE-I: angiotensin-converting enzyme inhibitor, AF: atrial fibrillation, ARB: angiotensin receptor blocker, BMI: body mass index, DOAC's: directly acting oral anticoagulants, eGFR: estimated glomerular filtration rate.

Imaging variables

Imaging variables of the total population, patients with and without AF recurrence are shown in Table 2. Patients with AF recurrence had significantly more often LVEF dysfunction (6 vs 2%, P=0.031), larger LA volumes (108 ± 32ml vs 97 ± 24ml, p<0.001) and more often higher attenuation (≥-96.4 HU) of the posterior LA adipose tissue (60 vs 50%, p=0.041). The sensitivity and specificity for the mean posterior LA adipose tissue was 60% and 50%, respectively. There was a weak but significant correlation between BMI and total EAT (r=0.27, p<0.0001) and between BMI and posterior LA adipose tissue mass (r=0.26, p<0.0001). No significant correlation was found for BMI and posterior LA adipose tissue attenuation (r=0.03, p=0.571) (Figure 1).

Table 2. Imaging variables of the total population and stratified according to recurrence

	Total patients (n=460)	With recurrence (n=168)	No recurrence (n=292)	p-value
Echocardiographic variables				
LVEF<50%, n(%)	16 (4)	10 (6)	6 (2)	0.031
E/A-ratio	1.2±0.4	1.2±0.4	1.2±0.4	0.557
CT variables				
LA volume (ml)	101±28	108±32	97±24	<0.001
Posterior LA adipose tissue mass (g)	10.1±5.1	10.0±5.0	10.1±5.1	0.923
Total epicardial adipose tissue mass (g)	109±44	111±43	108±45	0.488
Posterior LA adipose tissue attenuation (HU)	-96.4±7.9	-95.6±6.2	-96.8±8.7	0.098
Posterior LA adipose tissue attenuation ≥ -96.4 HU, n(%)	245 (53)	100 (60)	145 (50)	0.041

Values are mean ± standard deviation if normally distributed and median (interquartile range) if not normally distributed.
CT: computed tomography, HU: Hounsfield units, LA: left atrial, LVEF: left ventricular ejection fraction,

Figure 1. Correlations between BMI, total EAT, posterior LA adipose tissue mass and attenuation.

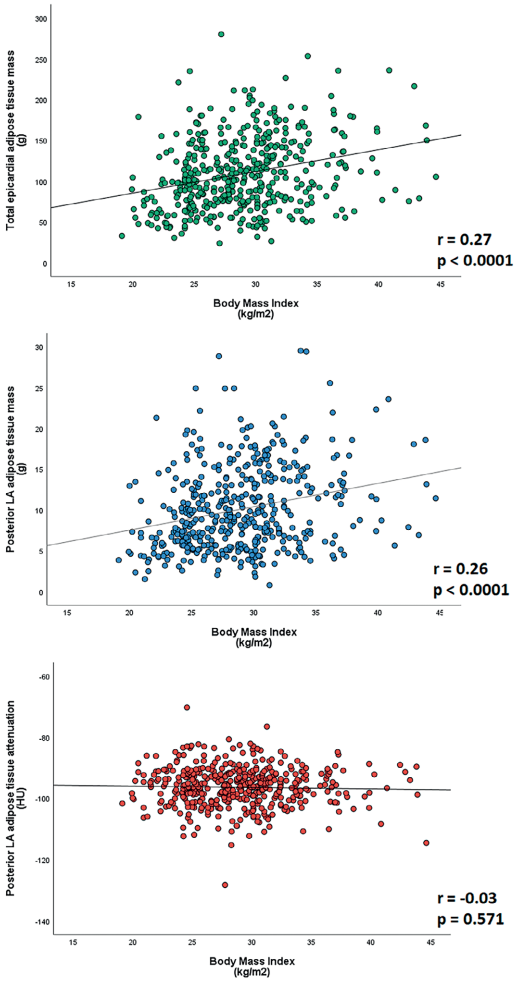

The relation between BMI and total EAT, BMI and posterior LA adipose tissue mass and attenuation.
BMI: body mass index, g: gram, HU: Hounsfield units, LA: left atrium.

Posterior LA adipose tissue attenuation and AF recurrence

Patients with higher posterior LA adipose tissue attenuation (≥-96.4 HU) had more cumulative recurrence rates of AF than patients with lower posterior LA adipose tissue attenuation (<-96.4 HU) by Kaplan-Meier analysis (log-rank test p=0.046; Figure 2). Table 3 summarizes the Cox regression analysis of the posterior LA

adipose tissue mass and attenuation for AF recurrence following catheter ablation. After correcting for known associates of AF recurrence posterior LA adipose tissue attenuation (HR 1.26; 95% CI 0.90-1.76; p=0.181) remained a promising predictor of AF recurrence following catheter ablation.

The inter-class correlation coefficient for inter-observer variability for posterior LA adipose tissue mass was 0.995 (95% CI 0.988-0.999; p<0.001) and for LA adipose tissue attenuation 0.990 (95% CI 0.971-0.997; p<0.001).

Figure 2. Kaplan-Meier curve for atrial fibrillation recurrence following catheter ablation according to posterior LA adipose tissue attenuation.

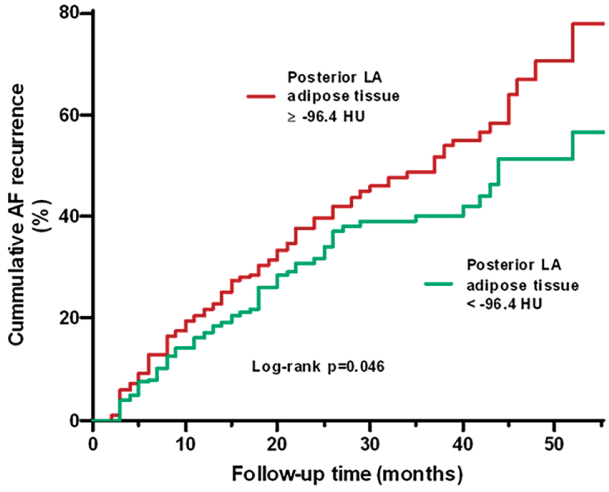

AF: atrial fibrillation, HU: Hounsfield units, LA: left atrial

Table 3. Uni- and multivariable Cox regression analysis for atrial fibrillation recurrence following catheter ablation.

	Univariable Hazard ratio (95% CI)	p-value	Multivariable Hazard ratio (95% CI)	p-value
Posterior LA adipose tissue mass (per one unit increase)	1.00 (0.97-1.03)	0.970	1.01 (0.97-1.04)	0.759
Posterior LA adipose tissue attenuation ≥ -96.4 HU(yes/no)	1.37 (1.00-1.86)	0.047	1.26 (0.90-1.76)	0.181

* Adjusted for age, sex, AF type, body mass index, use of antiarrhythmic drugs, left ventricular ejection fraction <50%, E/A-ratio and left atrial volume.
CI = confidence interval, HU = Hounsfield units, LA = left atrial

DISCUSSION

The current study demonstrated that patients with higher posterior LA adipose tissue attenuation had significantly more often AF recurrences following AF catheter ablation. After correction for several known risk factors for AF recurrences following catheter ablation, higher posterior LA adipose tissue attenuation remained a promising predictor of AF recurrence.

EAT and AF

Recently, obesity has been recognized as an important, and modifiable risk factor for AF development.[1,2] Although BMI has been used as a marker of general adiposity, it incorporates both subcutaneous and visceral adipose tissue, despite both structures being distinct.[20] Of note, higher levels of proinflammatory adipokines are secreted by visceral adipose tissue as compared to subcutaneous adipose tissue, and visceral adipose tissue has been associated with a greater risk for cardiovascular diseases.[6,8,9,20] EAT, the adipose tissue within the visceral layer of the pericardium, has demonstrated to be an important source of adipokines.[6] Total EAT is a stronger predictor for the presence of AF as compared to BMI.[5] More specifically, the relation between peri-atrial EAT and AF was examined in a population of 618 patients in sinus rhythm or with AF. Although, peri-atrial EAT thickness was higher in patients with AF compared to those in sinus rhythm, posterior LA adipose tissue thickness had the strongest correlation with the occurrence of AF of all LA adipose tissue pads.[13] Moreover, Batal et al. reported that only posterior LA adipose tissue thickness was significantly associated with AF burden.[12] Subsequently, Rosendael and colleagues quantified the posterior LA adipose tissue and found that each gram increase in posterior LA adipose tissue mass was associated with an increase of 32% in the risk of AF.[14] While some studies also demonstrated a relation between peri-atrial EAT assessed on CT and late AF recurrence after ablation,[21-23] others could not confirm this relation.[24,25] This discrepancy could be explained by methodological differences in assessment of peri-atrial EAT. Likewise, in the current study we could not demonstrate an association indicating that the quantity of posterior LA adipose tissue might not be an important measure for predicting AF recurrence. Another explanation could be related to the large posterior LA adipose tissue mass (mean 10.1 gram) found in our population. The higher BMI in the current population, compared to populations in previous studies, suggest higher adiposity and higher peri-atrial EAT in the current population. It may be that the posterior

LA adipose tissue mass has reached the maximum mass in both the recurrence and no-recurrence groups. This is further supported by the higher total EAT in the current population compared to previous studies.[21,25]

Inflammation and AF

Histological examination of atrial tissue in patients with AF has shown evidence of inflammation.[26] Various clinical studies have also reported a relation between inflammation and AF.[27,28] Specifically, systemic inflammatory biomarkers are increased in AF patients while anti-inflammatory therapy decreases the AF risk.[27-29] However, systemic inflammatory biomarkers might not represent inflammatory activity at the tissue level.[30] The close proximity of EAT to the LA, the ability of EAT to produce inflammatory adipokines and its association with AF makes EAT an attractive target for measuring inflammation in AF patients. Mazurek et al. quantified the inflammatory activity of EAT, visceral thoracic adipose tissue and subcutaneous adipose tissue using ^{18}F-fluorodeoxyglucose positron emission tomography in 21 patients with AF and 21 controls.[31] Inflammatory activity of EAT in AF patients was significantly higher compared to controls. Moreover, inflammatory activity of EAT was higher compared to subcutaneous adipose tissue and even thoracic visceral adipose tissue in AF patients.[31] Ciuffo et al. demonstrated in 143 patients that increased attenuation (as a marker of inflammation) of peri-atrial adipose tissue measured from a single slice four-chamber view on CT was a predictor of AF recurrence after catheter ablation.[10] However, in the same study attenuation of the peri-atrial adipose tissue measured from the two-chamber view was not associated with AF recurrence, highlighting the variability of the EAT at different myocardial regions and the importance of volumetric quantification of EAT.[11] The results from the current study demonstrate similar findings, using volumetric quantification in a larger patient population: more inflamed peri-atrial adipose tissue is associated with AF recurrence after catheter ablation. Several explanations for this relation could be considered. A more inflamed atrial wall might impede adequate lesion transmurality during ablation through the formation of edema.[32] Another explanation might be the formation of atrial fibrosis through localized inflammatory processes induced by EAT.[30] Atrial fibrosis might enable the formation of intra-atrial re-entry circuits and the presence of atrial fibrosis reduces catheter ablation success.[33] While we observed similar posterior LA adipose tissue mass between those patients that experienced AF recurrence and those patients that did not, patients with AF recurrence had larger LA volumes. Increasing LA

volumes leads to more enhanced stretching of the LA wall allowing for a larger contact area between the EAT and the LA wall. As the inflammatory adipokines of EAT directly exert their action on the LA wall through paracrine effects,[6] in addition to the attenuation of the posterior LA adipose tissue, the contact area between the EAT and the LA wall might also be an important factor in AF recurrences.

Assessment of the posterior LA adipose tissue attenuation on CT is a novel and easily accessible tissue specific biomarker of inflammation prior to AF catheter ablation. Moreover, attenuation of peri-vascular EAT assessed from CT could be a marker to track response to anti-inflammatory therapy.[34] In addition, several studies have demonstrated that anti-inflammatory therapy reduces the risk for AF.[28,29] Assessment of posterior LA adipose tissue attenuation may potentially guide/personalize the use of anti-inflammatory therapy to reduce AF recurrences.

Study limitations

This was a single center study with a retrospective design. Patients with inadequate CT quality were excluded, which may have introduced selection bias. Moreover, the attenuation values reported in this study may be limited to this specific CT scanner and should be validated with other CT scanners. The optimal cut-off values found in this study population should be confirmed in future studies including larger populations and using different CT scanners. Such validation is important to further assess the role of posterior LA adipose tissue attenuation before clinical implementation. Since AF recurrences were defined as documented episodes and we did not solely rely on reported complaints, some patients with recurrences might have been missed.

CONCLUSIONS

Posterior LA adipose tissue attenuation is a promising novel and tissue specific biomarker of AF recurrence. Higher attenuation of the posterior LA adipose tissue might signal local inflammation and serve as an imaging biomarker of increased risk of AF recurrence.

REFERENCES

1. Wang TJ, Parise H, Levy D, D'Agostino RB, Sr., Wolf PA, Vasan RS, et al. Obesity and the risk of new-onset atrial fibrillation. JAMA 2004;292:2471-2477.
2. Pathak RK, Middeldorp ME, Lau DH, Mehta AB, Mahajan R, Twomey D, et al. Aggressive risk factor reduction study for atrial fibrillation and implications for the outcome of ablation: the ARREST-AF cohort study. J Am Coll Cardiol 2014;64:2222-2231.
3. Sultan A, Luker J, Andresen D, Kuck KH, Hoffmann E, Brachmann J, et al. Predictors of Atrial Fibrillation Recurrence after Catheter Ablation: Data from the German Ablation Registry. Sci Rep 2017;7:16678.
4. Sacks HS, Fain JN. Human epicardial adipose tissue: a review. Am Heart J 2007;153:907-917.
5. Thanassoulis G, Massaro JM, O'Donnell CJ, Hoffmann U, Levy D, Ellinor PT, et al. Pericardial fat is associated with prevalent atrial fibrillation: the Framingham Heart Study. Circ Arrhythm Electrophysiol 2010;3:345-350.
6. Iacobellis G. Local and systemic effects of the multifaceted epicardial adipose tissue depot. Nat Rev Endocrinol 2015;11:363-371.
7. Maurovich-Horvat P, Massaro J, Fox CS, Moselewski F, O'Donnell CJ, Hoffmann U. Comparison of anthropometric, area- and volume-based assessment of abdominal subcutaneous and visceral adipose tissue volumes using multi-detector computed tomography. Int J Obes (Lond) 2007;31:500-506.
8. Goeller M, Achenbach S, Cadet S, Kwan AC, Commandeur F, Slomka PJ, et al. Pericoronary Adipose Tissue Computed Tomography Attenuation and High-Risk Plaque Characteristics in Acute Coronary Syndrome Compared With Stable Coronary Artery Disease. JAMA Cardiol 2018;3:858-863.
9. Oikonomou EK, Marwan M, Desai MY, Mancio J, Alashi A, Hutt Centeno E, et al. Non-invasive detection of coronary inflammation using computed tomography and prediction of residual cardiovascular risk (the CRISP CT study): a post-hoc analysis of prospective outcome data. Lancet 2018;392:929-939.
10. Ciuffo L, Nguyen H, Marques MD, Aronis KN, Sivasambu B, de Vasconcelos HD, et al. Periatrial Fat Quality Predicts Atrial Fibrillation Ablation Outcome. Circ Cardiovasc Imaging 2019;12:e008764.
11. Lemola K, Sneider M, Desjardins B, Case I, Han J, Good E, et al. Computed tomographic analysis of the anatomy of the left atrium and the esophagus: implications for left atrial catheter ablation. Circulation 2004;110:3655-3660.
12. Batal O, Schoenhagen P, Shao M, Ayyad AE, Van Wagoner DR, Halliburton SS, et al. Left atrial epicardial adiposity and atrial fibrillation. Circ Arrhythm Electrophysiol 2010;3:230-236.
13. Yorgun H, Canpolat U, Aytemir K, Hazirolan T, Sahiner L, Kaya EB, et al. Association of epicardial and peri-atrial adiposity with the presence and severity of non-valvular atrial fibrillation. Int J Cardiovasc Imaging 2015;31:649-657.
14. van Rosendael AR, Dimitriu-Leen AC, van Rosendael PJ, Leung M, Smit JM, Saraste A, et al. Association Between Posterior Left Atrial Adipose Tissue Mass and Atrial Fibrillation. Circ Arrhythm Electrophysiol 2017;10.
15. Kirchhof P, Benussi S, Kotecha D, Ahlsson A, Atar D, Casadei B, et al. 2016 ESC Guidelines for the management of atrial fibrillation developed in collaboration with EACTS. Europace 2016;18:1609-1678.

16. Bunch TJ, May HT, Bair TL, Jacobs V, Crandall BG, Cutler M, et al. The Impact of Age on 5-Year Outcomes After Atrial Fibrillation Catheter Ablation. J Cardiovasc Electrophysiol 2016;27:141-146.

17. Duytschaever M, Demolder A, Phlips T, Sarkozy A, El Haddad M, Taghji P, et al. PulmOnary vein isolation With vs. without continued antiarrhythmic Drug trEatment in subjects with Recurrent Atrial Fibrillation (POWDER AF): results from a multicentre randomized trial. Eur Heart J 2018;39:1429-1437.

18. Cha Y-M, Wokhlu A, Asirvatham SJ, Shen W-K, Friedman PA, Munger TM, et al. Success of Ablation for Atrial Fibrillation in Isolated Left Ventricular Diastolic Dysfunction. Circ Arrhythm Electrophysiol 2011;4:724-732.

19. Njoku A, Kannabhiran M, Arora R, Reddy P, Gopinathannair R, Lakkireddy D, et al. Left atrial volume predicts atrial fibrillation recurrence after radiofrequency ablation: a meta-analysis. *EP* Europace 2017;20:33-42.

20. Oikonomou EK, Antoniades C. The role of adipose tissue in cardiovascular health and disease. Nat Rev Cardiol 2019;16:83-99.

21. Nagashima K, Okumura Y, Watanabe I, Nakai T, Ohkubo K, Kofune T, et al. Association between epicardial adipose tissue volumes on 3-dimensional reconstructed CT images and recurrence of atrial fibrillation after catheter ablation. Circ J 2011;75:2559-2565.

22. Tsao HM, Hu WC, Wu MH, Tai CT, Lin YJ, Chang SL, et al. Quantitative analysis of quantity and distribution of epicardial adipose tissue surrounding the left atrium in patients with atrial fibrillation and effect of recurrence after ablation. Am J Cardiol 2011;107:1498-1503.

23. Kocyigit D, Gurses KM, Yalcin MU, Turk G, Evranos B, Yorgun H, et al. Periatrial epicardial adipose tissue thickness is an independent predictor of atrial fibrillation recurrence after cryoballoon-based pulmonary vein isolation. J Cardiovasc Comput Tomogr 2015;9:295-302.

24. Vroomen M, Olsthoorn JR, Maesen B, L'Espoir V, La Meir M, Das M, et al. Quantification of epicardial adipose tissue in patients undergoing hybrid ablation for atrial fibrillation. Eur J Cardiothorac Surg 2019;56:79-86.

25. Masuda M, Mizuno H, Enchi Y, Minamiguchi H, Konishi S, Ohtani T, et al. Abundant epicardial adipose tissue surrounding the left atrium predicts early rather than late recurrence of atrial fibrillation after catheter ablation. J Interv Card Electrophysiol 2015;44:31-37.

26. Frustaci A, Chimenti C, Bellocci F, Morgante E, Russo MA, Maseri A. Histological substrate of atrial biopsies in patients with lone atrial fibrillation. Circulation 1997;96:1180-1184.

27. Chung MK, Martin DO, Sprecher D, Wazni O, Kanderian A, Carnes CA, et al. C-reactive protein elevation in patients with atrial arrhythmias: inflammatory mechanisms and persistence of atrial fibrillation. Circulation 2001;104:2886-2891.

28. Peña JM, MacFadyen J, Glynn RJ, Ridker PM. High-sensitivity C-reactive protein, statin therapy, and risks of atrial fibrillation: an exploratory analysis of the JUPITER trial. Eur Heart J 2012;33:531-537.

29. Halonen J, Halonen P, Järvinen O, Taskinen P, Auvinen T, Tarkka M, et al. Corticosteroids for the prevention of atrial fibrillation after cardiac surgery: a randomized controlled trial. JAMA 2007;297:1562-1567.

30. Abe I, Teshima Y, Kondo H, Kaku H, Kira S, Ikebe Y, et al. Association of fibrotic remodeling and cytokines/chemokines content in epicardial adipose tissue with atrial myocardial fibrosis in patients with atrial fibrillation. Heart rhythm 2018;15:1717-1727.

31. Mazurek T, Kiliszek M, Kobylecka M, Skubisz-Gluchowska J, Kochman J, Filipiak K, et al. Relation of proinflammatory activity of epicardial adipose tissue to the occurrence of atrial fibrillation. Am J Cardiol 2014;113:1505-1508.

32. Taclas JE, Nezafat R, Wylie JV, Josephson ME, Hsing J, Manning WJ, et al. Relationship between intended sites of RF ablation and post-procedural scar in AF patients, using late gadolinium enhancement cardiovascular magnetic resonance. Heart rhythm 2010;7:489-496.

33. Verma A, Wazni OM, Marrouche NF, Martin DO, Kilicaslan F, Minor S, et al. Pre-existent left atrial scarring in patients undergoing pulmonary vein antrum isolation: an independent predictor of procedural failure. J Am Coll Cardiol 2005;45:285-292.

34. Elnabawi YA, Oikonomou EK, Dey AK, Mancio J, Rodante JA, Aksentijevich M, et al. Association of Biologic Therapy With Coronary Inflammation in Patients With Psoriasis as Assessed by Perivascular Fat Attenuation Index. JAMA Cardiol 2019;4:885-891.

8

Summary and Conclusions
Samenvatting en conclusies

Summary and Conclusions

The formation and growth of atherosclerotic plaques is a complex process which takes years before clinical symptoms occur. Chapter 2 demonstrates this dynamic process of coronary plaque evolution during long-term follow-up in a low-to-intermediate risk population. Men had more plaques in the coronary arteries on computed tomography (CT) than women, however the plaque burden normalized for the vessel volume on a per lesion analysis did not differ between men and women at baseline or during follow-up. Compositional plaque analysis demonstrated that women had lower fibro-fatty plaque volume at baseline and follow-up when compared to men. Furthermore, non-calcified and fibrous plaque volume regressed faster in women compared to men in the age category of less than 55 years of age. Conversely, no sex differences were noted in the patients aged 55 years or more. In Chapter 3, the relation between an anatomical marker of coronary artery disease (CAD), the coronary artery calcium (CAC) score, was compared with a functional marker of CAD, CT myocardial perfusion. The presence of inducible myocardial ischemia increased with increasing CAC score. Moreover, calcium score was the only determinant on multivariable analysis that significantly predicted the presence of inducible myocardial ischemia.

In Chapter 4, global left ventricular (LV) myocardial work efficiency was determined non-invasively using pressure-strain loops constructed from sphygmomanometric blood pressure measurements and 2D speckle tracking strain echocardiography. Global LV myocardial work efficiency was lower in individuals with structural heart disease: post ST-segment elevation myocardial infarction (STEMI) and heart failure with reduced LV ejection fraction. In individuals with cardiovascular risk factors but without structural heart disease, global LV myocardial work efficiency was similar to healthy subjects. In Chapter 5, segmental myocardial work efficiency and several other myocardial work indices were determined in patients following STEMI and compared to segmental hyperenhancement on late gadolinium contrast enhanced cardiac magnetic resonance (LGE CMR). Myocardial work index, constructive work and myocardial work efficiency were higher in non-infarcted segments, followed by segments with non-transmural infarction and transmural infarction respectively. Meanwhile, wasted work demonstrated an inverse relation.

Chapter 6 investigated the role of LV global longitudinal strain (GLS) and heart/mediastinum (H/M) ratio on myocardial innervation/denervation imaging (using 123I-MIBG scintigraphy) in predicting ventricular arrhythmias (defined as appropriate therapy (shocks, anti-tachycardia pacing) on implantable cardioverter defibrillator (ICD)) in patients with heart failure. Both LV GLS and the H/M-ratio, were significantly more impaired in individuals with appropriate ICD therapy compared to those without, while LV ejection fraction was similar in both groups. Multivariate Cox regression analysis identified LV GLS and H/M ratio on 123I-MIBG scintigraphy as independent predictors of appropriate ICD therapy. Finally, in Chapter 7, attenuation of posterior left atrial adipose tissue on CT (as marker of inflammation) was shown to be a promising predictor of atrial fibrillation recurrence following catheter ablation.

Conclusions

Multimodality imaging is an important tool to guide the management of patients with cardiovascular disease. Technological advancements in CT have allowed for increased image quality with reduced radiation exposure. This permits CT to be utilized in larger populations with lower risk, and provides increasingly more information, alone or combined with other imaging modalities. Advanced echocardiographic techniques including 2-dimensional speckle tracking imaging (permitting measurement of LV GLS, and more recently non-invasive myocardial work) may provide important information in the characterization and risk-stratification of patients.

Further prospective studies in larger patient populations are needed to confirm the current results, before widespread clinical implementation of these sophisticated imaging techniques can be recommended.

Samenvatting en conclusies

De vorming en groei van atherosclerotische plaques is een complex proces wat jaren in beslag neemt voordat klinische symptomen optreden. Hoofdstuk 2 demonstreert dit dynamische proces van coronaire plaque evolutie tijdens lange termijn follow-up in een populatie met een laag tot gemiddeld risico op hart- en vaatziekten. Mannen hadden meer plaques in de kransslagaders op computertomografie (CT) dan vrouwen, maar de *plaqueburden* genormaliseerd voor het vaatvolume in een per-laesie analyse verschilde niet tussen mannen en vrouwen bij aanvang of tijdens follow-up. Compositorisch plaque-analyse toonde aan dat vrouwen een lager *fibro-fatty* plaquevolume hadden bij aanvang en follow-up in vergelijking met mannen. Bovendien was er sprake van een snellere regressie van het *non-calcified* en *fibrous* plaquevolume bij vrouwen dan bij mannen in de leeftijdscategorie jonger dan 55 jaar. Daarentegen, bij de patiënten van 55 jaar of ouder werden geen sekseverschillen gezien. In Hoofdstuk 3 werd de relatie tussen een anatomische marker van coronaire hartziekte, de coronaire arteriële calcium (CAC) score, vergeleken met een functionele marker, CT myocardperfusie. De aanwezigheid van induceerbare myocardischemie op CT myocardperfusie nam toe met een toenemende CAC score. Bovendien was calcium score de enige determinant in multivariabele analyse die de aanwezigheid van induceerbare myocardischemie significant voorspelde. In Hoofdstuk 4 werd de *global left ventricular (LV) myocardial work efficiency* niet-invasief bepaald met een behulp van een nieuwe techniek dat *pressure-strain loops* construeert uit sfygmomanometrische bloeddrukmetingen in combinatie met 2-dimensionale *speckle tracking strain* echocardiografie. De *global LV myocardial work efficiency* was lager bij personen met structurele hartziekte: post-ST-segment elevatie myocardinfarct (STEMI) en hartfalen met verminderde LV ejectiefractie. Bij personen met cardiovasculaire risicofactoren maar zonder structurele hartziekte was de *global LV myocardial work efficiency* vergelijkbaar met die van gezonde proefpersonen. In Hoofdstuk 5 werden de segmentale waardes van *LV myocardial work efficiency* en andere *myocardial work* indexen bepaald bij patiënten na een STEMI en vergeleken met segmentale signaalintensiteit op *late gadolinium contrast enhanced* (LGE) cardiale magnetische resonantie (CMR). *Myocardial work index, constructive work* en *myocardial work efficiency* waren allen het hoogst in niet geïnfarceerde segmenten, gevolgd door respectievelijk niet-transmuraal geïnfarceerd en transmuraal geïnfarceerd segmenten. Integendeel, m*yocardial wasted work* toonde een omgekeerde relatie.

In hoofdstuk 6 wordt de rol van LV *global longitudinale strain* (GLS) en hart/mediastinum (H/M) ratio op myocardiale innervatie/denervatie beeldvorming (met behulp van 123I-MIBG scintigrafie) onderzocht op het voorspellen van ventriculaire aritmieën (gedefinieerd als correcte therapie (shocks of antitachycardie pacing) op implanteerbare cardioverter defibrillator (ICD)) bij patiënten met hartfalen. Zowel LV GLS als de H/M-ratio waren significant meer aangetast bij personen met correcte ICD-therapie in vergelijking met personen zonder, hoewel LV ejectiefractie vergelijkbaar was in beide groepen. Multivariate Cox-regressie analyse identificeerde LV GLS en H/M-ratio op 123I-MIBG-scintigrafie als onafhankelijke voorspellers voor correcte ICD-therapie. Tot slot, in hoofdstuk 7 werd aangetoond dat de attenuatie van het posterieur linker atrium vetweefsel op CT (als marker van inflammatie) een veelbelovende voorspeller is voor recidief van atriumfibrilleren na katheterablatie.

Conclusie

Multimodale beeldvorming is een belangrijk hulpmiddel in de behandeling van patiënten met hart- en vaatziekten. Technologische vooruitgang in CT hebben gezorgd voor toenemende beeldkwaliteit met verminderde blootstelling aan straling. Hierdoor kan CT, alleen of in combinatie met andere beeldvormende modaliteiten, worden gebruikt in steeds grotere populaties met een lager risico en wordt tevens steeds meer informatie verstrekt. Geavanceerde echocardiografische technieken, waaronder 2-dimensionale *speckle tracking imaging* (voor de meting van LV GLS en recentelijk non-invasieve *myocardial work*) kunnen belangrijke informatie opleveren bij de karakterisering en risicostratificatie van patiënten met hart- en vaatziekten.

Prospectieve studies in grotere patiëntenpopulaties zijn nodig om de bevindingen die in dit proefschrift staan beschreven te bevestigen voordat klinische implementatie van deze geavanceerde beeldvormingstechnieken kan worden aanbevolen.

Dankwoord
List of publications
Curriculum Vitae

Dankwoord

Graag zou ik iedereen willen bedanken die heeft bijgedragen aan de totstandkoming van dit proefschrift, zowel op de afdeling cardiologie van het Leids Universitair Medisch Centrum als daarbuiten. Ik wil een aantal personen in het bijzonder noemen.

Prof. dr. Bax, beste Jeroen, bedankt voor je vertrouwen en de enthousiaste begeleiding afgelopen jaren ondanks je drukke schema. Prof. dr. Jukema, beste Wouter dank voor je inspirerende woorden en wijze levenslessen. Prof. dr. Schalij, beste Martin, jouw leiderschap van de afdeling cardiologie heb ik tijdens mijn periode op de afdeling als erg fijn ervaren.

Dear Victoria, thank you for your critical feedback, suggestions and always letting us strive for the best. Beste Arthur, dank voor de begeleiding en dat ik altijd langs kon komen bij vragen.

Ik zou het secretariaat van het stafcentrum en de research verpleegkundigen willen bedanken voor alle hulp en gezelligheid.

Graag zou ik ook al mijn tuincollega's willen bedanken voor de fantastische periode samen, leerzaam en gezellig! I would like to thank the imaging foreign fellows for the wonderful time together. Mijn imaging room maatjes wil ik in het bijzonder noemen en bedanken: Rohit dank voor je gezelligheid en je "down-to-earth" advies. Alexander, bedankt voor je hulp bij het opstarten van mijn projecten. Rachid, bedankt voor je gezelligheid, je kritische houding en je rechtdoorzee advies. Bedankt dat je mijn paranimf wilt zijn! Jeff, de lange dagen werken in de imaging room aan metingen, analyses en stukken schrijven had ik niet kunnen doen zonder jouw constructieve feedback, gezelligheid en humor. Canada en de VS waren fantastisch. Ik voel me vereerd dat je mijn paranimf wilt zijn!

Gert, bedankt voor je begeleiding tot nu toe, ik hoop dat we dit nog jaren kunnen voortzetten. Jeffrey, leuk dat ik je na onze tijd in het Slootje weer ben tegengekomen.

Ik zou graag Saarig, Khurshed, Kinaci, Kupeli, AA en Abderrahman willen bedanken voor de onderwijsmomenten en gezelligheid. Ik heb veel van jullie mogen leren gedurende onze discussies over wetenschap, klinische problemen en het leven.

Familie en schoonfamilie, dank voor jullie ondersteuning.

Hamdi, Rini, beide Abdou families dank voor de gezelligheid en de mooie momenten samen.

Jema, Abi, Achmed en Zaid dank voor de omgeving waarin ik kon opgroeien en jullie continue steun en adviezen. Zonder jullie was dit proefschrift er niet geweest.

Lieve Sahar, je bent een onuitputtelijke bron van steun, vertrouwen en liefde. Het is moeilijk om de woorden te vinden die recht doen aan mijn dankbaarheid. Lieve Moesa, je bent geweldig in zoveel opzichten maar jouw vrolijkheid raakt mij het meest.

List of publications

Veldhuis-Vlug AG, **El Mahdiui M**, Endert E, Heijboer AC, Fliers E, Bisschop PH. Bone resorption is increased in pheochromocytoma patients and normalizes following adrenalectomy. *J Clin Endocrinol Metab* 2012;97:E2093-2097.

Manabe O, Kikuchi T, Scholte A, **El Mahdiui M**, Nishii R, Zhang MR, et al. Radiopharmaceutical tracers for cardiac imaging. *J Nucl Cardiol* 2018;25:1204-1236.

Hensen LCR, **El Mahdiui M**, van Rosendael AR, Smit JM, Jukema JW, Bax JJ, et al. Prevalence and Prognostic Implications of Mitral and Aortic Valve Calcium in Patients With Chronic Kidney Disease. *Am J Cardiol* 2018;122:1732-1737.

Smit JM, **El Mahdiui M**, van Rosendael AR, Jukema JW, Koning G, Reiber JHC, et al. Comparison of Diagnostic Performance of Quantitative Flow Ratio in Patients With Versus Without Diabetes Mellitus. *Am J Cardiol* 2019;123:1722-1728.

El Mahdiui M, Smit JM, van Rosendael AR, Delgado V, Ajmone Marsan N, Jukema JW, et al. Characterization of the left ventricular arrhythmogenic substrate with multimodality imaging: role of innervation imaging and left ventricular global longitudinal strain. *Eur J Hybrid Imaging* 2019;3:14.

El Mahdiui M, van der Bijl P, Abou R, Ajmone Marsan N, Delgado V, Bax JJ. Global Left Ventricular Myocardial Work Efficiency in Healthy Individuals and Patients with Cardiovascular Disease. *J Am Soc Echocardiogr* 2019;32:1120-1127.

Smit JM, Koning G, van Rosendael AR, **El Mahdiui M**, Mertens BJ, Schalij MJ, et al. Referral of patients for fractional flow reserve using quantitative flow ratio. *Eur Heart J Cardiovasc Imaging* 2019;20:1231-1238.

van der Bijl P, Kostyukevich M, **El Mahdiui M**, Hansen G, Samset E, Ajmone Marsan N, et al. A Roadmap to Assess Myocardial Work: From Theory to Clinical Practice. *JACC Cardiovasc Imaging* 2019.

Smit JM, van Rosendael AR, **El Mahdiui M**, Neglia D, Knuuti J, Saraste A, et al. Impact of Clinical Characteristics and Statins on Coronary Plaque Progression by Serial Computed Tomography Angiography. *Circ Cardiovasc Imaging* 2020;13:e009750.

Lustosa RP, van der Bijl P, **El Mahdiui M**, Montero-Cabezas JM, Kostyukevich MV, Ajmone Marsan N, et al. Noninvasive Myocardial Work Indices 3 Months after ST-Segment Elevation Myocardial Infarction: Prevalence and Characteristics of Patients with Postinfarction Cardiac Remodeling. *J Am Soc Echocardiogr* 2020;33:1172-1179.

Hiemstra YL, van der Bijl P, **El Mahdiui M**, Bax JJ, Delgado V, Marsan NA. Myocardial Work in Nonobstructive Hypertrophic Cardiomyopathy: Implications for Outcome. *J Am Soc Echocardiogr* 2020;33:1201-1208.

Abou R, Prihadi EA, Goedemans L, van der Geest R, **El Mahdiui M**, Schalij MJ, et al. Left ventricular mechanical dispersion in ischaemic cardiomyopathy: association with myocardial scar burden and prognostic implications. *Eur Heart J Cardiovasc Imaging* 2020;21:1227-1234.

Butcher SC, Fortuni F, Montero-Cabezas JM, Abou R, **El Mahdiui M**, van der Bijl P, et al. Right ventricular myocardial work: proof-of-concept for non-invasive assessment of right ventricular function. *Eur Heart J Cardiovasc Imaging* 2021;22:142-152.

Lustosa RP, Fortuni F, van der Bijl P, Goedemans L, **El Mahdiui M**, Montero-Cabezas JM, et al. Left ventricular myocardial work in the culprit vessel territory and impact on left ventricular remodelling in patients with ST-segment elevation myocardial infarction after primary percutaneous coronary intervention. *Eur Heart J Cardiovasc Imaging* 2021;22:339-347.

Lustosa RP, Butcher SC, van der Bijl P, **El Mahdiui M**, Montero-Cabezas JM, Kostyukevich MV, et al. Global Left Ventricular Myocardial Work Efficiency and Long-Term Prognosis in Patients After ST-Segment-Elevation Myocardial Infarction. *Circ Cardiovasc Imaging* 2021;14:e012072.

El Mahdiui M, Simon J, Smit JM, Kuneman JH, van Rosendael AR, Steyerberg EW, et al. Posterior Left Atrial Adipose Tissue Attenuation Assessed by Computed

Tomography and Recurrence of Atrial Fibrillation After Catheter Ablation. *Circ Arrhythm Electrophysiol* 2021;14:e009135.

El Mahdiui M, Smit JM, van Rosendael AR, Neglia D, Knuuti J, Saraste A, et al. Sex differences in coronary plaque changes assessed by serial computed tomography angiography. *Int J Cardiovasc Imaging* 2021;37:2311-2321.

El Mahdiui M, van der Bijl P, Abou R, de Paula Lustosa R, van der Geest R, Ajmone Marsan N, et al. Myocardial Work, an Echocardiographic Measure of Post Myocardial Infarct Scar on Contrast-Enhanced Cardiac Magnetic Resonance. *Am J Cardiol* 2021;151:1-9.

El Mahdiui M, Smit JM, van Rosendael AR, Jukema JW, Bax JJ, Scholte A. Relationship between coronary artery calcification and myocardial ischemia on computed tomography myocardial perfusion in patients with stable chest pain. *J Nucl Cardiol* 2021;28:1707-1714.

Abou R, Goedemans L, Montero-Cabezas JM, Prihadi EA, **El Mahdiui M**, Schalij MJ, et al. Prognostic Value of Multilayer Left Ventricular Global Longitudinal Strain in Patients with ST-segment Elevation Myocardial Infarction with Mildly Reduced Left Ventricular Ejection Fractions. *Am J Cardiol* 2021;152:11-18.

Smit JM, Simon J, **El Mahdiui M**, Szaraz L, van Rosendael PJ, Kolassváry M, et al. Anatomical Characteristics of the Left Atrium and Left Atrial Appendage in Relation to the Risk of Stroke in Patients With Versus Without Atrial Fibrillation. *Circ Arrhythm Electrophysiol* 2021;14:e009777.

Lustosa RP, Fortuni F, van der Bijl P, **El Mahdiui M**, Montero-Cabezas JM, Kostyukevich MV, et al. Changes in Global Left Ventricular Myocardial Work Indices and Stunning Detection 3 Months After ST-Segment Elevation Myocardial Infarction. *Am J Cardiol* 2021;157:15-21.

Caselli C, De Caterina R, Smit JM, Campolo J, **El Mahdiui M**, Ragusa R, et al. Triglycerides and low HDL cholesterol predict coronary heart disease risk in patients with stable angina. *Sci Rep* 2021;11:20714.

van Driest FY, van der Geest RJ, Broersen A, Dijkstra J, **El Mahdiui M**, Jukema JW, et al. Quantification of myocardial ischemia and subtended myocardial mass at adenosine stress cardiac computed tomography: a feasibility study. *Int J Cardiovasc Imaging* 2021;37:3313-3322.

Di Giorgi N, Michelucci E, Smit JM, Scholte A, **El Mahdiui M**, Knuuti J, et al. A specific plasma lipid signature associated with high triglycerides and low HDL cholesterol identifies residual CAD risk in patients with chronic coronary syndrome. *Atherosclerosis* 2021;339:1-11.

Simon J, **El Mahdiui M**, Smit JM, Száraz L, van Rosendael AR, Herczeg S, et al. Left atrial appendage size is a marker of atrial fibrillation recurrence after radiofrequency catheter ablation in patients with persistent atrial fibrillation. *Clin Cardiol* 2021.

Kuneman JH, **El Mahdiui M**, van Rosendael AR, van den Hoogen IJ, Patel MR, Nørgaard BL, et al. Coronary volume to left ventricular mass ratio in patients with diabetes mellitus. *J Cardiovasc Comput Tomogr 2022.*

Curriculum vitae

De auteur van dit proefschrift werd geboren op 24 januari 1989 te Midar, Marokko. Na het behalen van zijn middelbareschooldiploma aan het Calandlyceum in 2008 begon hij met zijn geneeskunde opleiding aan het Academisch Medisch Centrum te Amsterdam. Tijdens zijn opleiding volgde hij het honourstraject wat hij ook succesvol heeft afgerond en heeft hij vroeg kennis mogen maken met het uitvoeren van wetenschappelijk onderzoek als student op de afdeling endocrinologie van het Academisch Medisch Centrum. Hij volgde tijdens zijn studie ook verschillende Masterclasses, was hij betrokken bij maatschappelijke organisaties en heeft verschillende stages gelopen in het buitenland. Na het behalen van zijn geneeskunde diploma in 2014 startte hij als arts-assistent niet in opleiding op de afdeling interne geneeskunde, longziekten en cardiologie in het toenmalige MC Slotervaart te Amsterdam. Nadien was hij werkzaam op de afdelingen Intensive Care en Neurologie wat de basis legde voor brede medische kennis. Na een korte periode werkzaam te zijn als arts-assistent op de afdeling cardiologie van het Leids Universitair Medisch Centrum startte hij met zijn promotieonderzoek aan dezelfde universiteit onder begeleiding van professor J.J. Bax en professor J.W. Jukema. De resultaten van dit promotieonderzoek staan in dit proefschrift beschreven.